

# Constraining the Equation of State of Neutron Stars from Binary Mergers

COMPACT STARS IN THE QCD PHASE DIAGRAM VII

CUNY ADVANCED SCIENCE RESEARCH CENTER  
NEW YORK, USA, 13. JUNE 2018

MATTHIAS HANAUSKE, KENTARO TAKAMI, LUKE BOVARD, JOSE FONT, FILIPPO GALEAZZI, JENS PAPENFORT, LUKAS WEIH, ELIAS MOST, FEDERICO GUERCILENA, ZEKIYE SIMAY YILMAZ, CHRISTINA MITROPOULOS, JAN STEINHEIMER, STEFAN SCHRAMM, VERONICA DEXHEIMER, DAVID BLASCHKE, MARK ALFORD, KAI SCHWENZER, ANDREAS ZACCHI, JÜRGEN SCHAFFNER-BIELICH, LAURA TOLOS, GLORIA MONTANA, MICHAEL RATTAY, HORST STÖCKER AND LUCIANO REZZOLLA

FRANKFURT INSTITUTE FOR ADVANCED STUDIES  
JOHANN WOLFGANG GOETHE UNIVERSITÄT  
INSTITUT FÜR THEORETISCHE PHYSIK  
ARBEITSGRUPPE RELATIVISTISCHE ASTROPHYSIK  
D-60438 FRANKFURT AM MAIN

# Content

- GW170817 - The long-awaited event
  - Constraining the EOS using data from GW170817
- Hypermassive neutron stars and the QCD phase diagram
  - Neutron star mergers and the EOS of elementary matter
  - The hadron-quark phase transition and the neutron star merger product
- Detecting the hadron-quark phase transition with gravitational waves
  - The twin star collapse
  - Rotational behavior of deconfined quark matter
- Summary and Outlook

# The long-awaited event GW170817

	Low-spin priors ( $ \chi  \leq 0.05$ )	High-spin priors ( $ \chi  \leq 0.89$ )
Primary mass $m_1$	$1.36-1.60 M_\odot$	$1.36-2.26 M_\odot$
Secondary mass $m_2$	$1.17-1.36 M_\odot$	$0.86-1.36 M_\odot$
Chirp mass $\mathcal{M}$	$1.188^{+0.004}_{-0.002} M_\odot$	$1.188^{+0.004}_{-0.002} M_\odot$
Mass ratio $m_2/m_1$	$0.7-1.0$	$0.4-1.0$
Total mass $m_{\text{tot}}$	$2.74^{+0.04}_{-0.01} M_\odot$	$2.82^{+0.47}_{-0.09} M_\odot$
Radiated energy $E_{\text{rad}}$	$> 0.025 M_\odot c^2$	$> 0.025 M_\odot c^2$
Luminosity distance $D_L$	$40^{+8}_{-14}$ Mpc	$40^{+8}_{-14}$ Mpc
Viewing angle $\Theta$	$\leq 56^\circ$	$\leq 56^\circ$
Using NGC 4993 location	$\leq 28^\circ$	$\leq 28^\circ$
Combined dimensionless tidal deformability $\tilde{\Lambda}$	$\leq 800$	$\leq 700$
Dimensionless tidal deformability $\Lambda(1.4M_\odot)$	$\leq 800$	$\leq 1400$

# GW170817: Constraining the Neutron Star Radius and EOS

Talk by Bangalore Sathyaprakash and James Lattimer

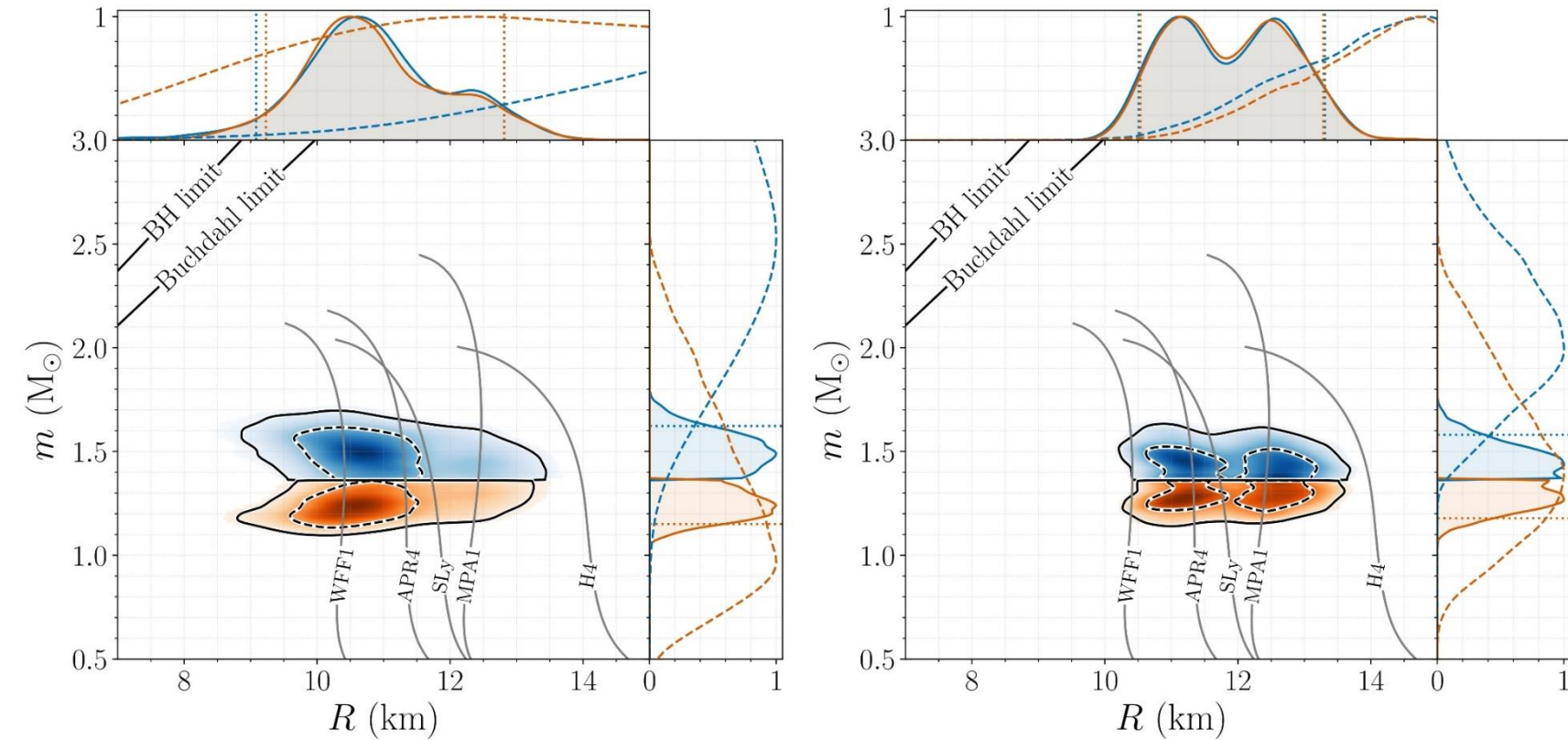


FIG. 3. Marginalized posterior for the mass  $m$  and areal radius  $R$  of each binary component using EOS-insensitive relations (left panel) and a parametrized EOS where we impose a lower limit on the maximum mass of  $1.97 M_{\odot}$  (right panel). The top blue (bottom orange) posterior corresponds to the heavier (lighter) NS. Example mass-radius curves for selected EOSs are overplotted in grey. The lines in the top left denote the Schwarzschild BH ( $R = 2m$ ) and Buchdahl ( $R = 9m/4$ ) limits. In the one-dimensional plots, solid lines are used for the posteriors, while dashed lines are used for the corresponding parameter priors. Dotted vertical lines are used for the bounds of the 90% credible intervals.

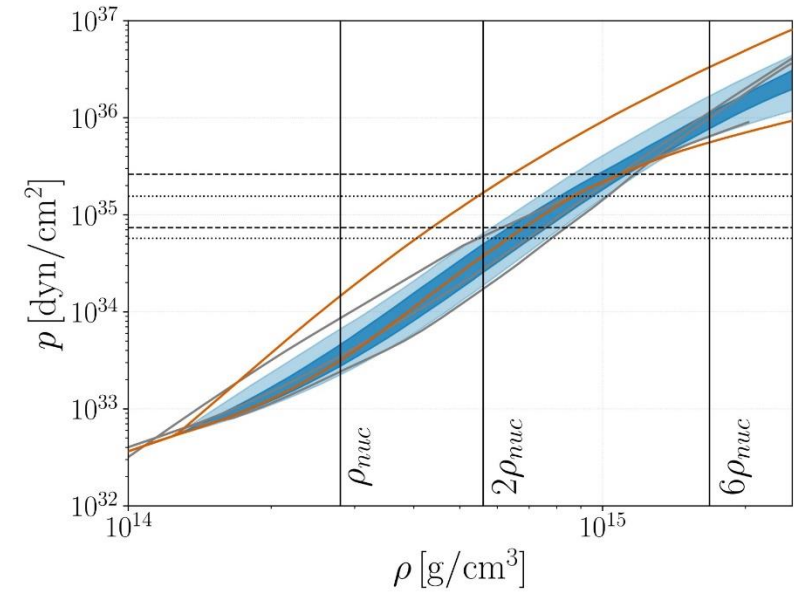
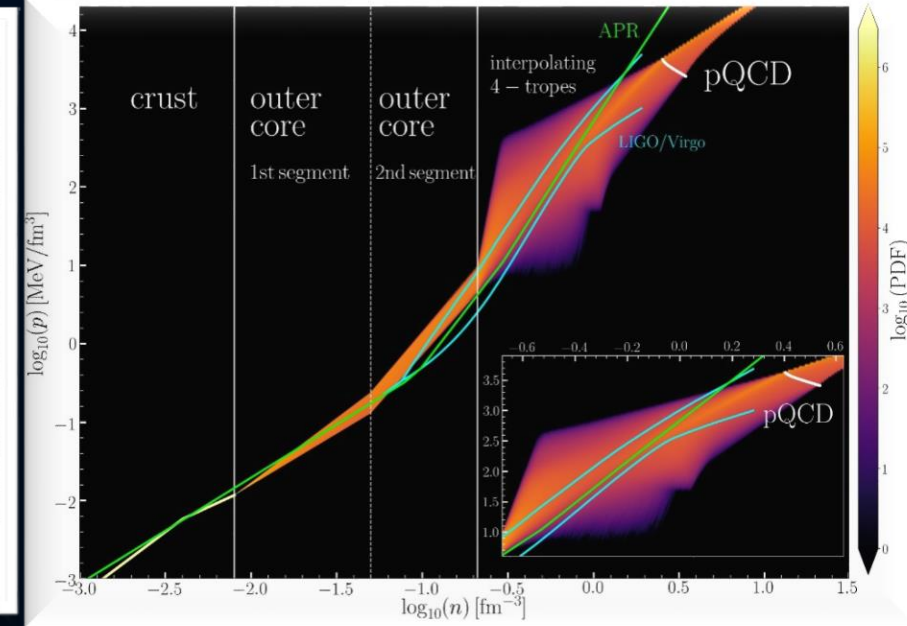
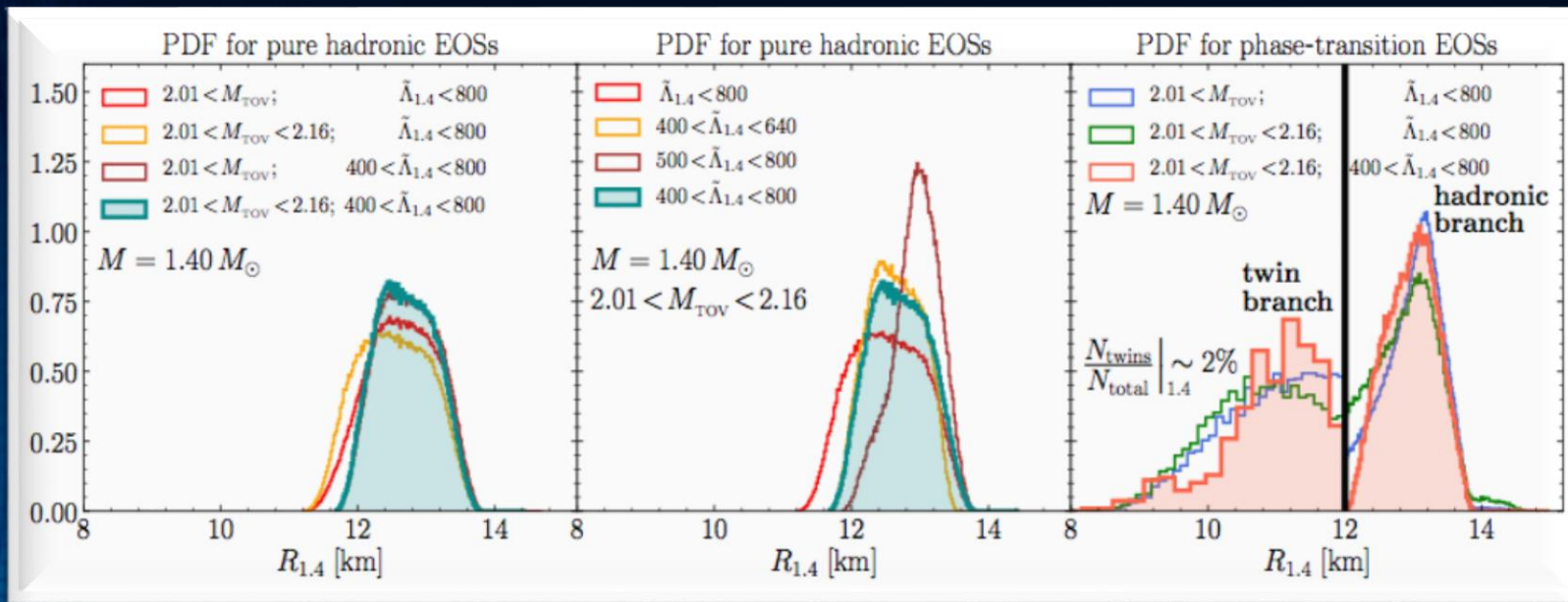


FIG. 2. Marginalized posterior (blue) and prior (orange) for the pressure  $p$  as a function of the rest-mass density  $\rho$  of the NS interior using the spectral EOS parametrization and imposing a lower limit on the maximum NS mass supported by the EOS of  $1.97 M_{\odot}$ . The dark (light) blue shaded region corresponds to the 50% (90%) posterior credible level and the orange lines show the 90% prior credible interval. Horizontal lines denote the 90% credible interval for the central pressure of the heavier (dashed) and the lighter (dotted) binary components. Vertical lines correspond to once, twice, and six times the nuclear saturation density. Overplotted in grey are representative EOS models [121, 122, 124], using data taken from [19]; from top to bottom at  $2\rho_{\text{nuc}}$  we show H4, APR4, and WFF1.

# GW170817: Constraining the Neutron Star Radius

## Impact of Phase Transitions



$$12.00 < R_{1.4}/\text{km} < 13.45 \quad \bar{R}_{1.4} = 12.45 \text{ km}$$

EOSs without phase transitions

$$8.53 < R_{1.4}/\text{km} < 13.74 \quad \bar{R}_{1.4} = 13.06 \text{ km}$$

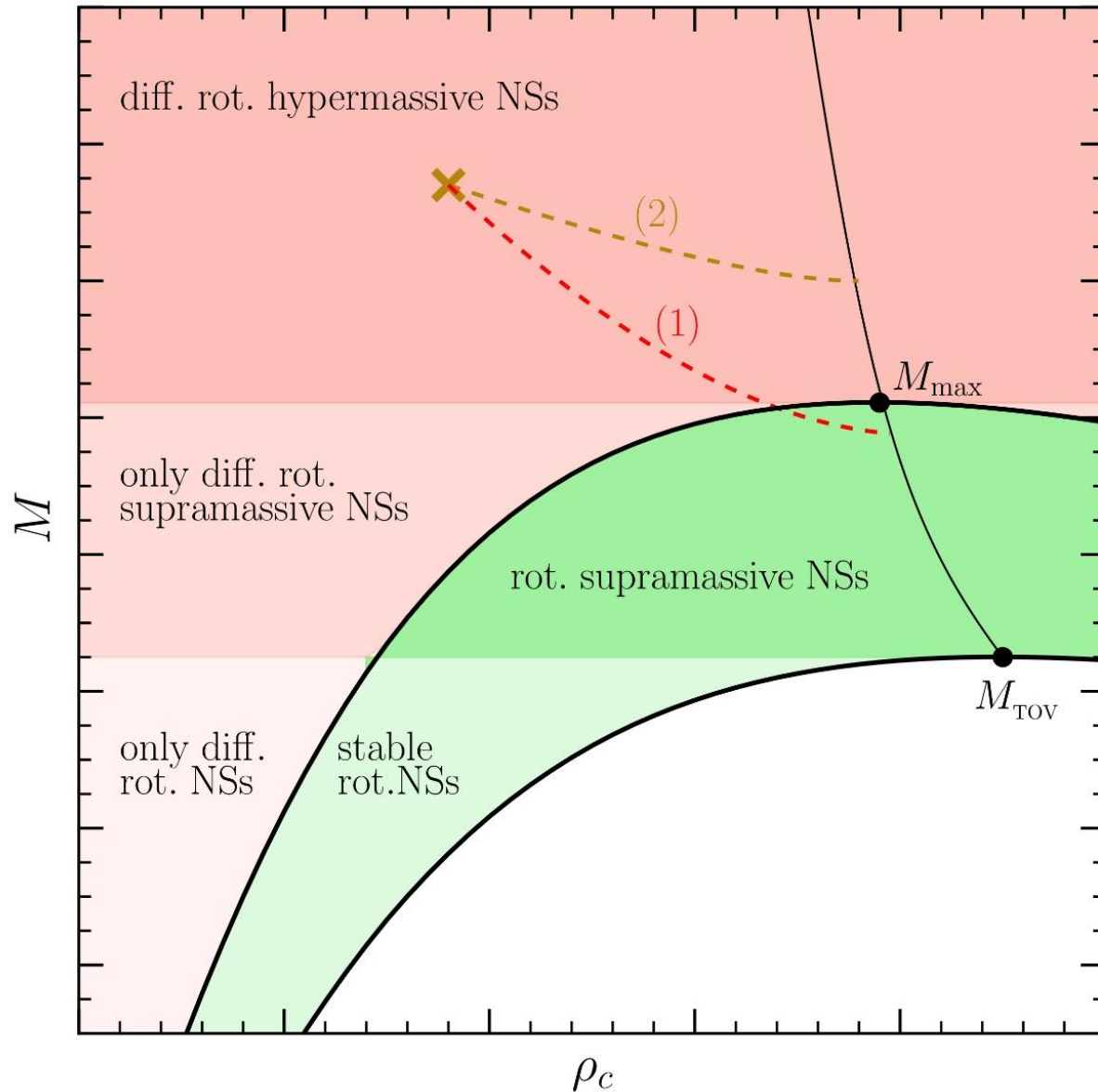
EOSs with phase transitions

E. Most, L. Weih, L. Rezzolla, J. Schaffner-Bielich "New constraints on radii and tidal deformabilities of neutron stars from GW170817", arXiv:1803.00549, (accepted in PRL)

See also: De, Finstad, Lattimer, Brown, Berger, Bower, (2018), arXiv:1804.08583 ; Bauswein, Just, Janka, N. Stergioulas, APJL 850, L34 (2017) ; Fattoyev, Piekarewicz, Horowitz, PRL 120, 172702 (2018) ; Nandi & Char, Astrophys. J. 857, 12 (2018) ; Paschalidis, Yagi, Alvarez-Castillo, Blaschke, Sedrakian, PRD 97, 084038 ; Ruiz, Shapiro, Tsokaros, PRD 97, 021501 (2018) ; Annala, Gorda, Kurkela, Vuorinen, PRL 120, 172703 (2018) ; Raithel, Özel, Psaltis, (2018) arXiv:1803.07687

# GW170817: Constraining the maximum mass of Neutron Stars

Talk by Cole Miller



The highly differentially rotating hypermassive/supramassive neutron star will spin down and redistribute its angular momentum (e.g. due to viscosity effects, magnetic braking). After  $\sim 1$  second it will cross the stability line as a uniformly rotating supramassive neutron star (close to  $M_{\max}$ ) and collapse to a black hole. Parts of the ejected matter will fall back into the black hole producing the gamma-ray burst.

L.Rezzolla, E.Most, L.Weih, "Using Gravitational Wave Observations and Quasi-Universal Relations to constrain the maximum Mass of Neutron Stars", *The Astrophysical Journal Letters* 852, L25 (2018):  
 $2.01 \pm 0.04 < M_{\text{TOV}} < 2.16 \pm 0.17$

See also: S.Lawrence et al. ,*APJ*808,186, 2015  
Margalit & Metzger, *The Astrophysical Journal Letters* 850, L19 (2017):  $M_{\text{TOV}} < 2.17$  (90%)  
Zhou, Zhou, Li, *PRD* 97, 083015 (2018)  
Ruiz, Shapiro, Tsokaros, *PRD* 97,021501 (2018)

# Numerical Relativity and Relativistic Hydrodynamics of Binary Neutron Star Mergers

Numerical simulations of a merger of two compact stars are based on a (3+1) decomposition of spacetime of the Einstein and hydrodynamic equations.

$$R_{\mu\nu} - \frac{1}{2}g_{\mu\nu}R = 8\pi T_{\mu\nu}$$

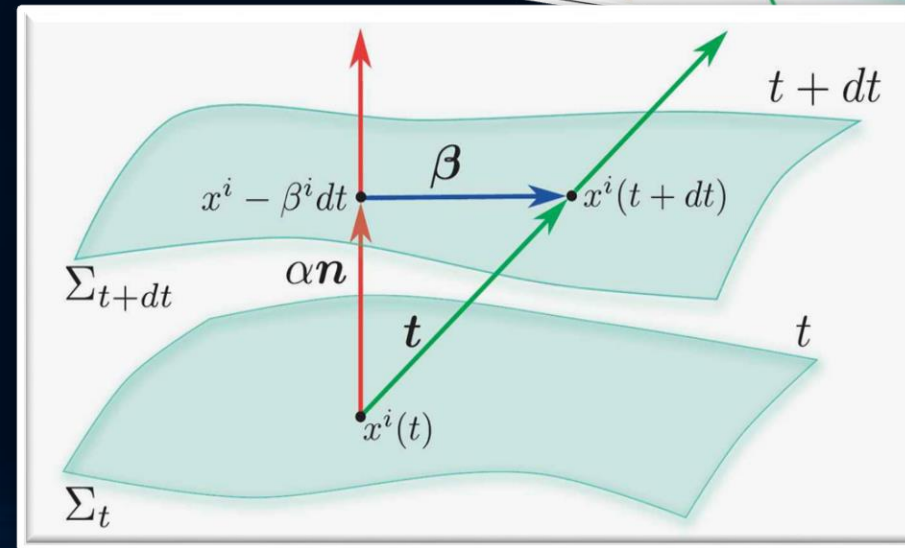
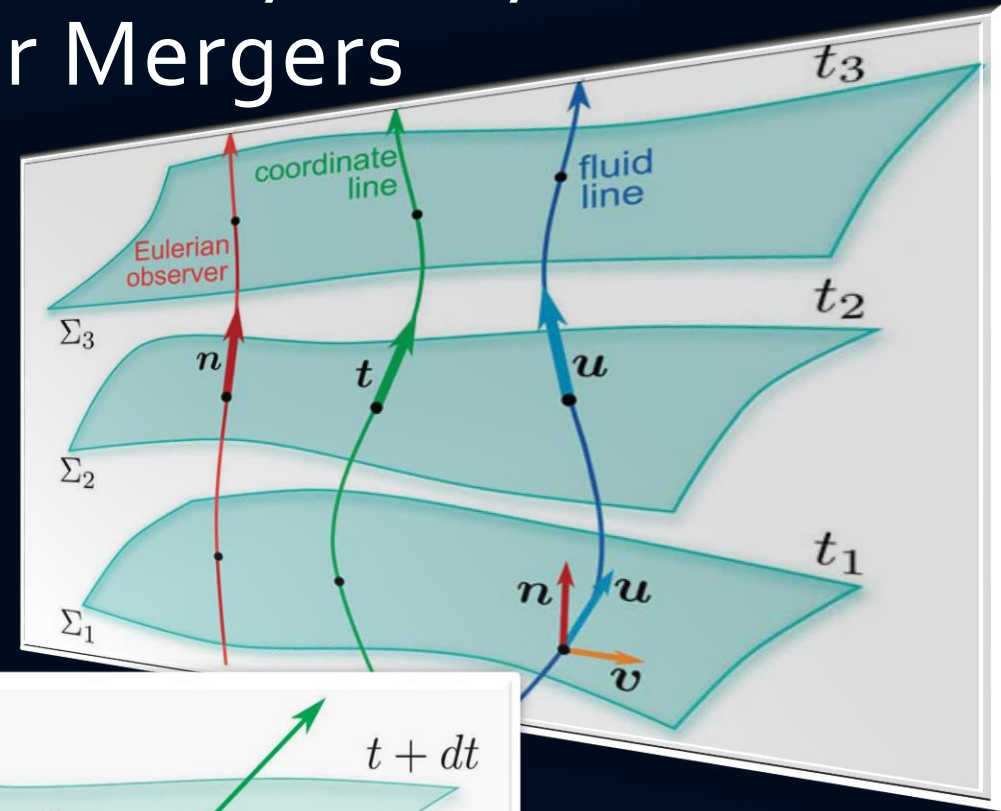
$$\begin{aligned}\nabla_{\mu}(\rho u^{\mu}) &= 0, \\ \nabla_{\nu}T^{\mu\nu} &= 0.\end{aligned}$$

(3+1) decomposition of spacetime

$$g_{\mu\nu} = \begin{pmatrix} -\alpha^2 + \beta_i\beta^i & \beta_i \\ \beta_i & \gamma_{ij} \end{pmatrix}$$

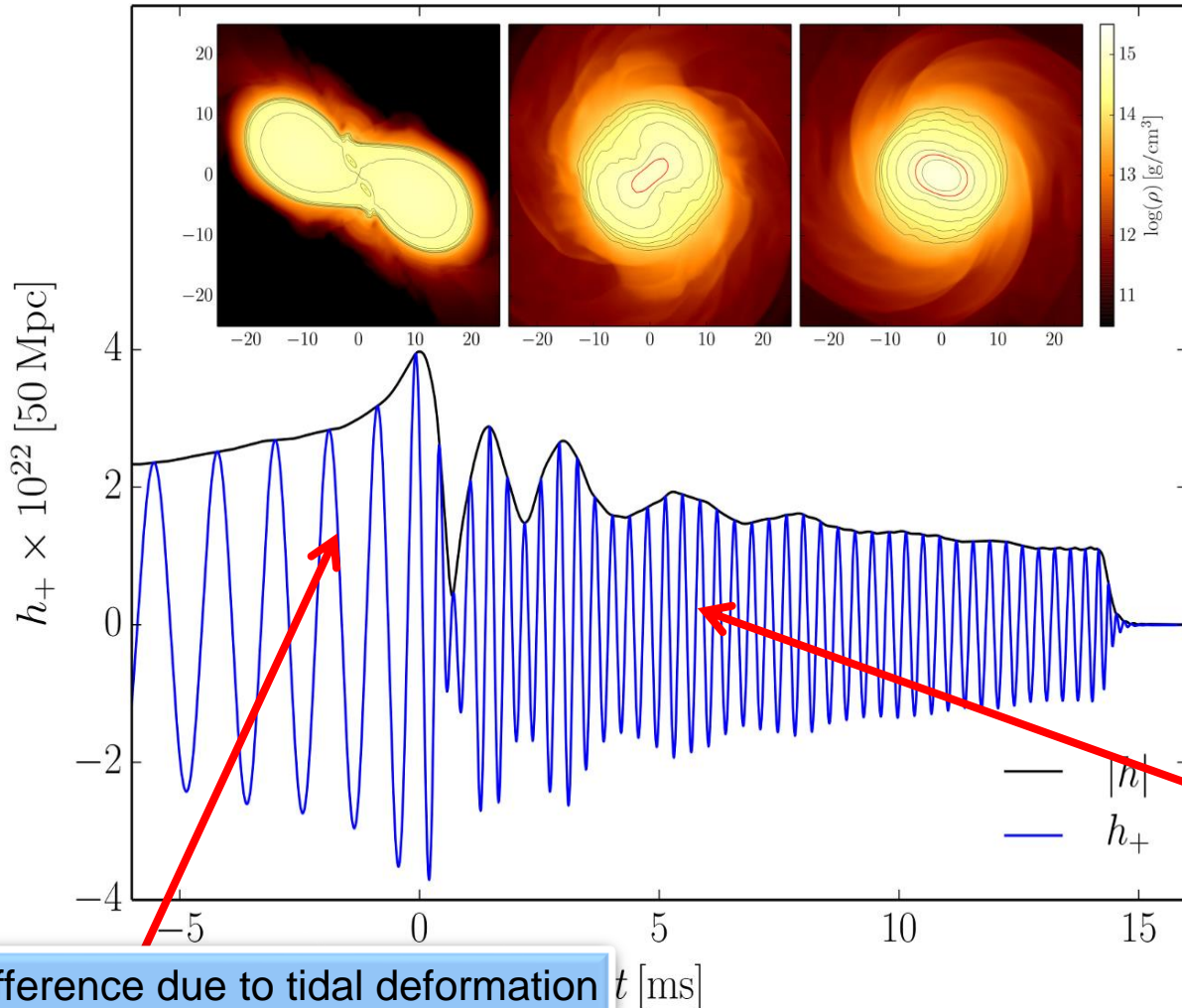
$$d\tau^2 = \alpha^2(t, x^j)dt^2$$

$$x^i_{t+dt} = x^i_t - \beta^i(t, x^j)dt$$



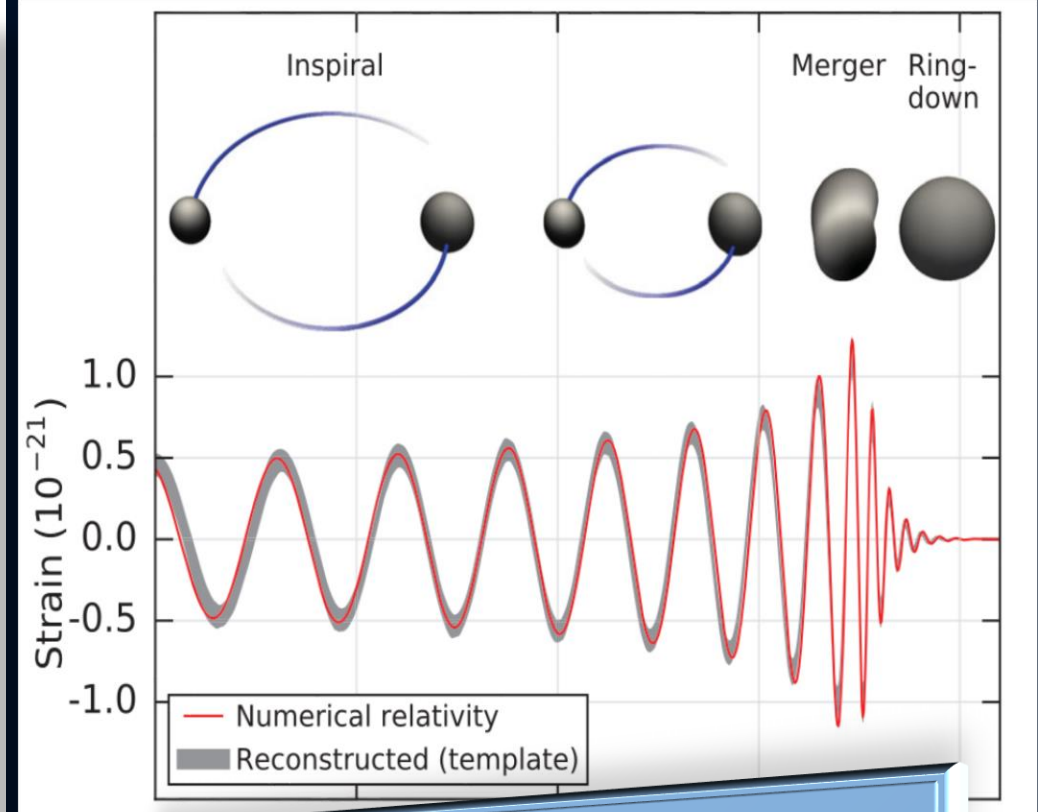
# Gravitational Waves from Neutron Star Mergers

## Neutron Star Collision (Simulation)



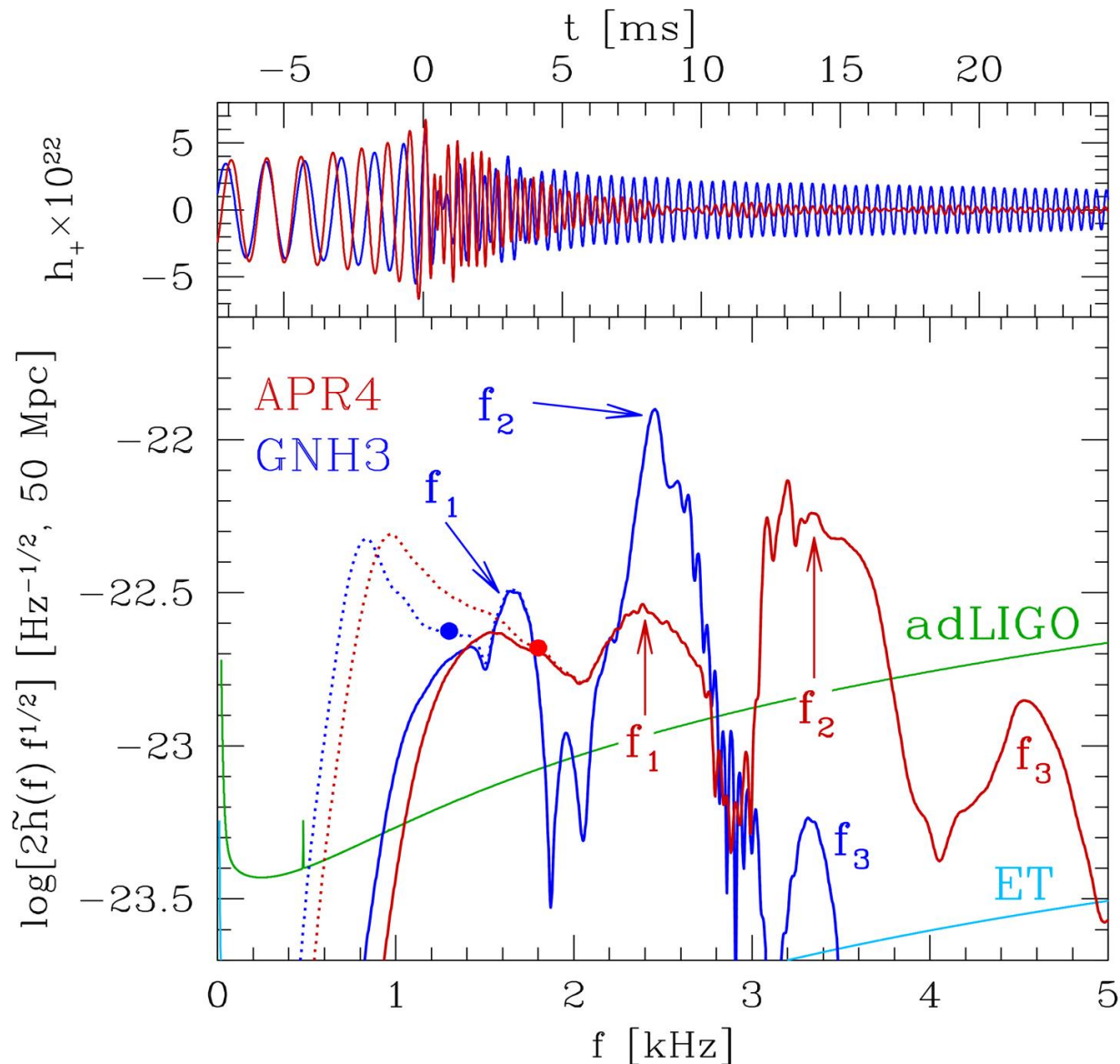
Difference due to tidal deformation in the late inspiral phase

## Collision of two Black Holes GW150914



Main difference:  
In binary neutron star mergers a **Post-Merger Phase** often exists

# GW-Spectrum for different EOSs



See:

Oechslin+2007, Baiotti+2008, Bauswein+ 2011, 2012, Stergioulas+ 2011, Hotokezaka+ 2013, Takami 2014, 2015, Bernuzzi 2014, 2015, Bauswein+ 2015, Clark+ 2016, Rezzolla+2016, de Pietri+ 2016, Feo+ 2017, Bose+ 2017

Kentaro Takami, Luciano Rezzolla, and Luca Baiotti, Physical Review D 91, 064001 (2015)

Hotokezaka, K., Kiuchi, K., Kyutoku, K., Muranushi, T., Sekiguchi, Y. I., Shibata, M., & Taniguchi, K. (2013). Physical Review D, 88(4), 044026.

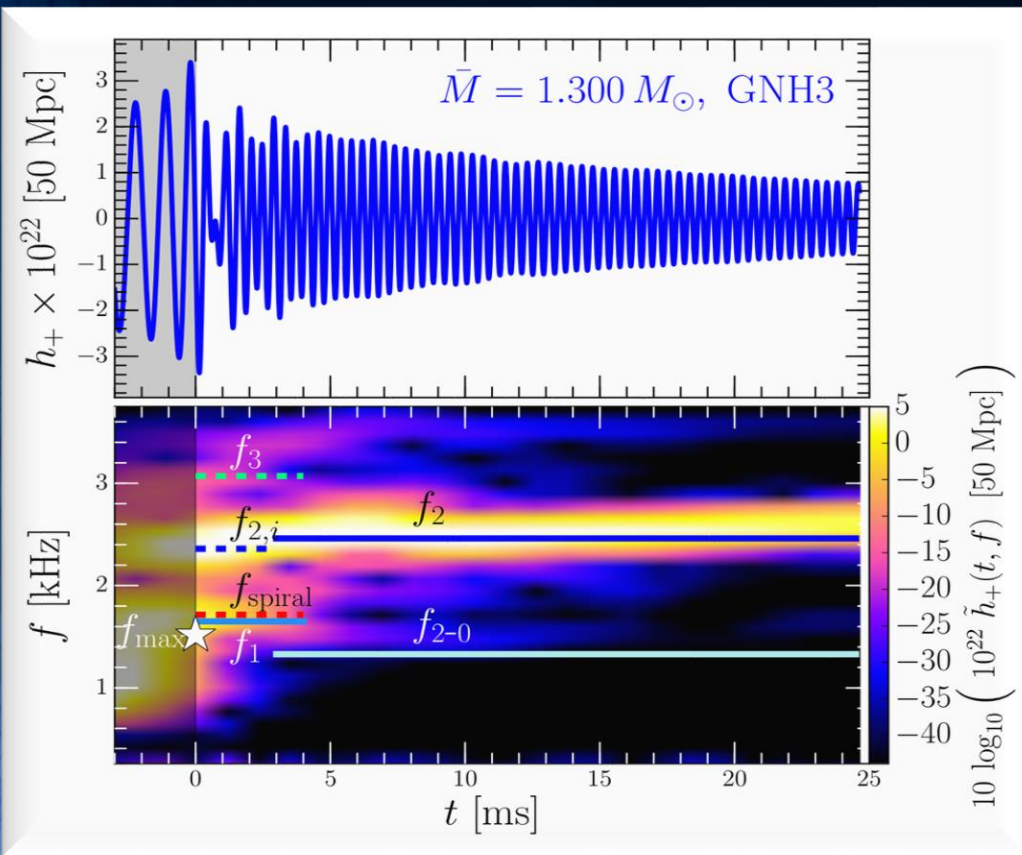
Bauswein, A., & Janka, H. T. (2012). Physical review letters, 108(1), 011101.

Clark, J. A., Bauswein, A., Stergioulas, N., & Shoemaker, D. (2015). arXiv:1509.08522.

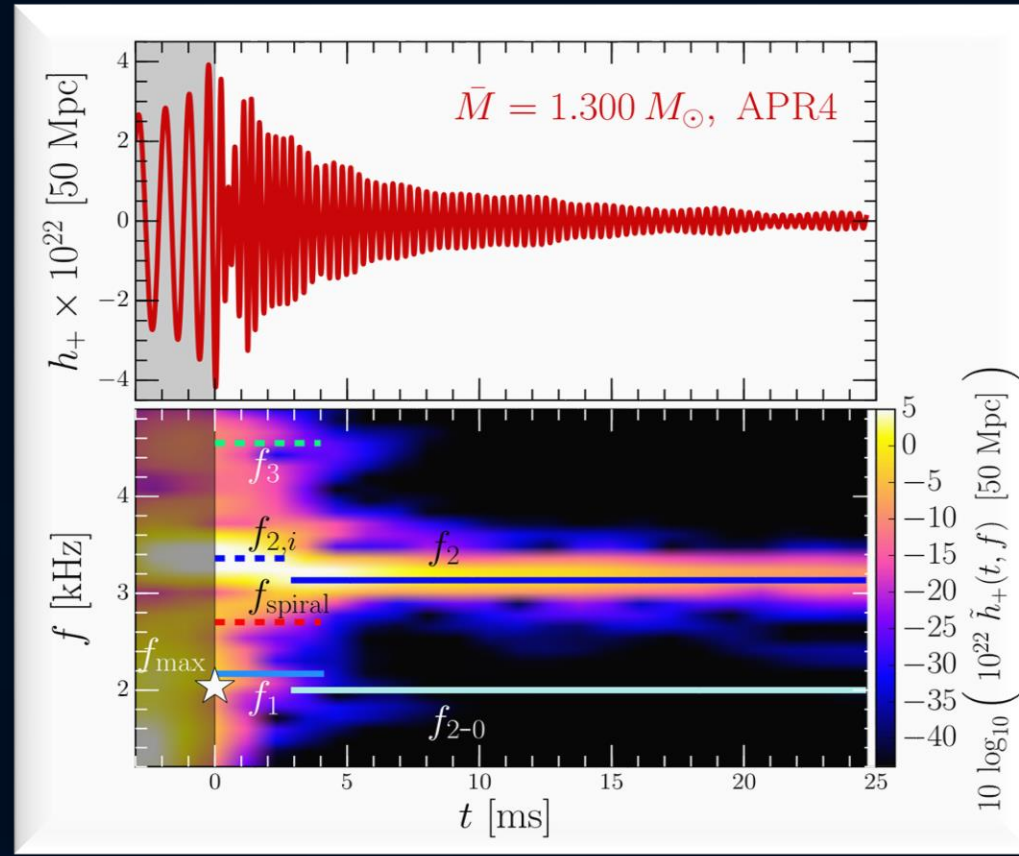
Bernuzzi, S., Dietrich, T., & Nagar, A. (2015). Physical review letters, 115(9), 091101.

# Time Evolution of the GW-Spectrum

The power spectral density profile of the post-merger emission is characterized by several distinct frequencies. After approximately 5 ms after merger, the only remaining dominant frequency is the  $f_2$ -frequency (see e.g. L.Rezzolla and K.Takami, PRD, 93(12), 124051 (2016))



Stiff EOS



Soft EOS

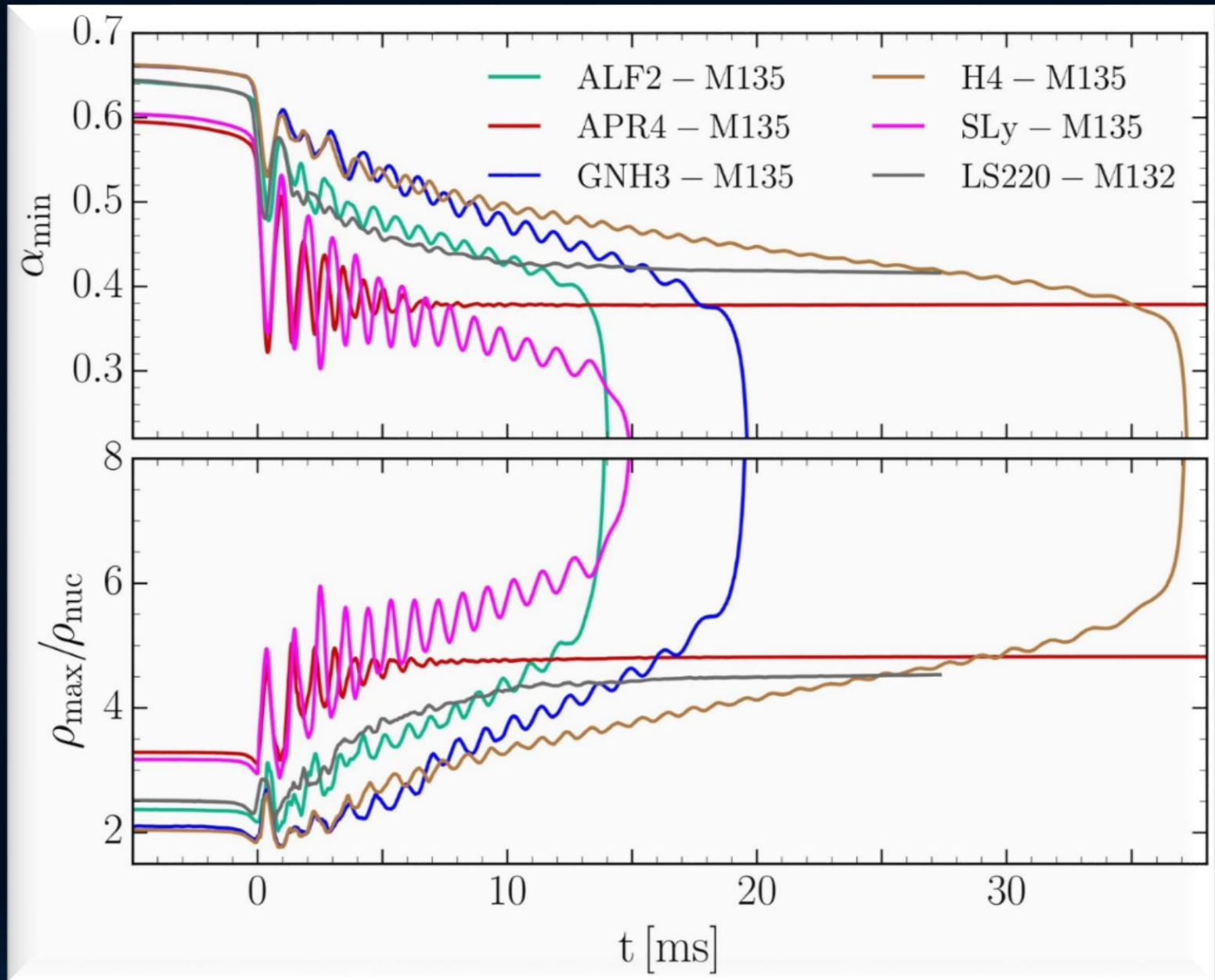
Unfortunately, due to the low sensitivity at high gravitational wave frequencies, no post-merger signal has been found in GW170817.

But advanced detectors / next-generation detectors might be able to detect!!?

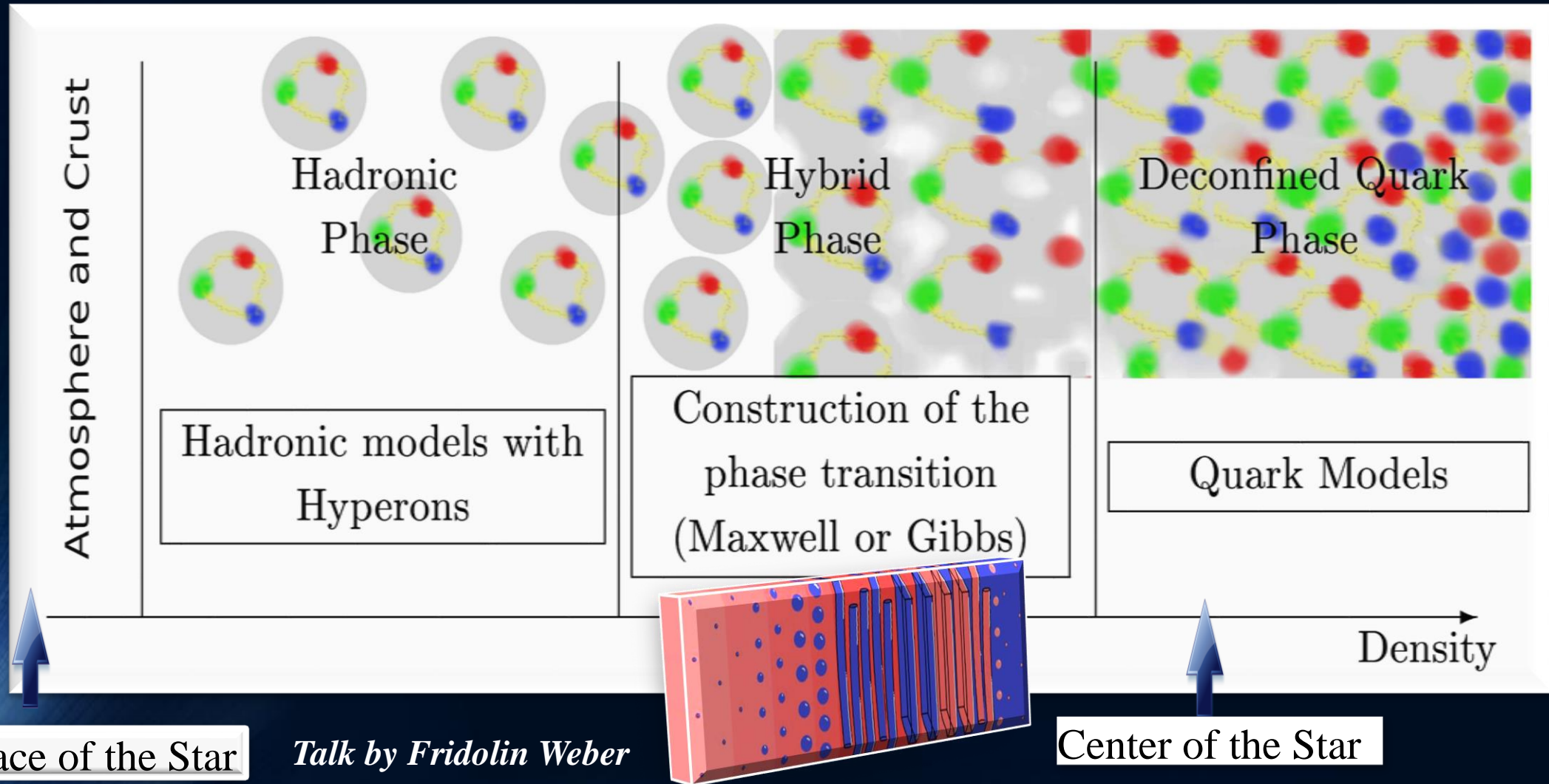
# Binary Merger of two Neutron Stars for different EoSs

High mass simulations  
( $M=1.35 M_{\text{solar}}$ )

Central value of the lapse function  $\alpha_c$  (upper panel) and maximum of the rest mass density  $\rho_{\text{max}}$  in units of  $\rho_0$  (lower panel) versus time for the high mass simulations.



# The QCD – Phase Transition and the Interior of a Hybrid Star

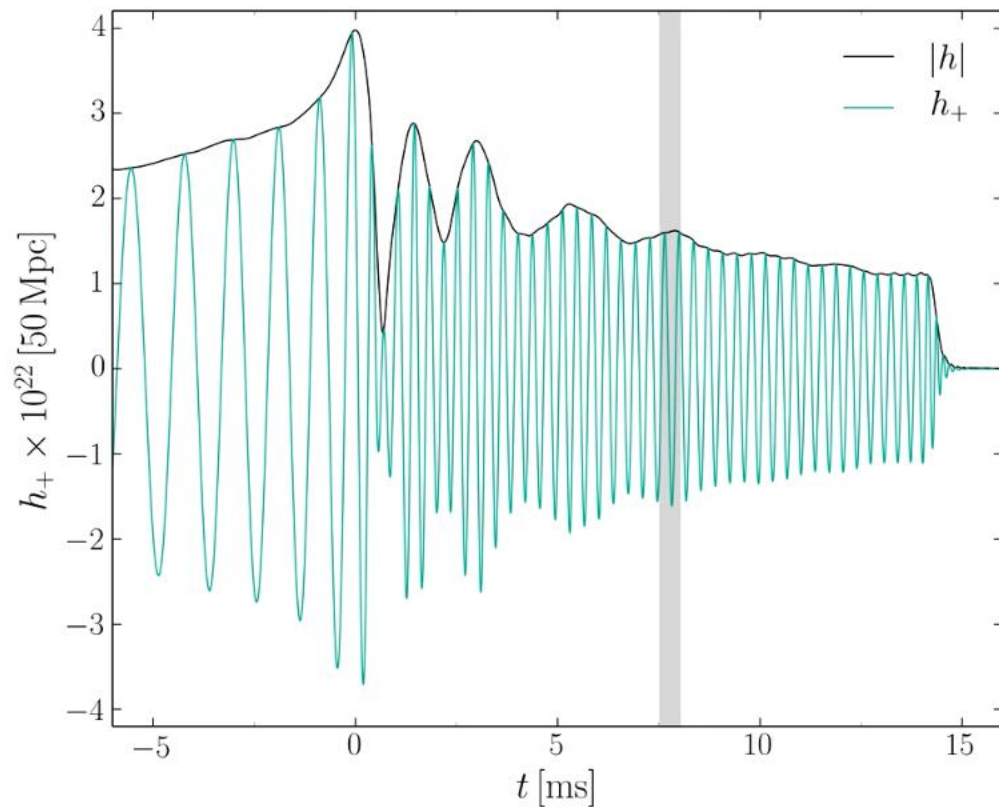


*Matthias Hanauske; Doctoral Thesis:*

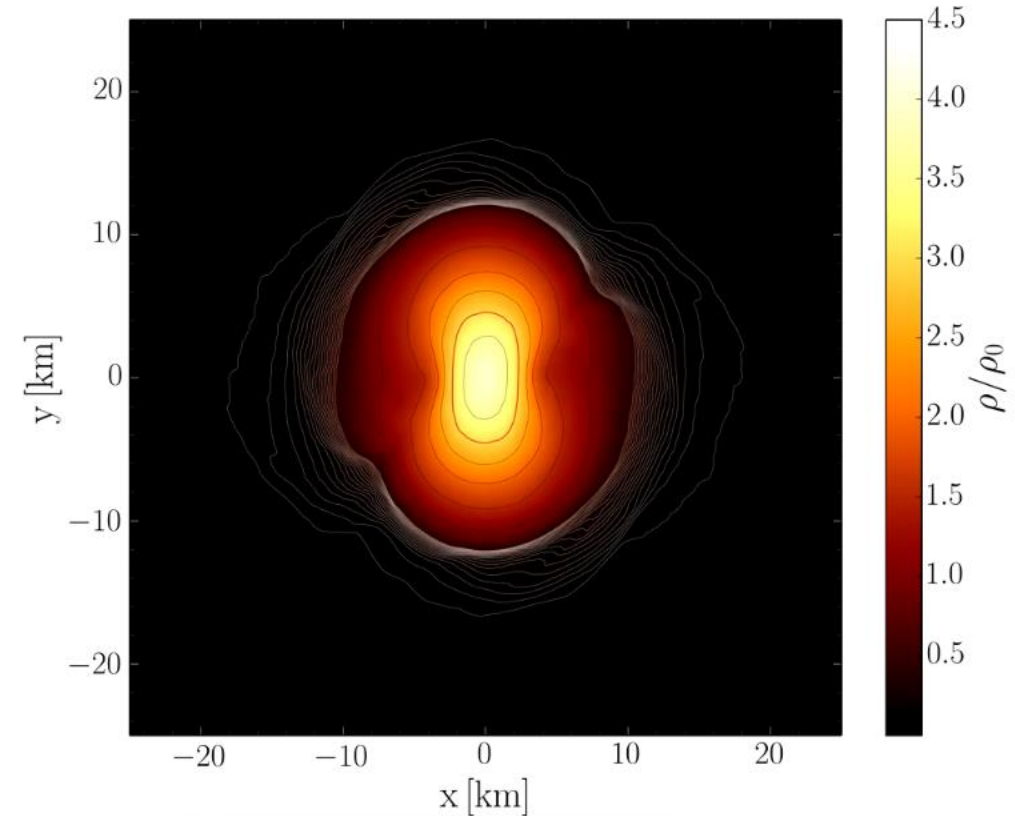
*Properties of Compact Stars within QCD-motivated Models; University Library Publication Frankfurt (2004)*

# Evolution of the density in the post merger phase

ALF2-EOS: Mixed phase region starts at  $3\rho_0$  (see red curve), initial NS mass:  $1.35 M_{\text{solar}}$

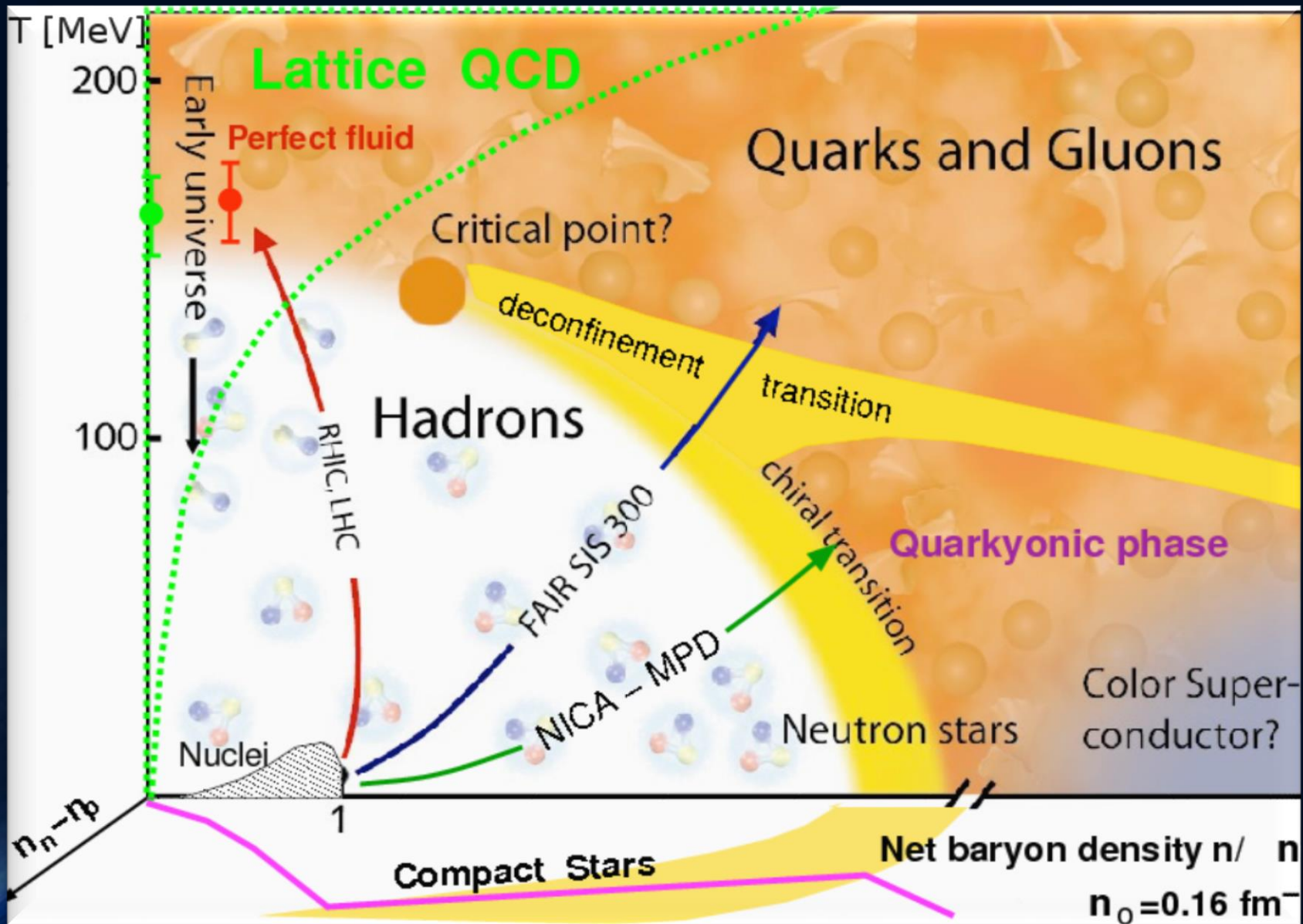


Gravitational wave amplitude  
at a distance of 50 Mpc



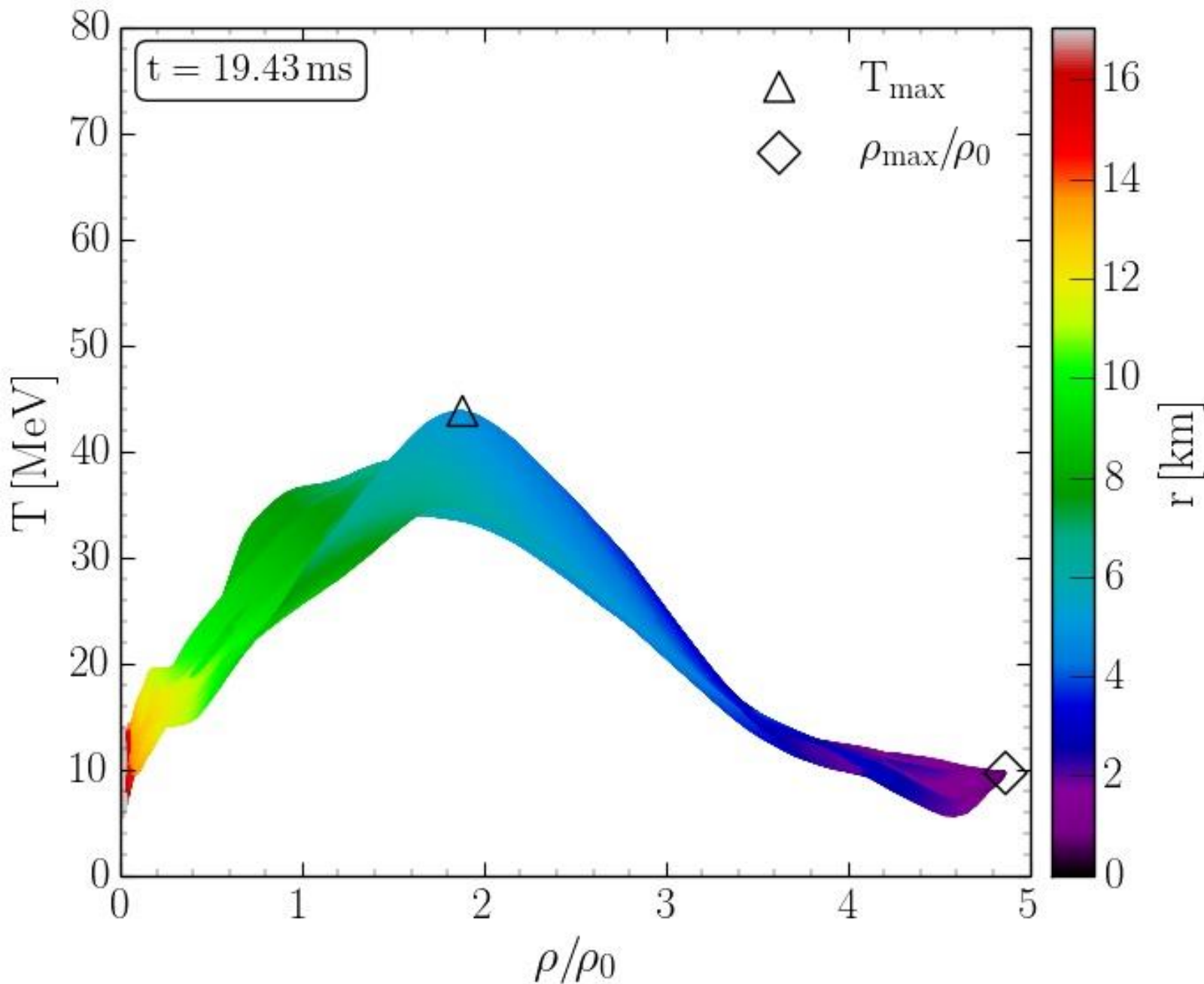
Rest mass density distribution  $\rho(x,y)$   
in the equatorial plane  
in units of the nuclear matter density  $\rho_0$

# The QCD Phase Diagram



Credits to [http://inspirehep.net/record/823172/files/phd\\_qgp3D\\_quarkyonic2.png](http://inspirehep.net/record/823172/files/phd_qgp3D_quarkyonic2.png)

# Hypermassive Neutron Stars in the QCD Phase Diagram

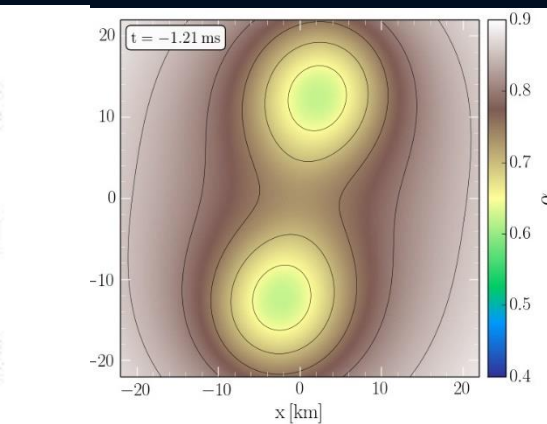
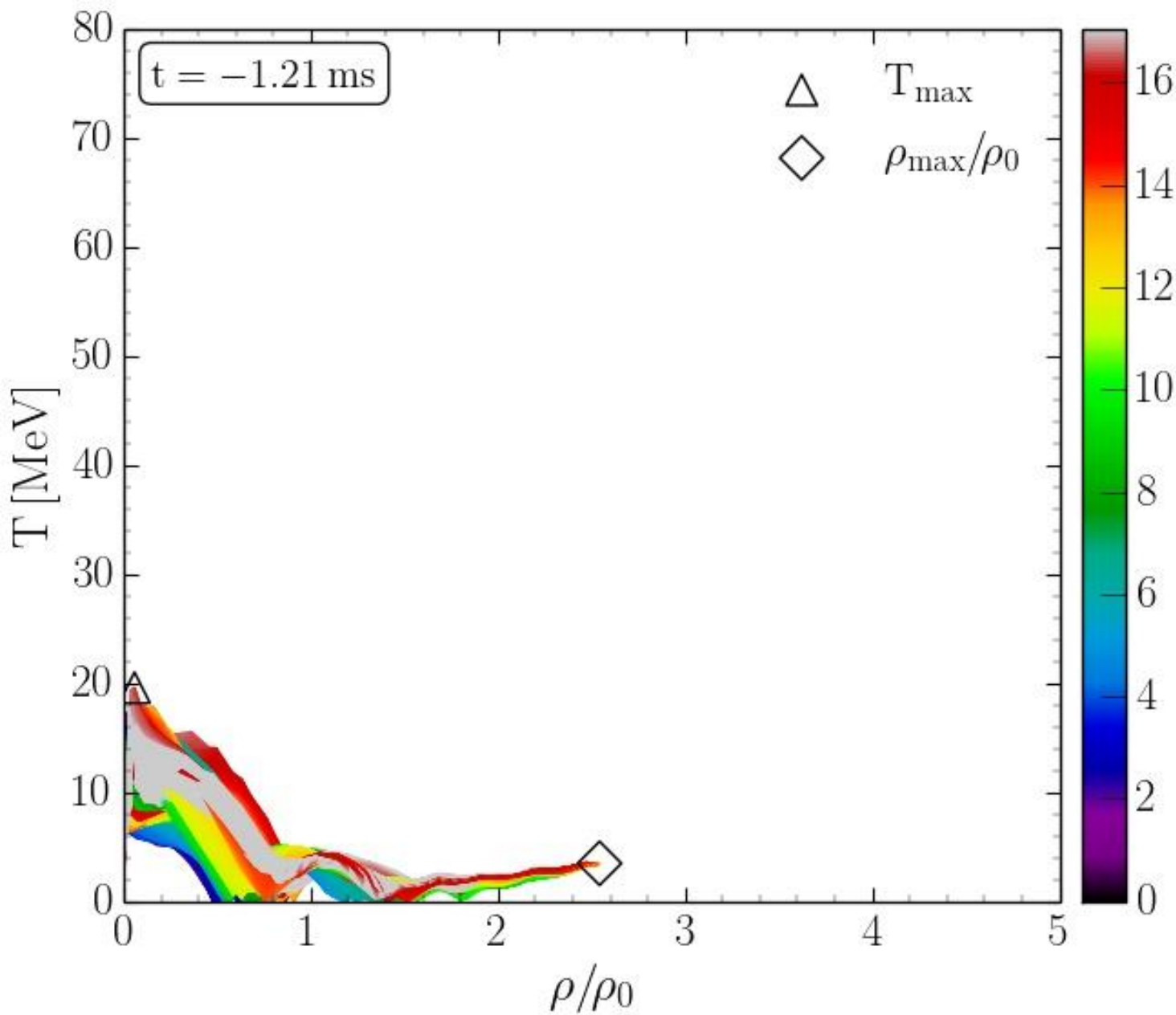


Density-temperature profiles inside the inner area of a hypermassive neutron star simulated within the LS220 EOS (☺ see talk by J.Lattimer) with a total mass of  $M_{\text{total}} = 2.7 M_{\text{solar}}$  in the style of a  $(T - \rho)$  QCD phase diagram plot at  $t = 19.43$  ms after the merger.

The color-coding indicates the radial position  $r$  of the corresponding  $(T - \rho)$  fluid element measured from the origin of the simulation  $(x, y) = (0, 0)$  on the equatorial plane at  $z = 0$ .

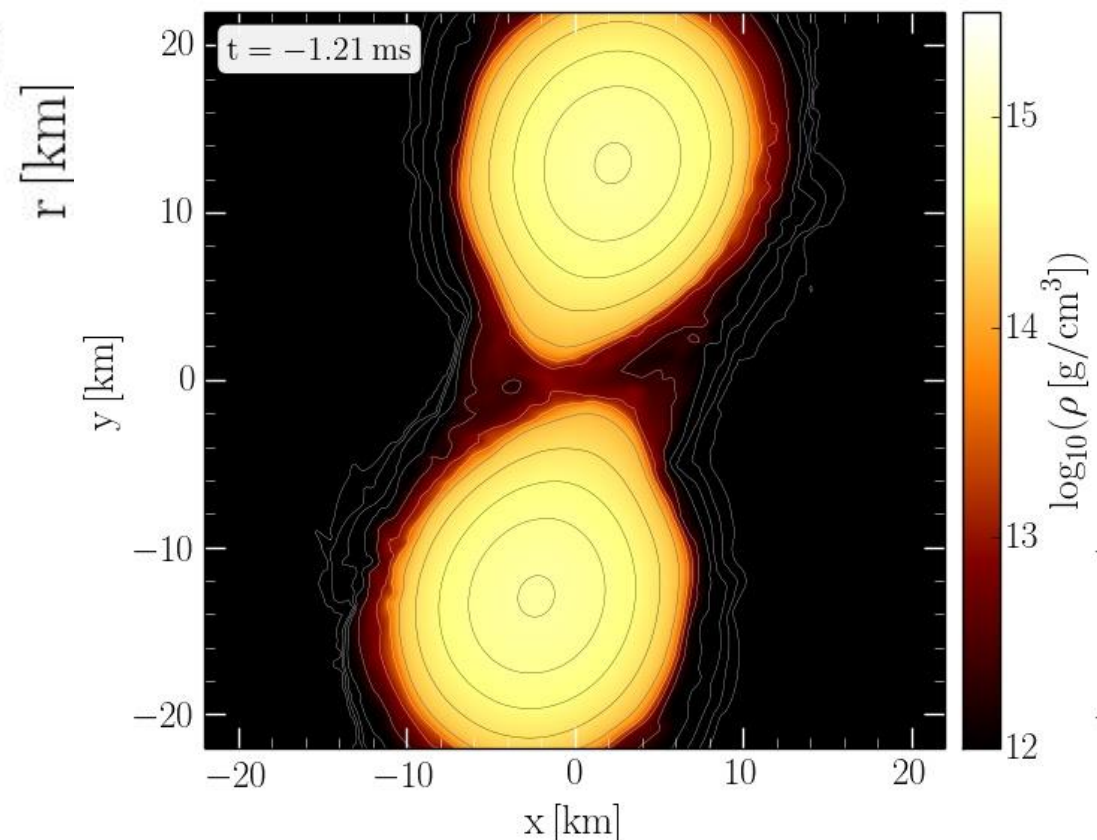
The open triangle marks the maximum value of the temperature while the open diamond indicates the maximum of the density.

# QCD Phase Diagram: The Late Inspiral Phase

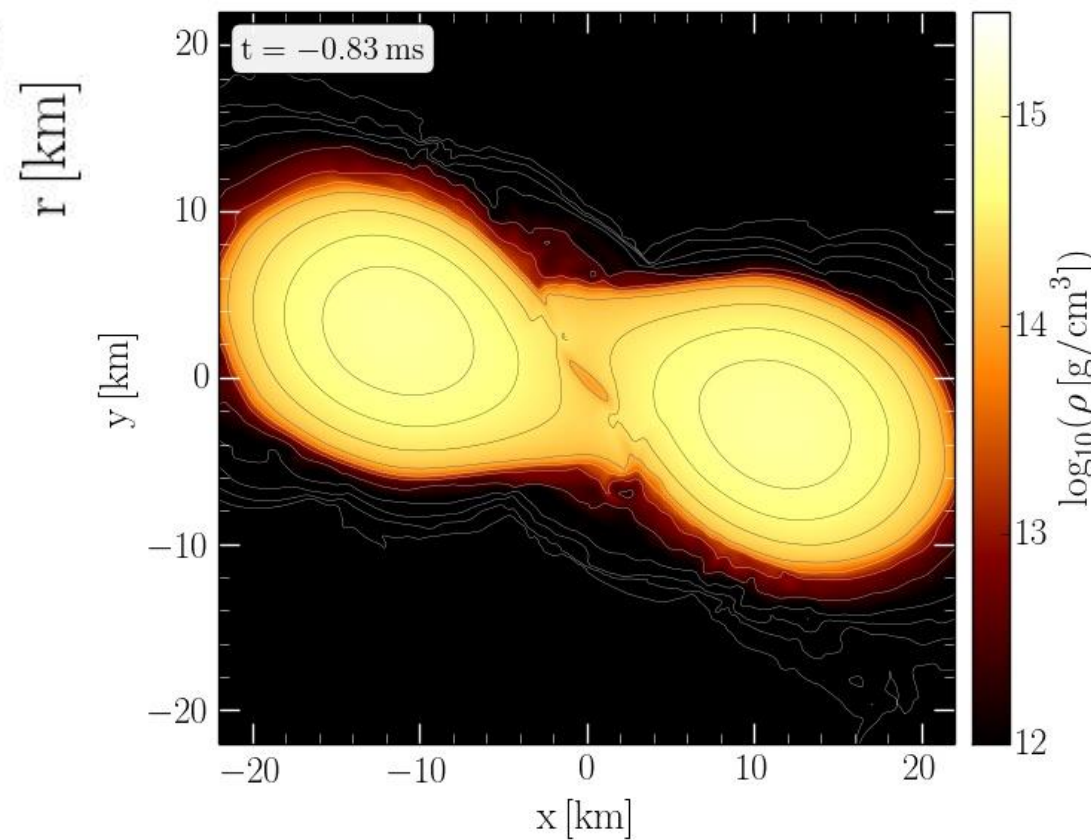
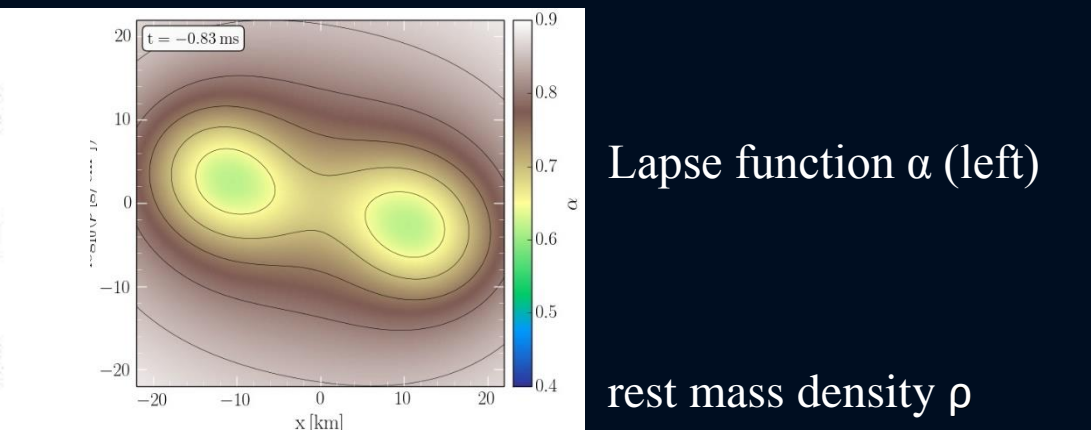
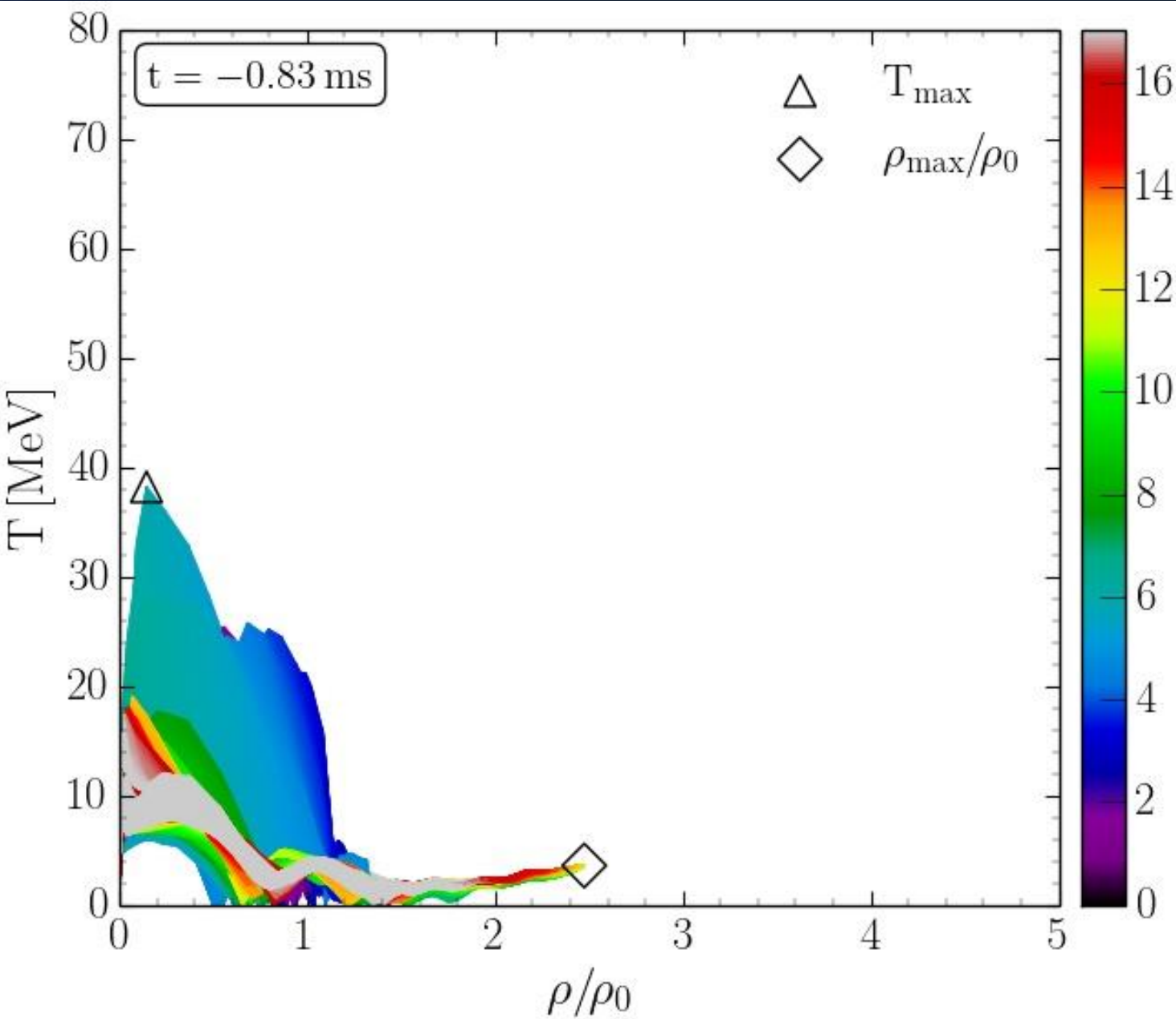


Lapse function  $\alpha$  (left)

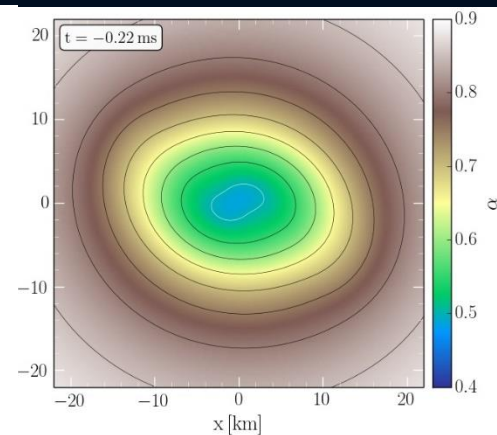
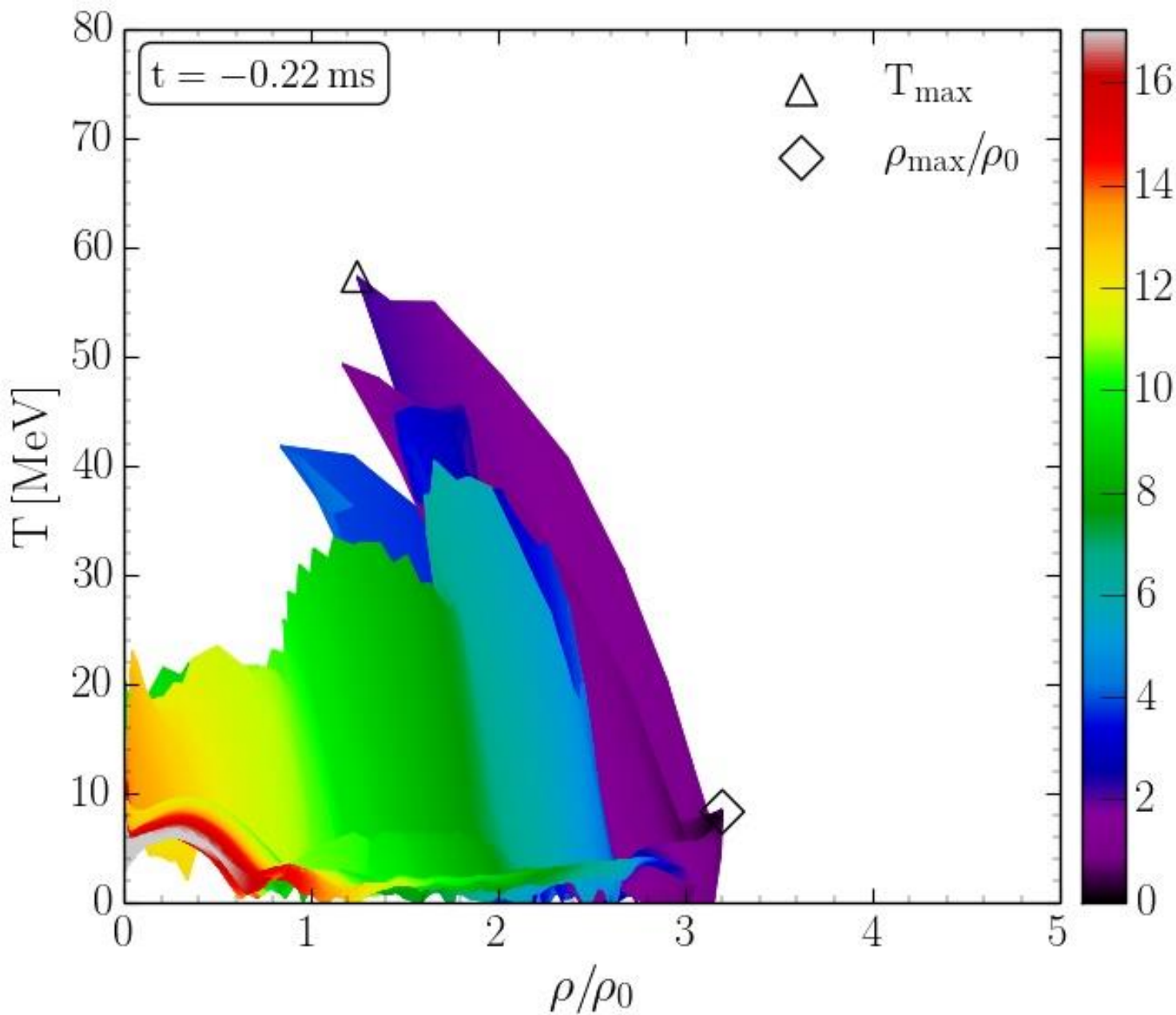
rest mass density  $\rho$



# QCD Phase Diagram: The Late Inspiral Phase

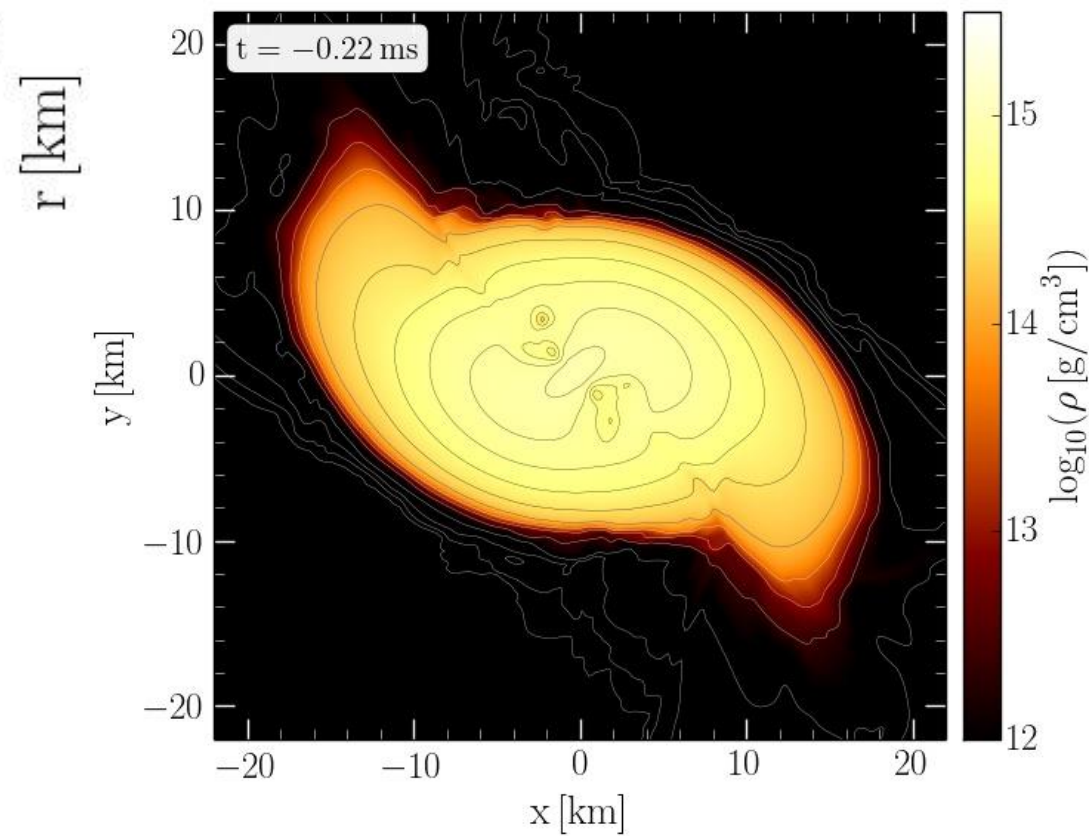


# QCD Phase Diagram: The Late Inspiral Phase

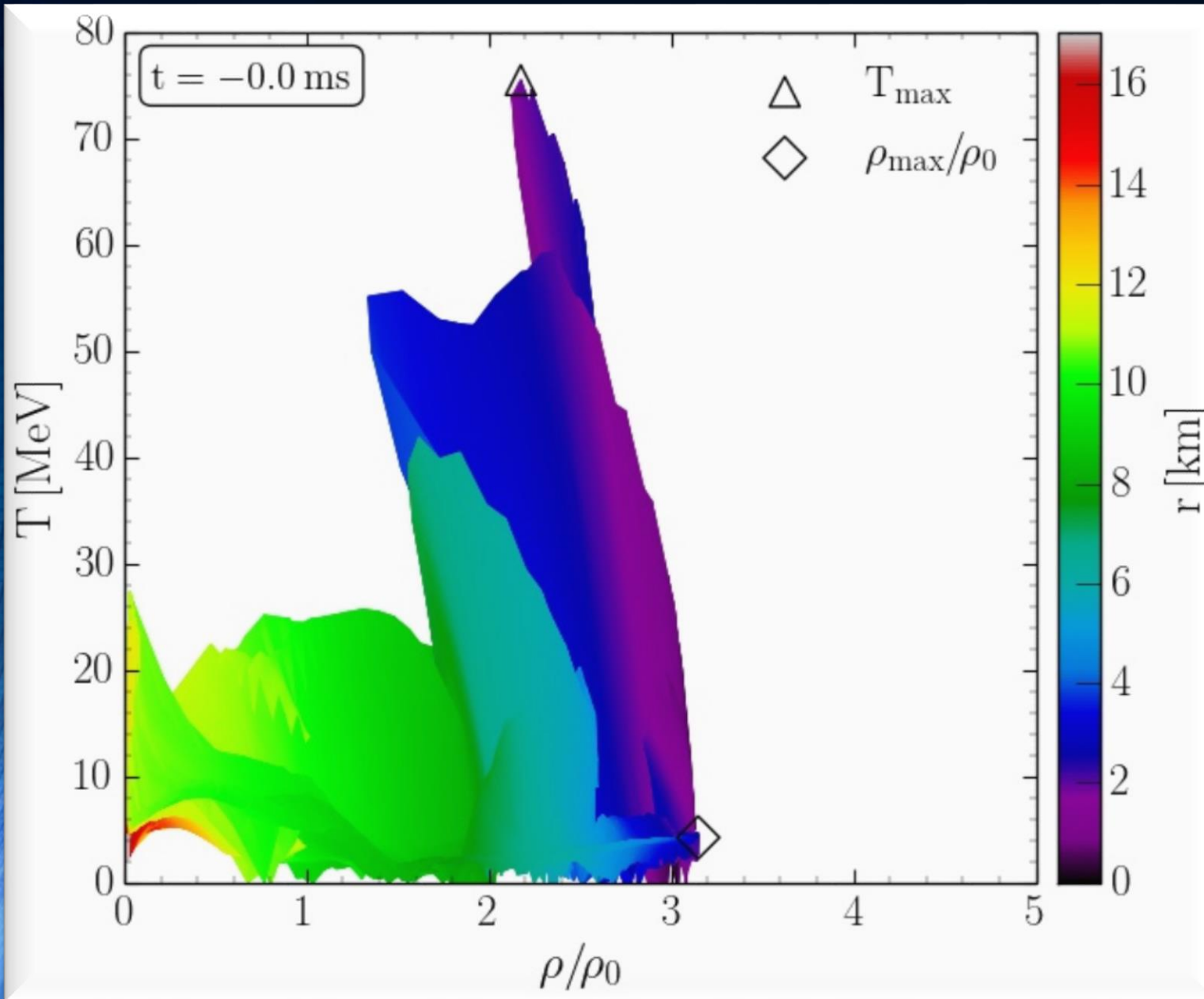


Lapse function  $\alpha$  (left)

rest mass density  $\rho$



# Binary Neutron Star Mergers in the QCD Phase Diagram

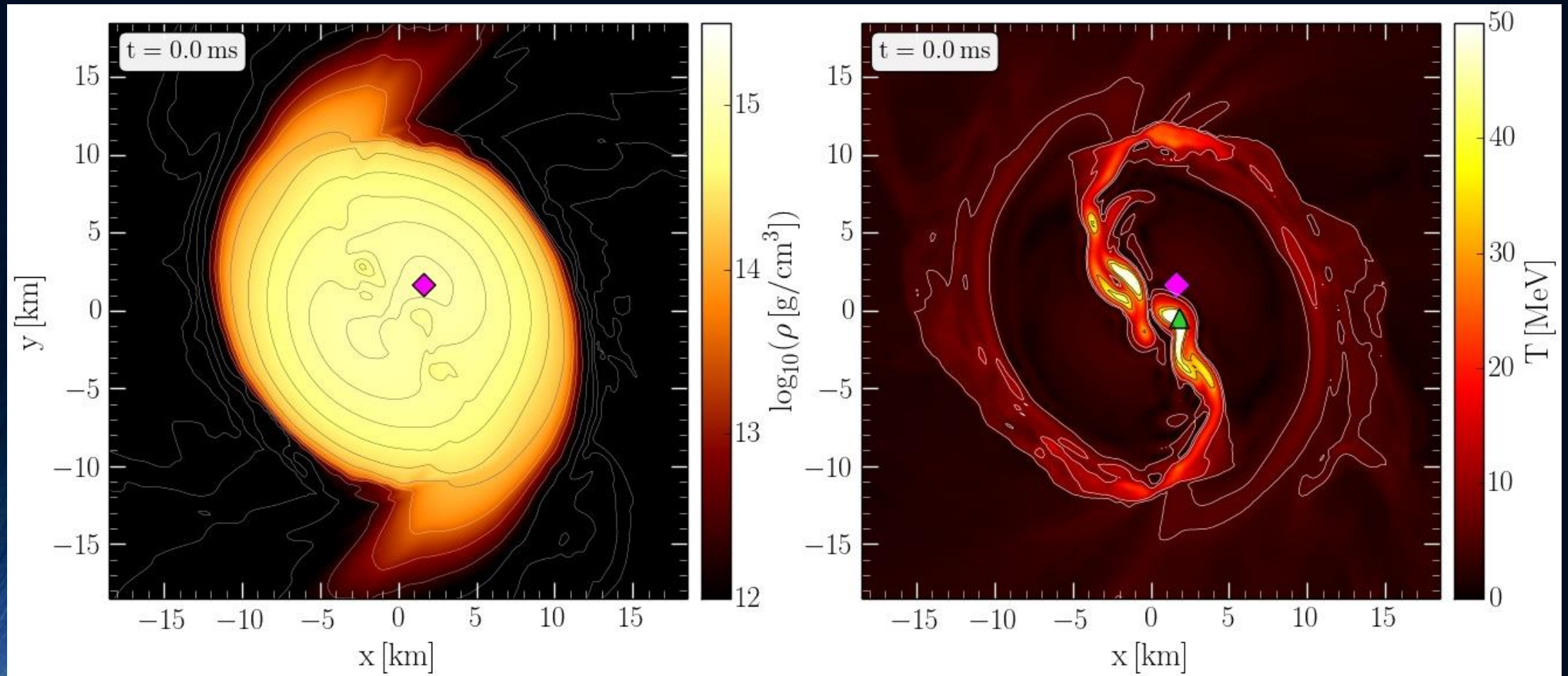


Density-temperature profiles inside the inner area of the LS220-M135 simulation in the style of a  $(T-\rho)$  QCD phase diagram plot at merger time ( $t=0$  ms).

The color-coding indicates the radial position  $r$  of the corresponding  $(T-\rho)$  fluid element measured from the origin of the simulation  $(x,y) = (0,0)$  on the equatorial plane ( $z = 0$ ).

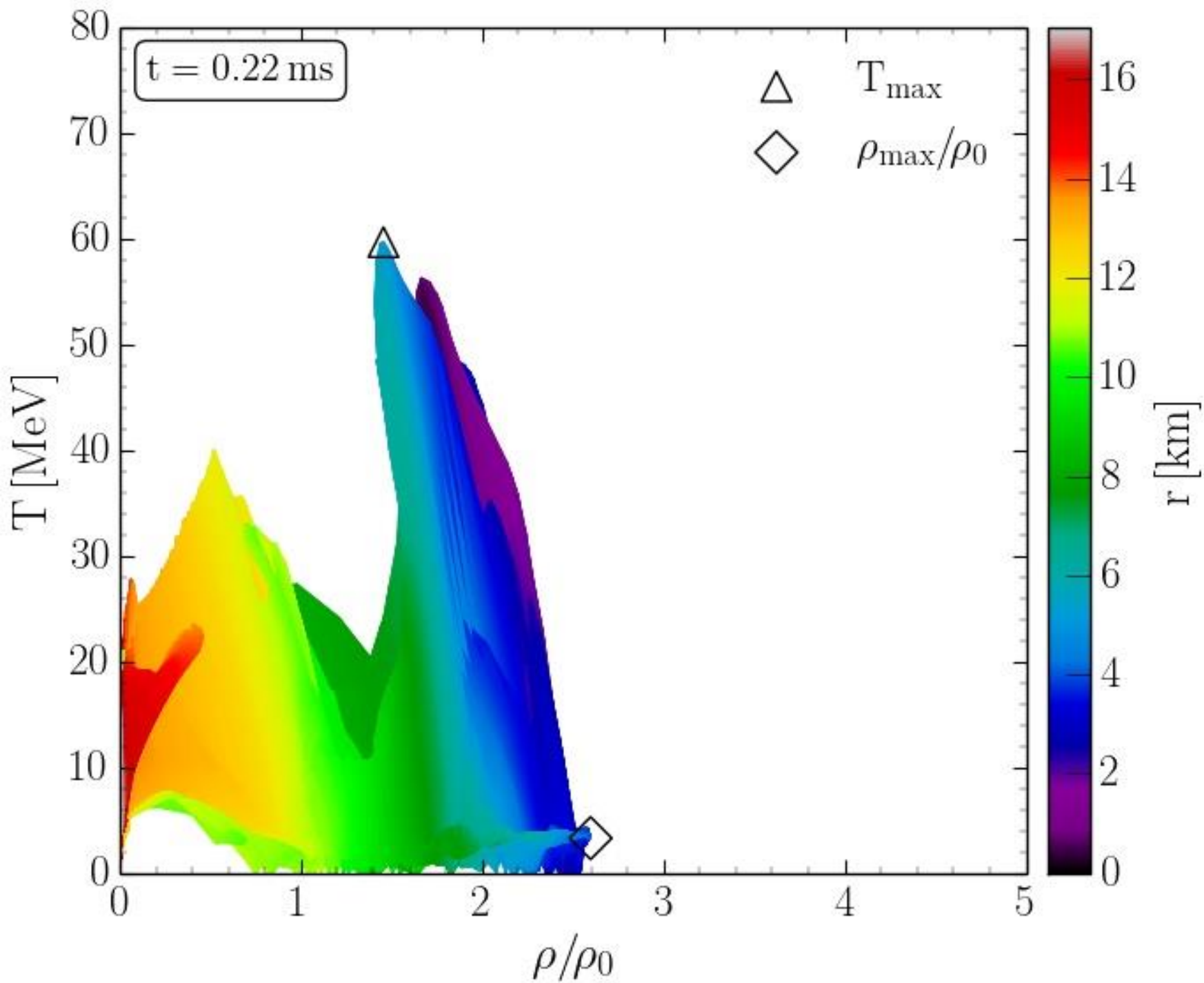
The open triangle marks the maximum value of the temperature while the open diamond indicates the maximum of the density.

# Binary Neutron Star Mergers in the QCD Phase Diagram



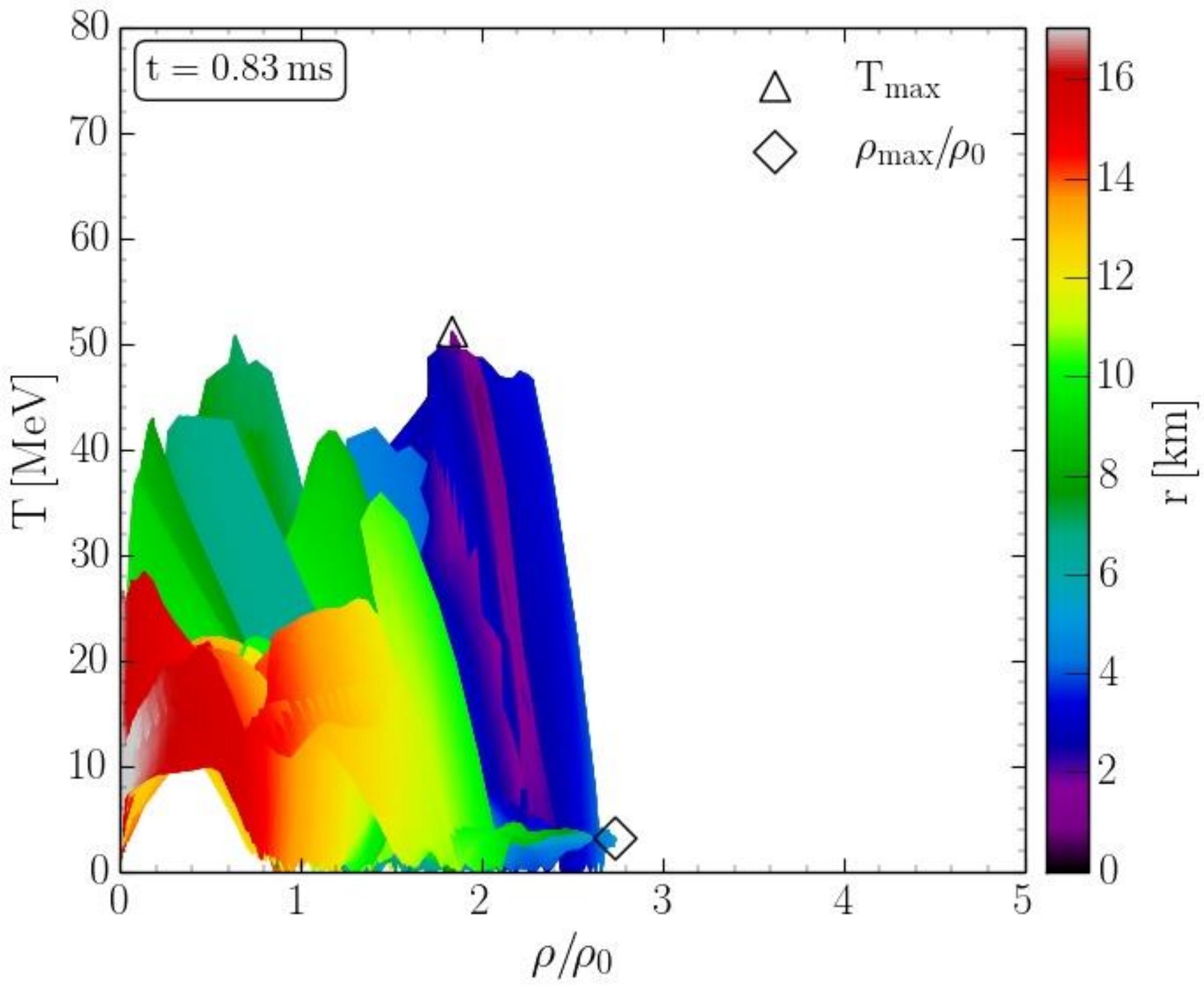
Logarithm of the rest mass density and temperature in the  $xy$ -plane at merger time. The black density contour lines were taken at  $\rho = [0.5, 1, 1.5, \dots] \rho_0$  while the white density contours have a logarithmic distance to indicate the low density regions. The black temperature contour lines were taken at  $T = [30, 40]$  MeV while the white contours indicate the low temperature values ( $T = [5, 10]$  MeV). The green triangle marks the maximum value of the temperature, while the magenta diamond indicates the maximum of the density.

# Binary Neutron Star Mergers in the QCD Phase Diagram



Evolution of hot and dense matter inside the inner area of a hypermassive neutron star in the style of a  $(T-\rho)$  QCD phase diagram plot at  $t=0.22 \text{ ms}$ . The violent, early post-merger phase is characterized by a pronounced density double-core structure and hot temperature regions which are smeared out in areas between the double-core density maxima.

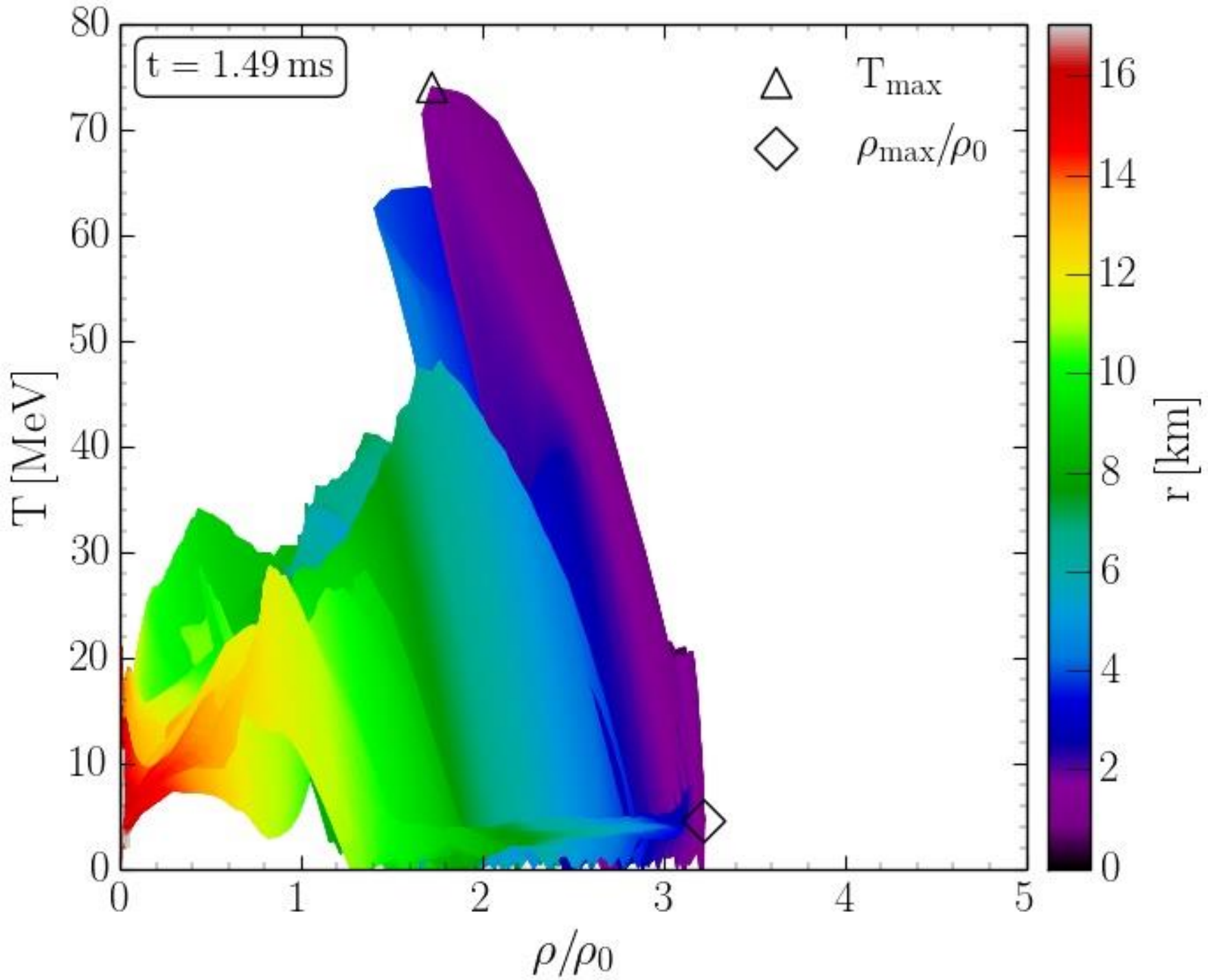
M.Hanuske & L.Bovard, Neutron Star Mergers in the Context of the Hadron-Quark Phase Transition (submitted to the *Journal of Astrophysics and Astronomy*)



Evolution of hot and dense matter inside the inner area of a hypermassive neutron star in the style of a  $(T-\rho)$  QCD phase diagram plot at  $t=0.83 \text{ ms}$ .

The maximum value of the temperature is located near the origin, while the density maxima are placed in the two low temperature centers of the density double-core of the HMNS (see diamond symbol, which is located at the tip of the green cusp in the left figure).

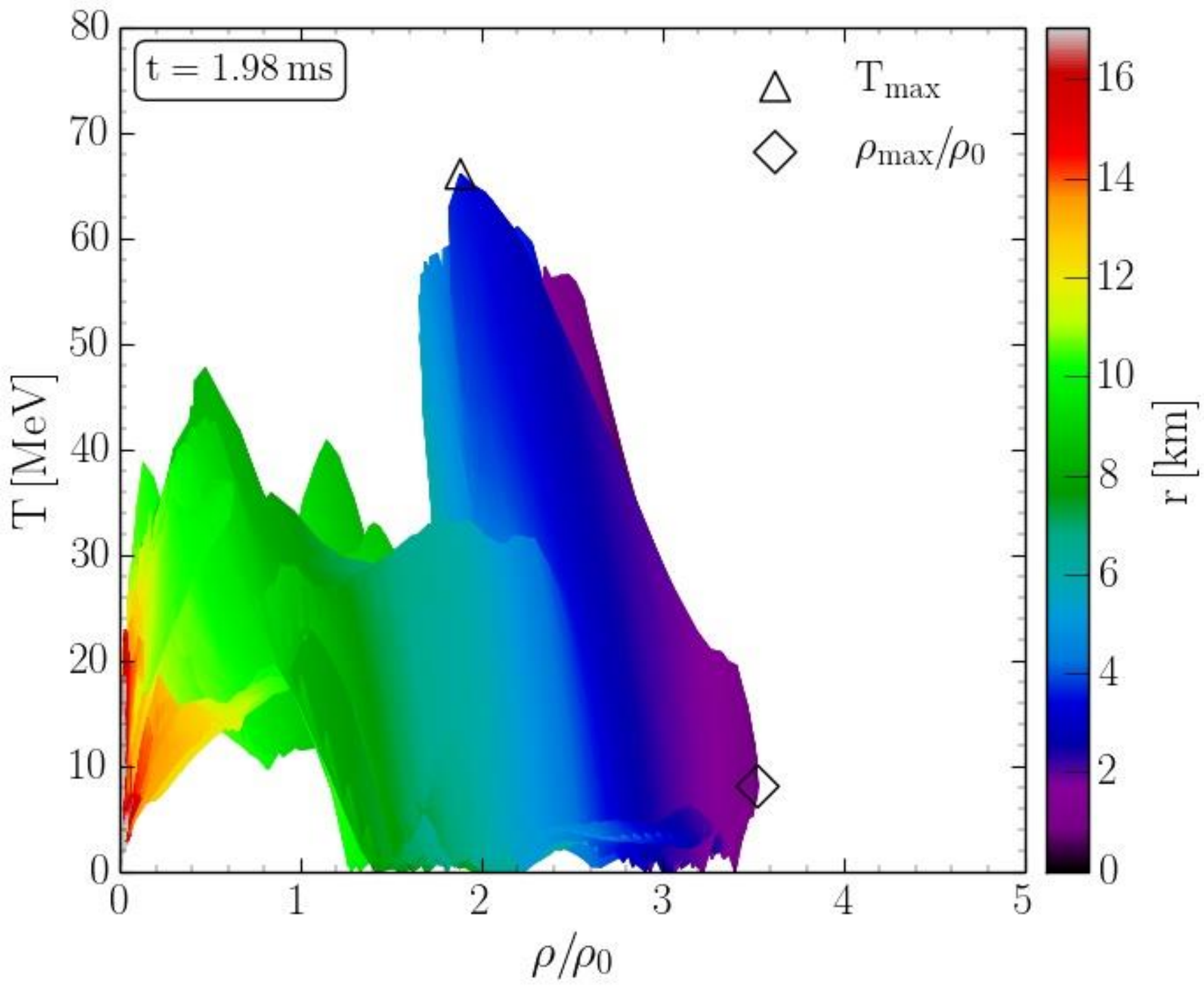
Binary Neutron Star Mergers  
in the QCD Phase Diagram



Evolution of hot and dense matter inside the inner area of a hypermassive neutron star in the style of a  $(T-\rho)$  QCD phase diagram plot at  $t=1.49 \text{ ms}$ .

M.Hanuske & L.Bovard,  
Neutron Star Mergers in the Context of the Hadron-Quark Phase Transition  
(submitted to the *Journal of Astrophysics and Astronomy*)

Binary Neutron Star Mergers  
in the QCD Phase Diagram



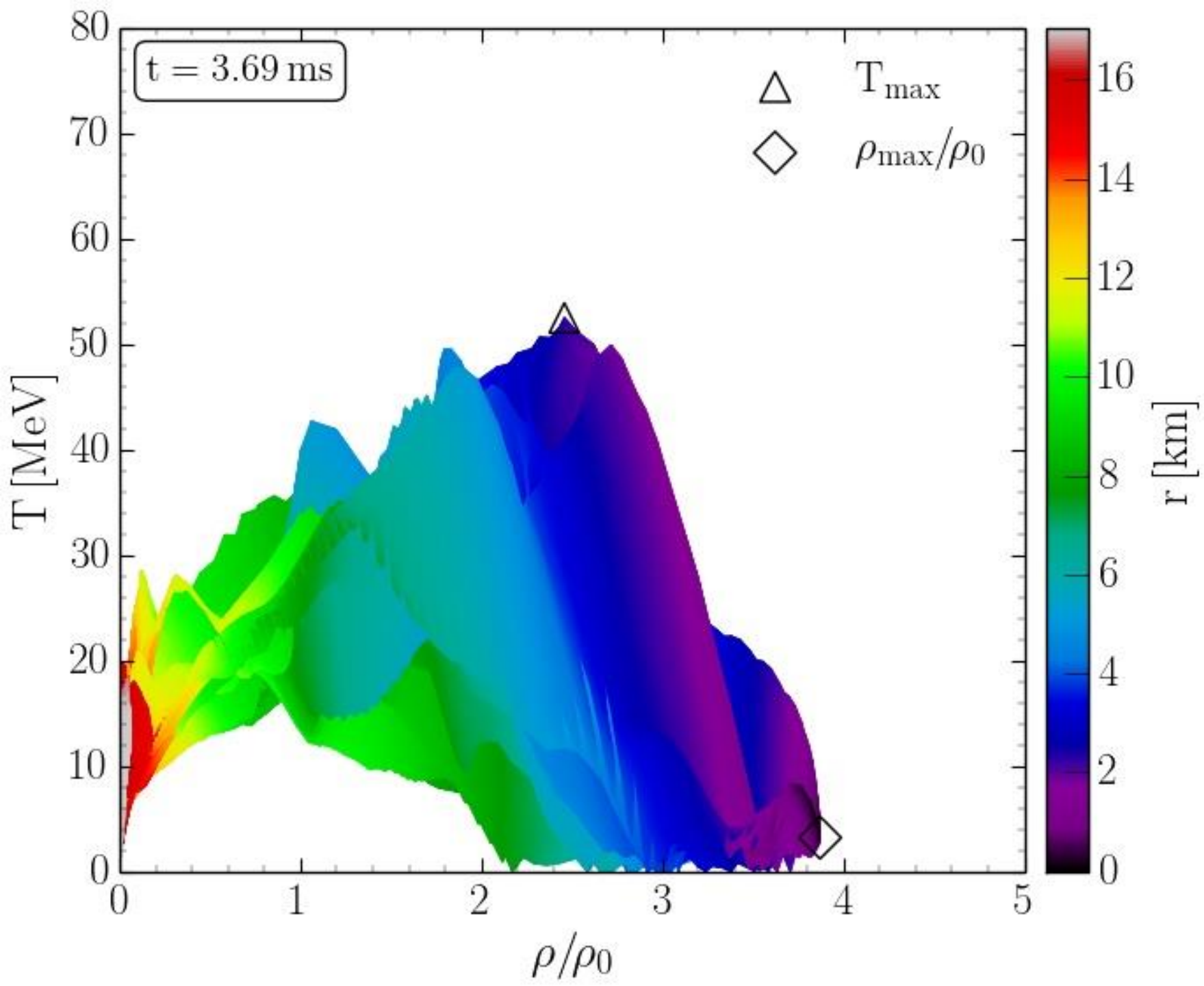
Evolution of hot and dense matter inside the inner area of a hypermassive neutron star in the style of a  $(T-\rho)$  QCD phase diagram plot at  $t=1.98 \text{ ms}$ .

In the time interval  $1.5 \text{ ms} < t < 3 \text{ ms}$  the double-core structure disappears and the maximum density value shifts to the central region of the HMNS.

M.Hanuske & L.Bovard, Neutron Star Mergers in the Context of the Hadron-Quark Phase Transition (submitted to the *Journal of Astrophysics and Astronomy*)

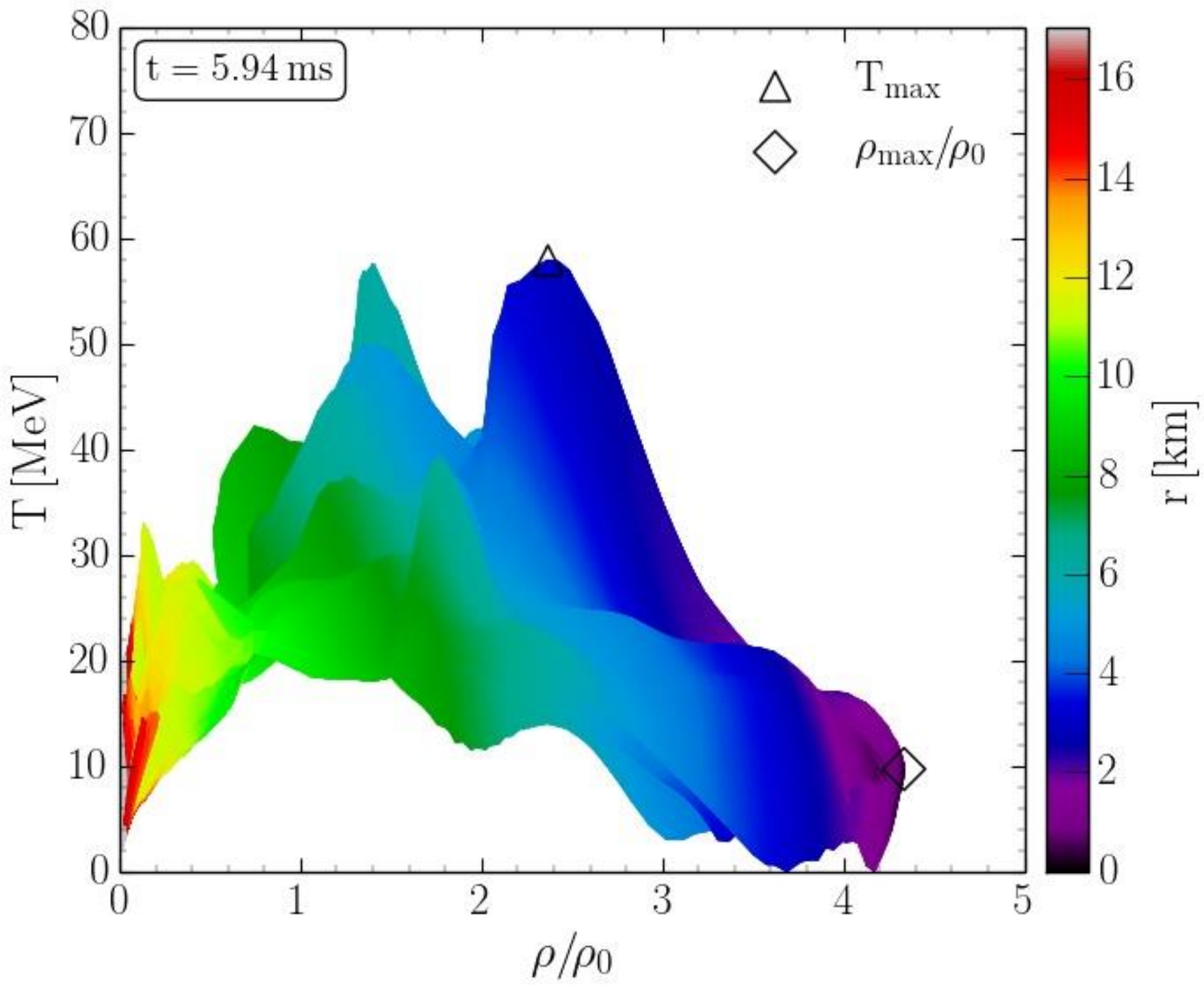
Binary Neutron Star Mergers  
in the QCD Phase Diagram

# Binary Neutron Star Mergers in the QCD Phase Diagram



Evolution of hot and dense matter inside the inner area of a hypermassive neutron star in the style of a  $(T-\rho)$  QCD phase diagram plot at  $t=3.69$  ms.

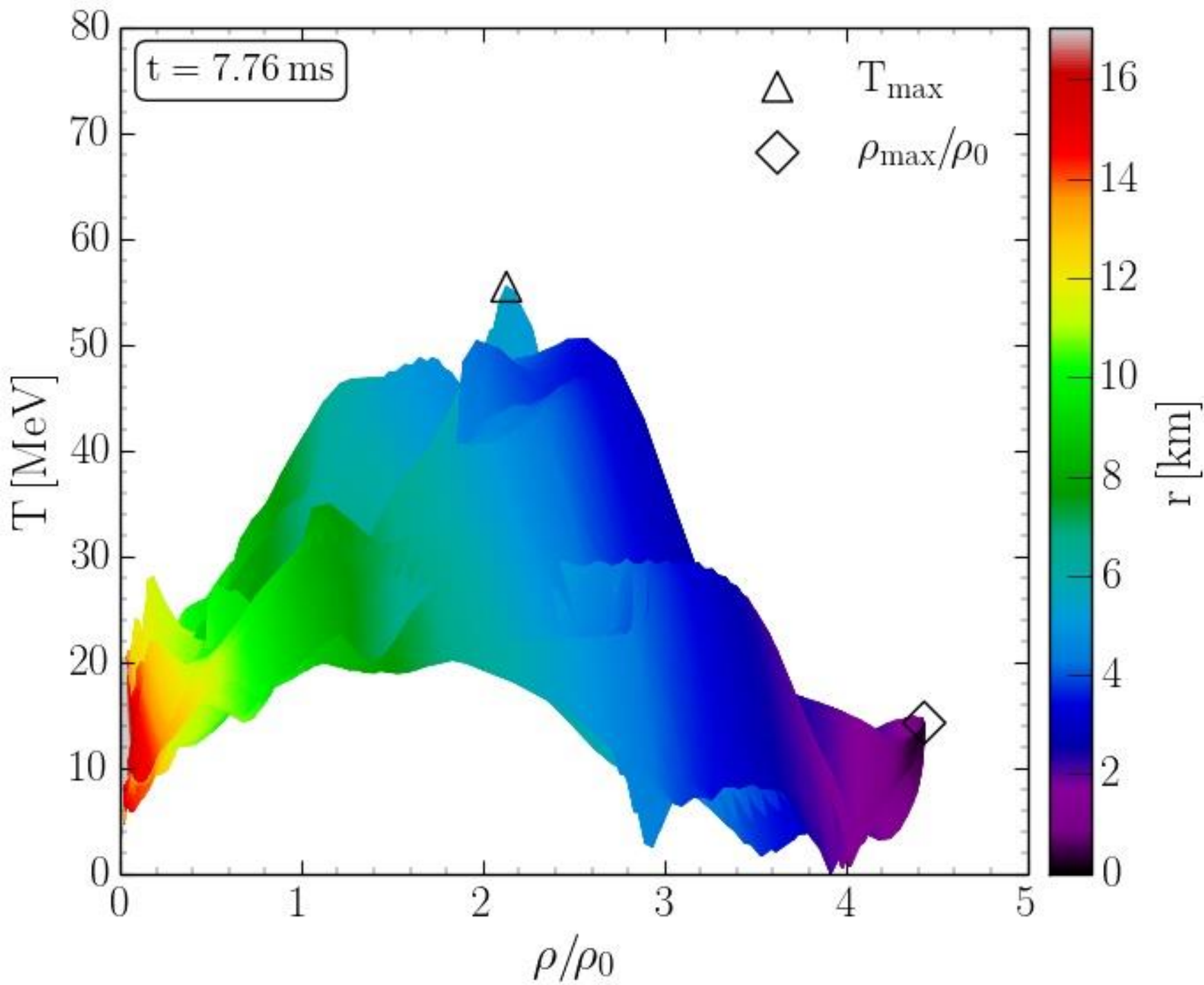
The density distribution at this post-merger time has an pronounced 'peanut' shape but the highest value of the density is now placed in the center of the HMNS. The maximum density value (diamond symbol) is located at the center of the HMNS, while the temperature maximum (triangle) is placed in one of the temperature hot spots at  $r \sim 3$  km.



Evolution of hot and dense matter inside the inner area of a hypermassive neutron star in the style of a  $(T-\rho)$  QCD phase diagram plot at  $t=5.94 \text{ ms}$ .

M.Hanuske & L.Bovard,  
Neutron Star Mergers in the Context of the Hadron-Quark Phase Transition  
(submitted to the *Journal of Astrophysics and Astronomy*)

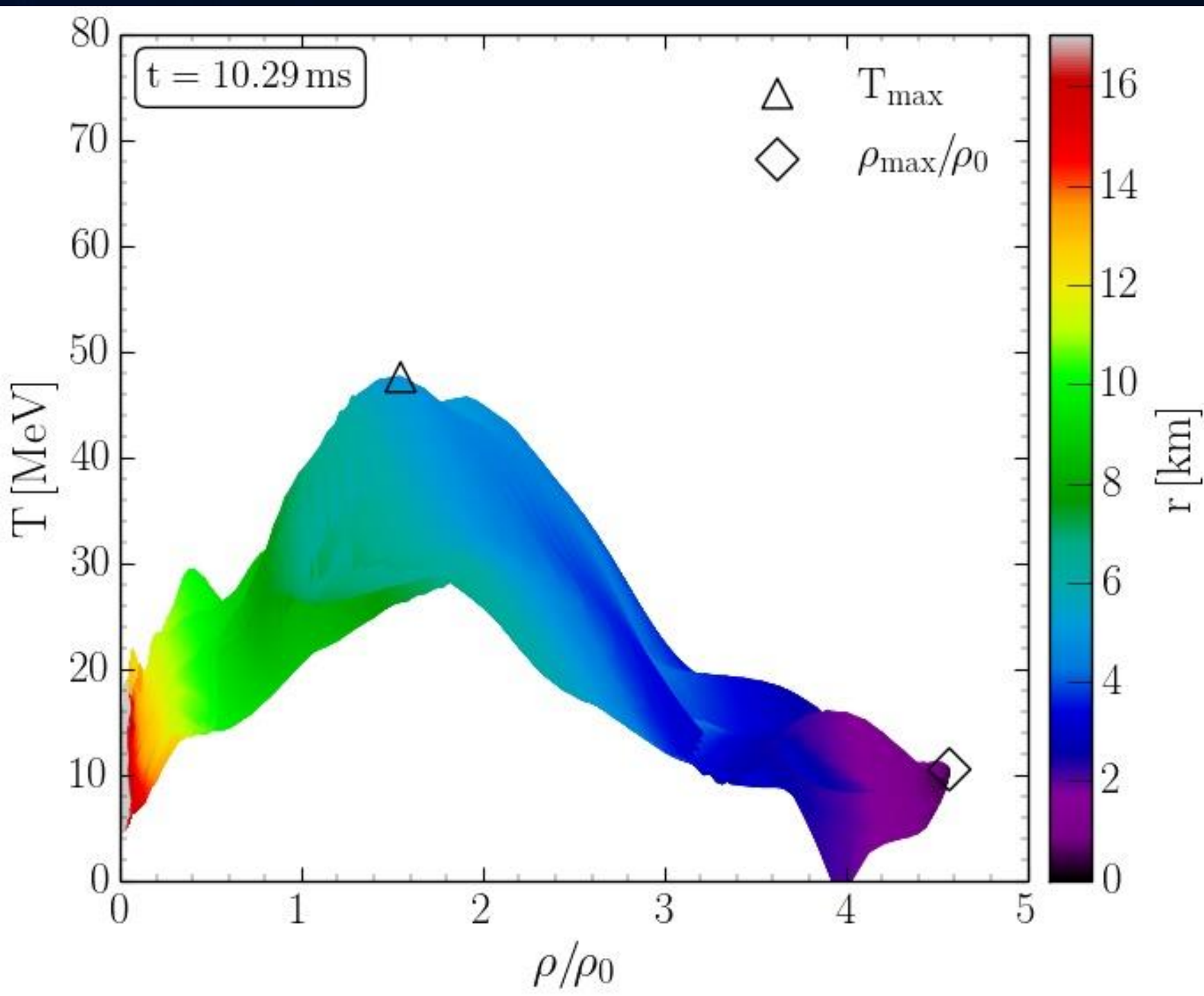
Binary Neutron Star Mergers  
in the QCD Phase Diagram



Evolution of hot and dense matter inside the inner area of a hypermassive neutron star in the style of a  $(T-\rho)$  QCD phase diagram plot at  $t=7.76 \text{ ms}$ .

M.Hanuske & L.Bovard,  
Neutron Star Mergers in the Context of the Hadron-Quark Phase Transition  
(submitted to the *Journal of Astrophysics and Astronomy*)

Binary Neutron Star Mergers  
in the QCD Phase Diagram



Evolution of hot and dense matter inside the inner area of a hypermassive neutron star in the style of a  $(T-\rho)$  QCD phase diagram plot at  $t=10.29 \text{ ms}$ .

M.Hanuske & L.Bovard,  
Neutron Star Mergers in the Context of the Hadron-Quark Phase Transition  
(submitted to the *Journal of Astrophysics and Astronomy*)

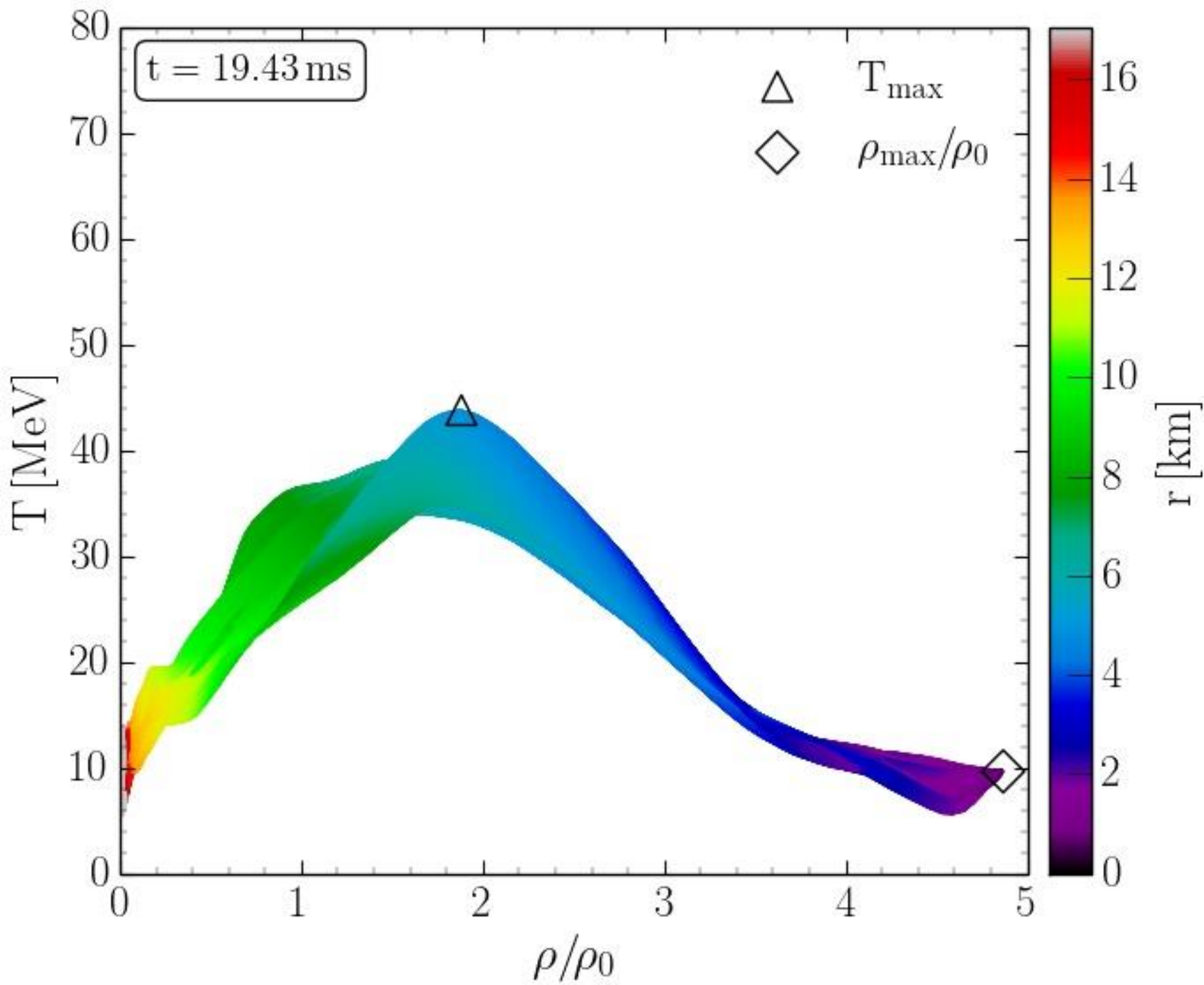
Binary Neutron Star Mergers  
in the QCD Phase Diagram

# Binary Neutron Star Mergers

## in the QCD Phase Diagram

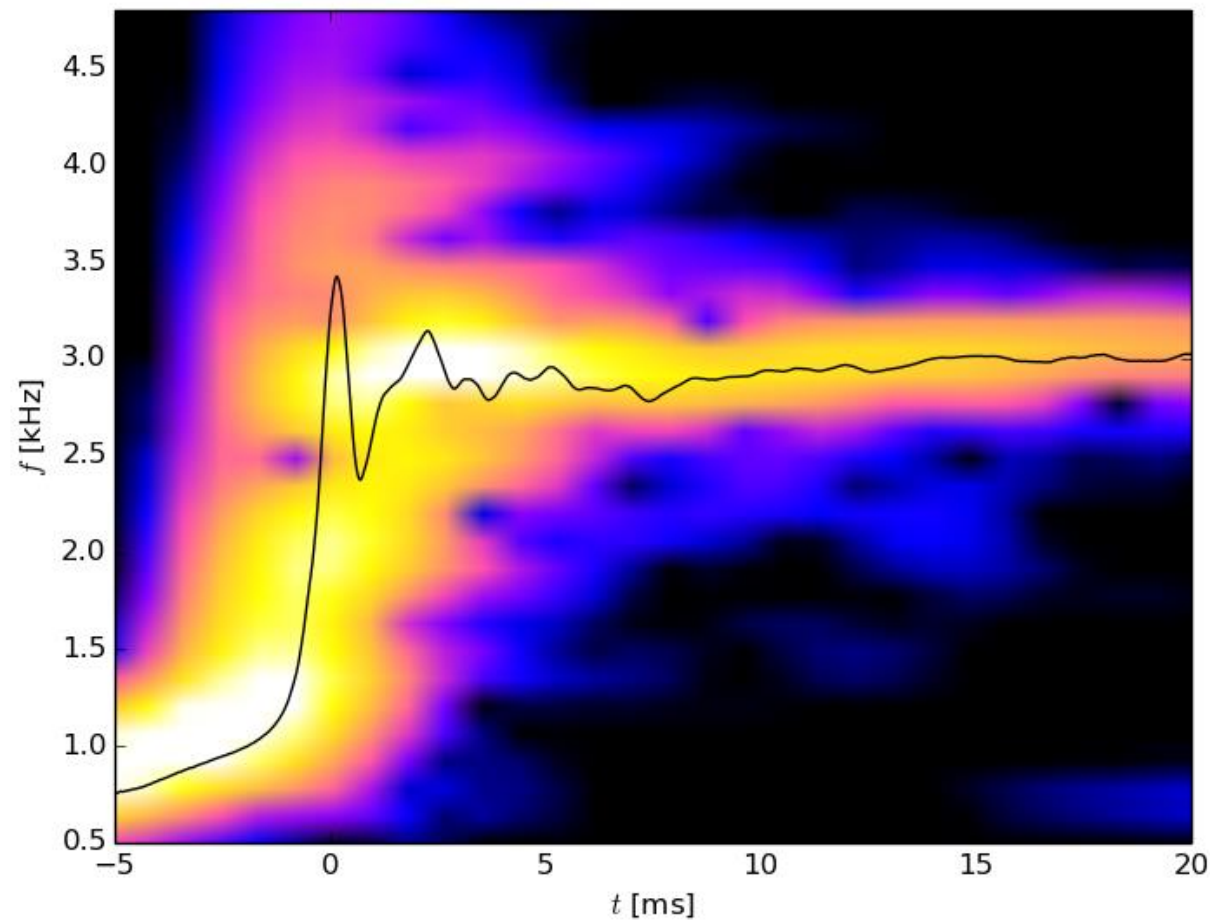
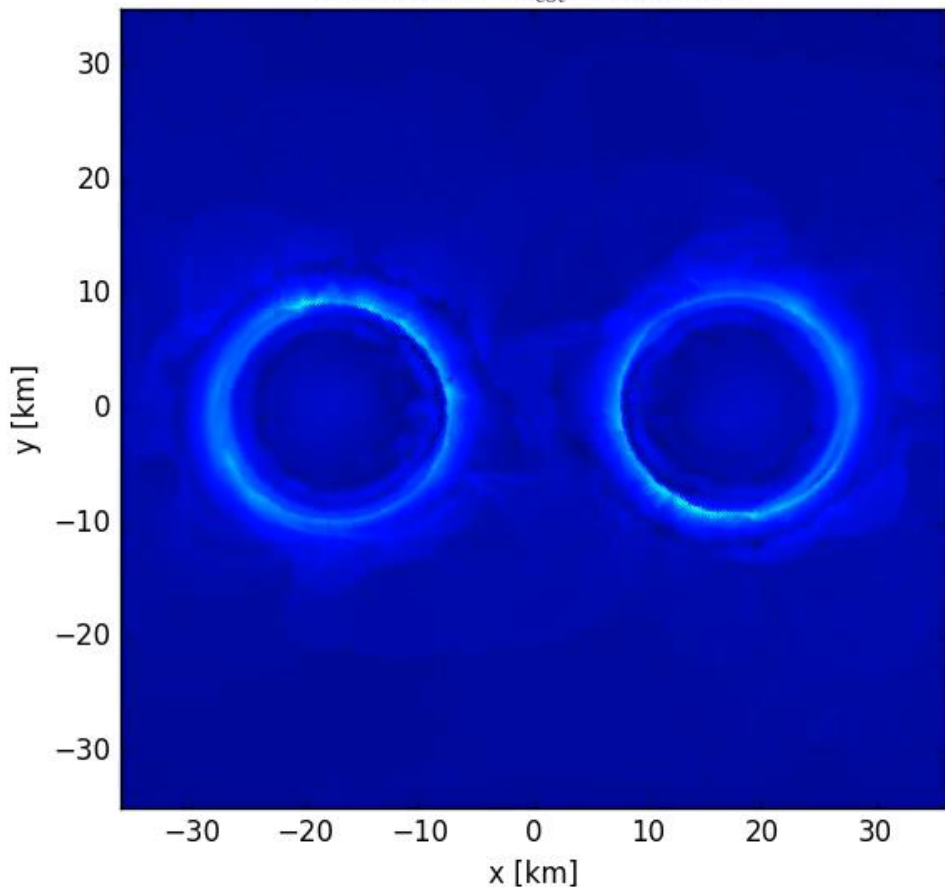
Evolution of hot and dense matter inside the inner area of a hypermassive neutron star in the style of a  $(T-\rho)$  QCD phase diagram plot at  $t=19.43$  ms.

At late post-merger times, the area populated in the  $(T-\rho)$  plane has been constricted to a small quasi stable region. The central region of the HMNS consists of highly dense matter ( $\rho \sim 5 \rho_0$ ) at moderate temperature values  $T \sim 10$  MeV while the maximum of the temperature is reached at the top of the temperature ring like structure at  $r \sim 6$  km at moderate density values  $\rho \sim 2 \rho_0$ .



# The Co-Rotating Frame

$t = 9.58\text{ms}$   $\Omega_{\text{cot}} = 387.20\text{Hz}$

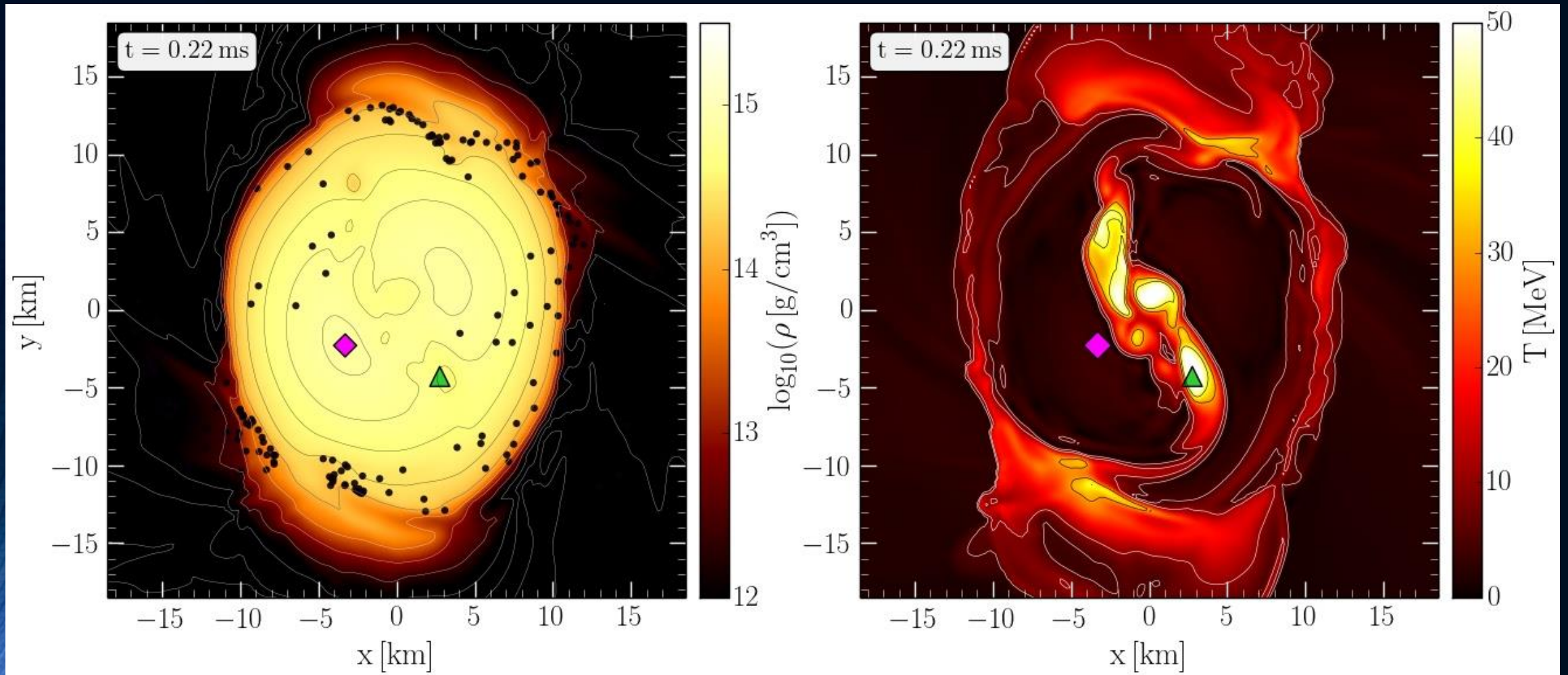


Simulation and movie has been produced by Luke Bovard

Hanuske, et.al. PRD, 96(4), 043004 (2017)

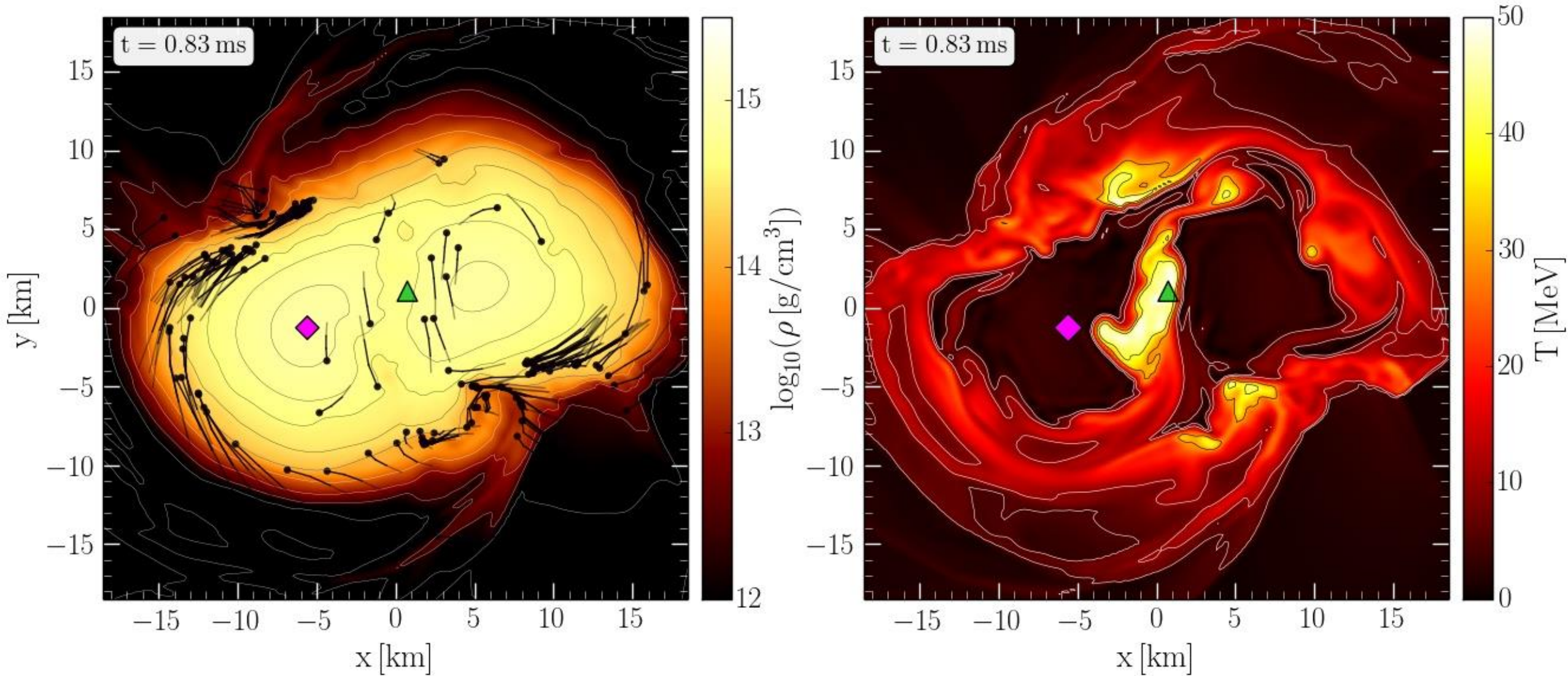
<sup>2</sup> Note that the angular-velocity distribution in the lower central panel of Fig. 10 refers to the corotating frame and that this frame is rotating at half the angular frequency of the emitted gravitational waves,  $\Omega_{\text{GW}}$ . Because the maximum of the angular velocity  $\Omega_{\text{max}}$  is of the order of  $\Omega_{\text{GW}}/2$  (cf. left panel of Fig. 12), the ring structure in this panel is approximately at zero angular velocity.

# Density and Temperature Evolution inside the HMNS



Logarithm of the rest mass density and temperature in the  $xy$ -plane at merger time. Additionally the flowlines of several tracer particles that remain close to the equatorial plane will be visualized. The final part of the tracer flowlines for the last  $t = 0.19$  ms are shown and the small black dots are used to indicate the tracer position at the time indicated in the frame. The initial parts of the trajectories have increasing transparency so as to highlight the final part of the trajectories.

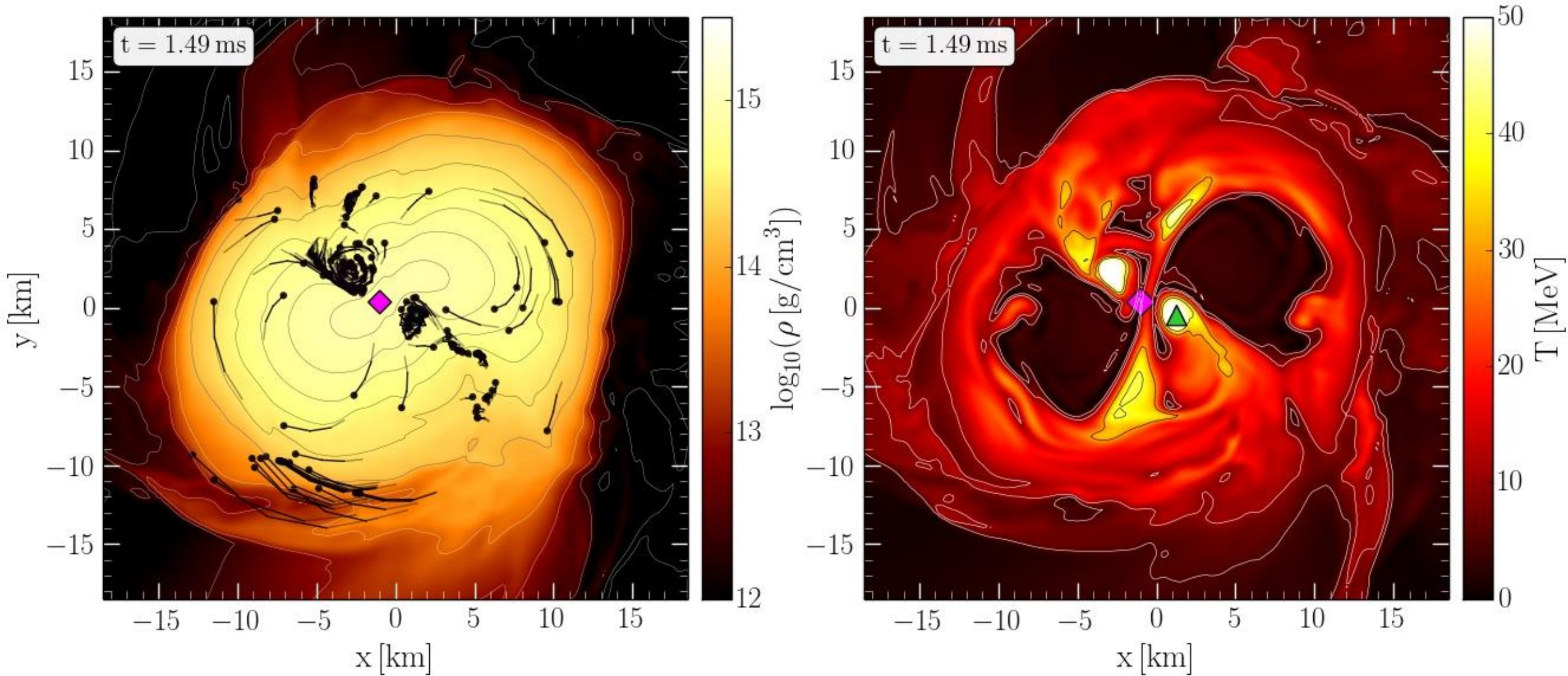
# Density and Temperature Evolution inside the HMNS



Rest mass density on the equatorial plane

Temperature on the equatorial plane

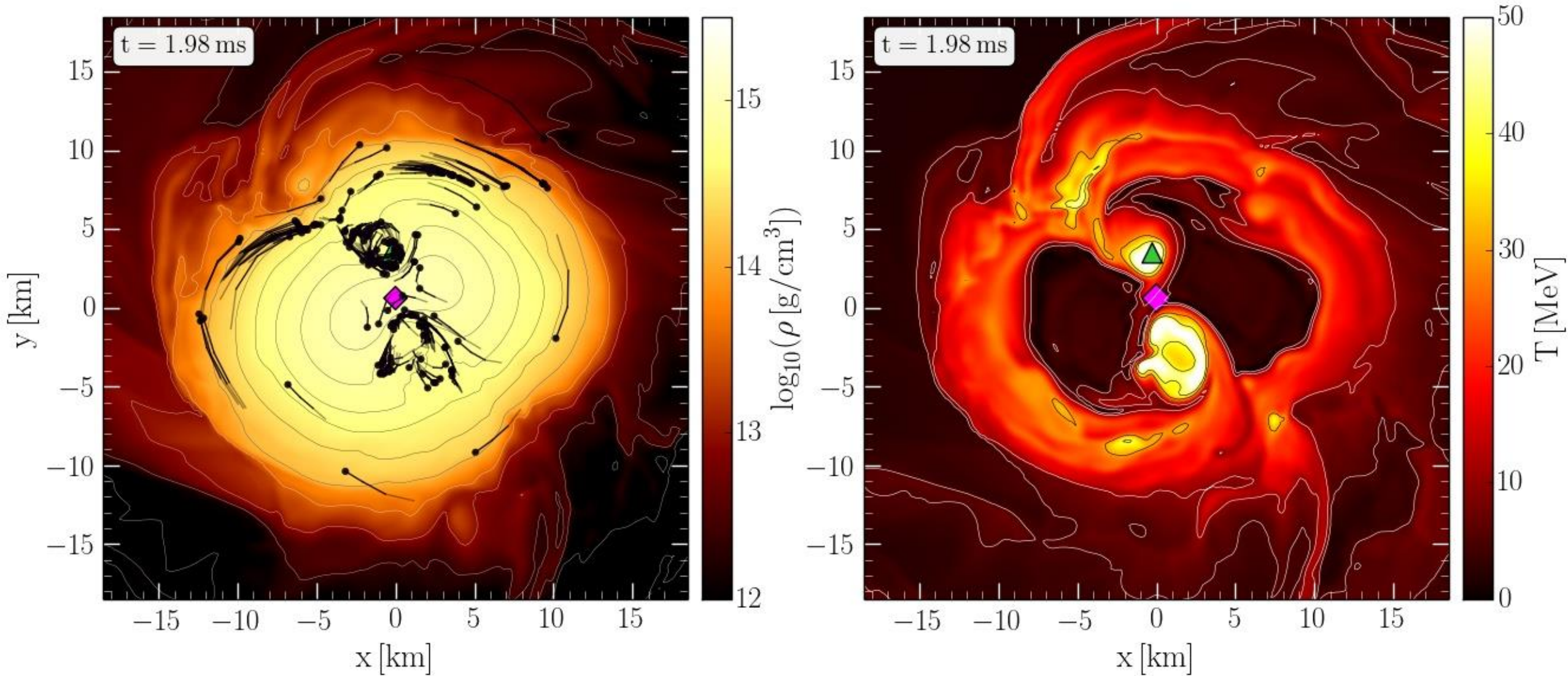
# Density and Temperature Evolution inside the HMNS



Rest mass density on the equatorial plane

Temperature on the equatorial plane

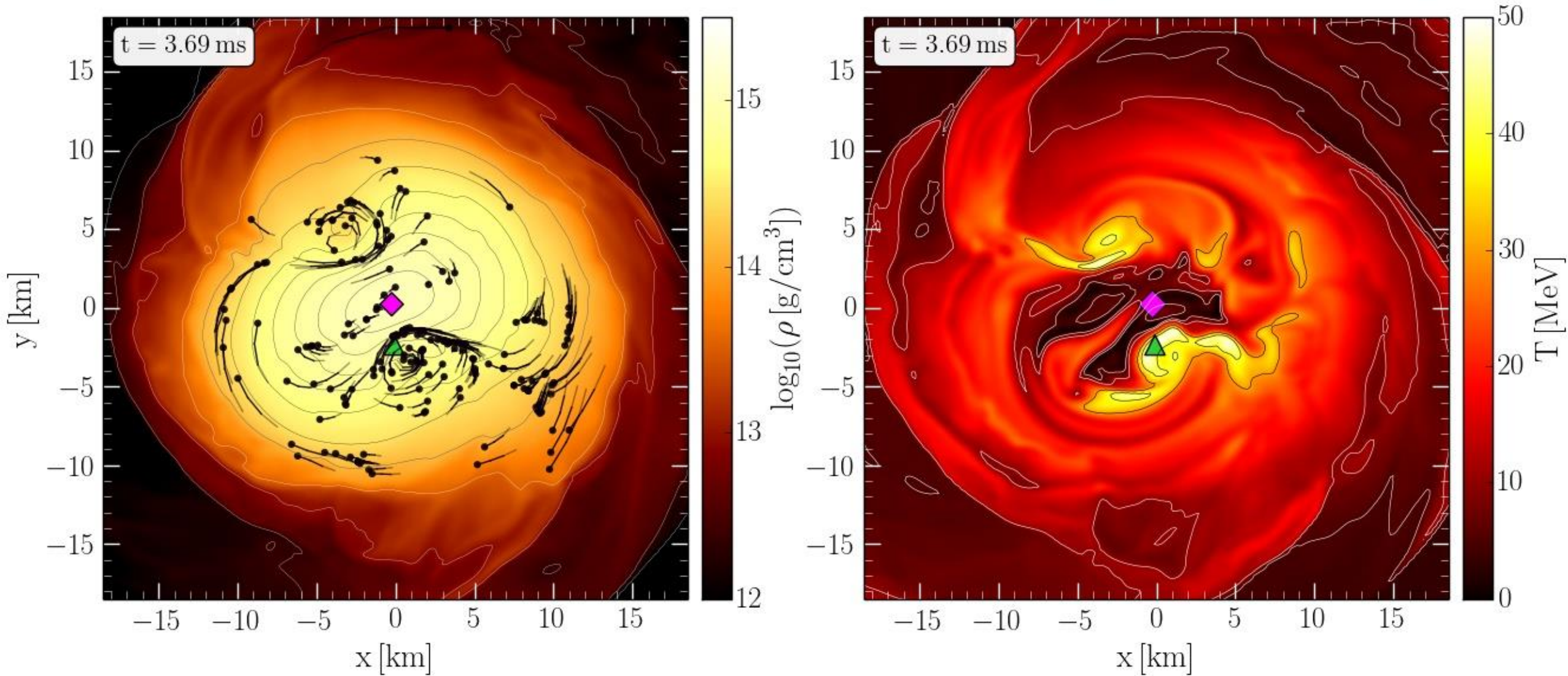
# Density and Temperature Evolution inside the HMNS



Rest mass density on the equatorial plane

Temperature on the equatorial plane

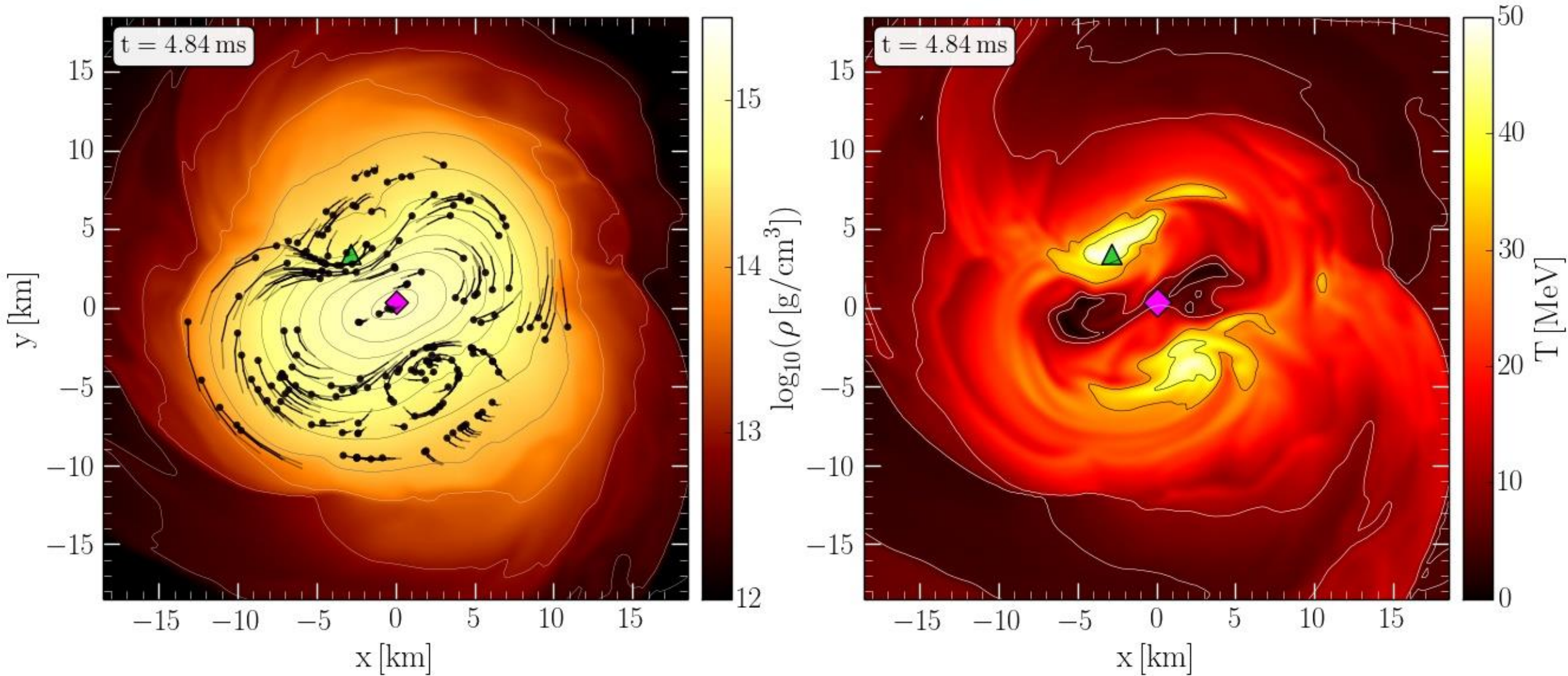
# Density and Temperature Evolution inside the HMNS



Rest mass density on the equatorial plane

Temperature on the equatorial plane

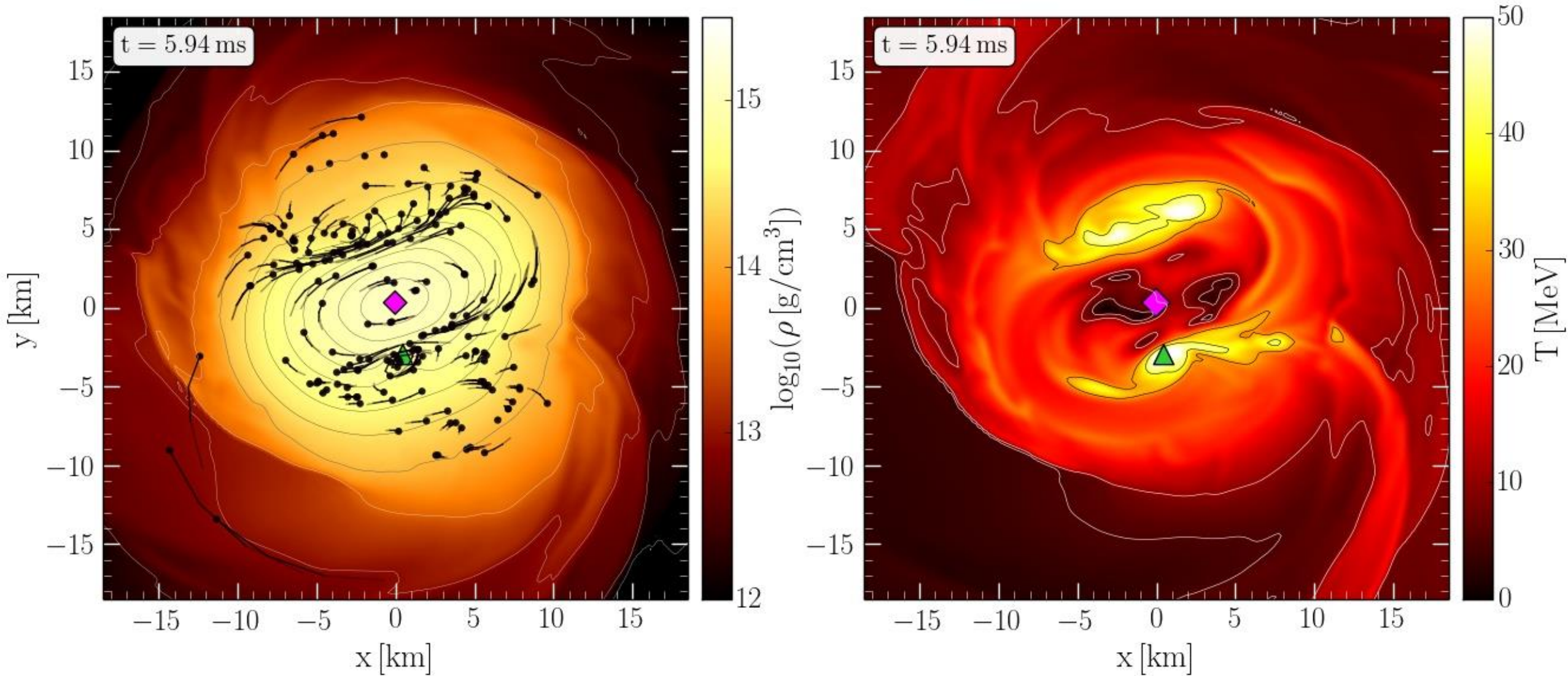
# Density and Temperature Evolution inside the HMNS



Rest mass density on the equatorial plane

Temperature on the equatorial plane

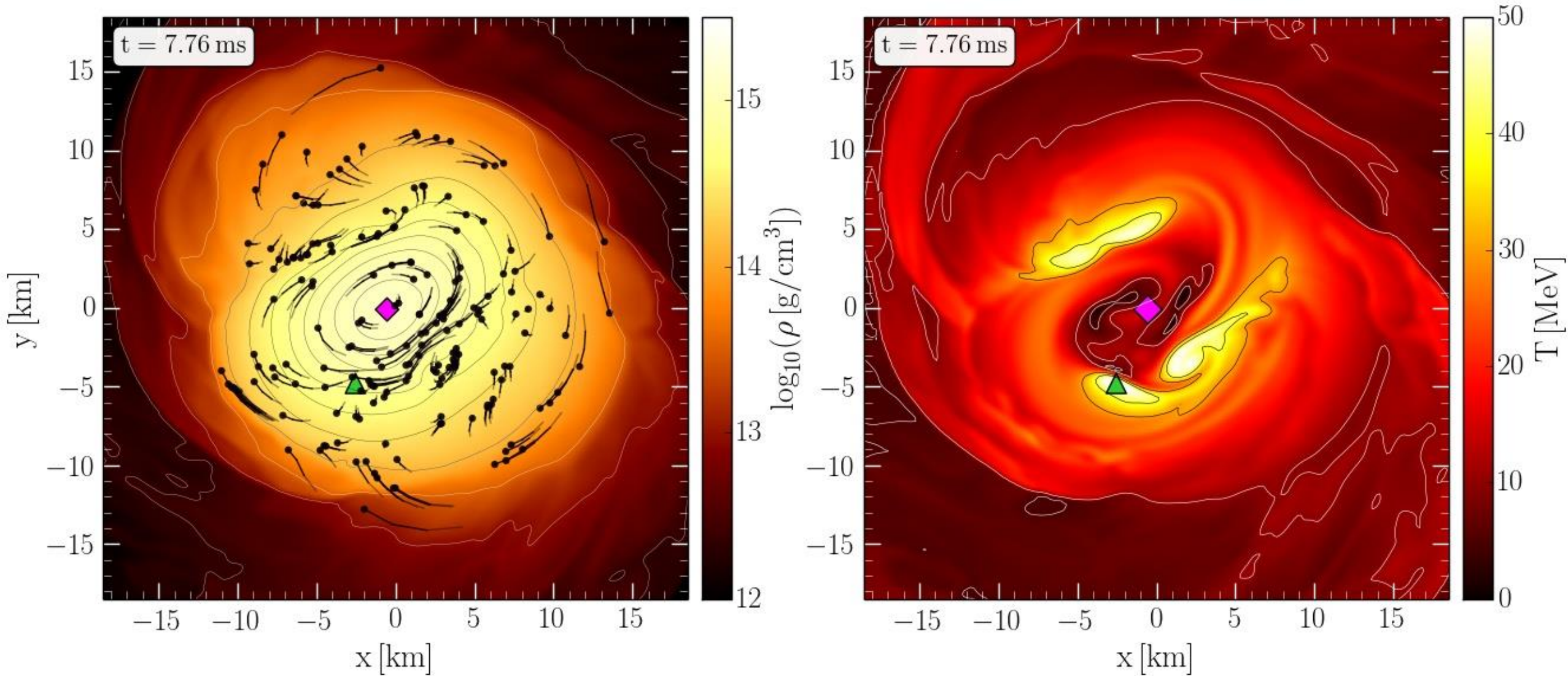
# Density and Temperature Evolution inside the HMNS



Rest mass density on the equatorial plane

Temperature on the equatorial plane

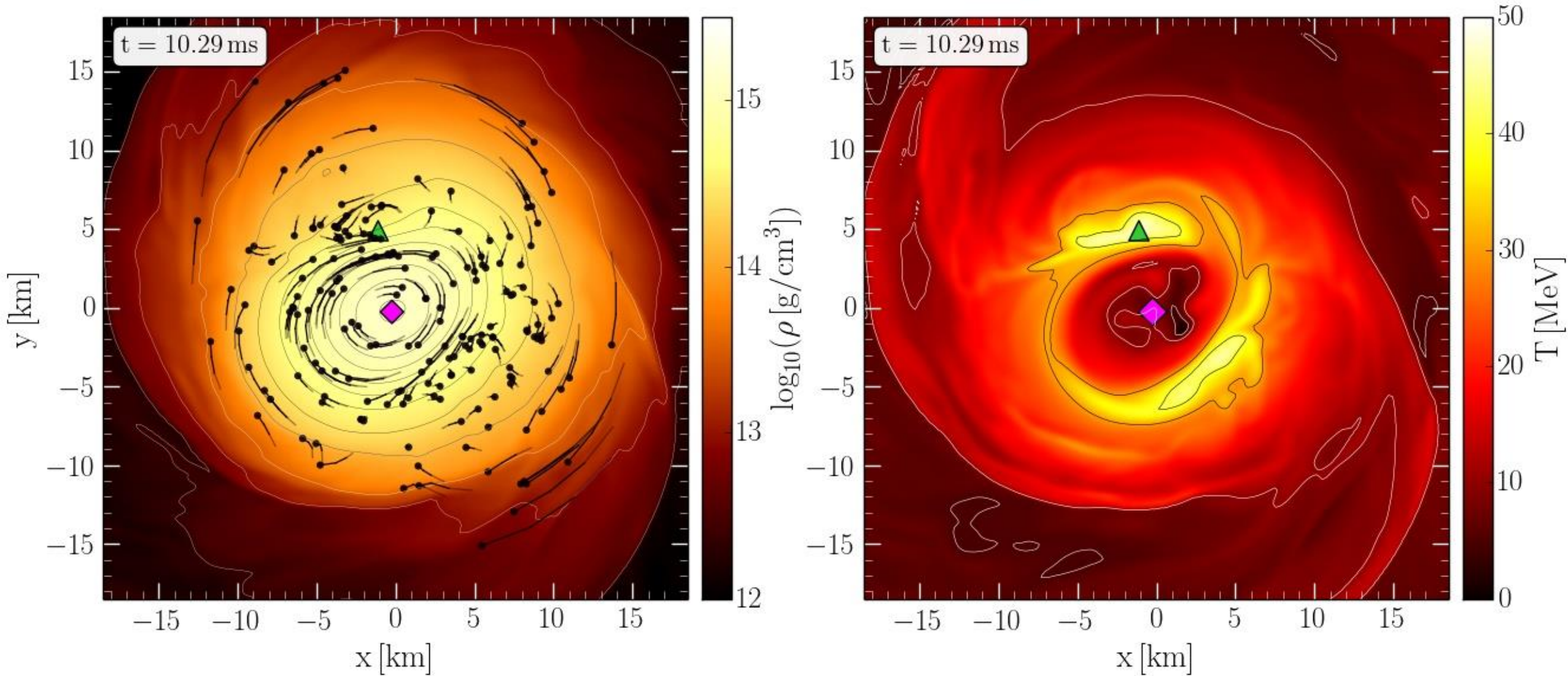
# Density and Temperature Evolution inside the HMNS



Rest mass density on the equatorial plane

Temperature on the equatorial plane

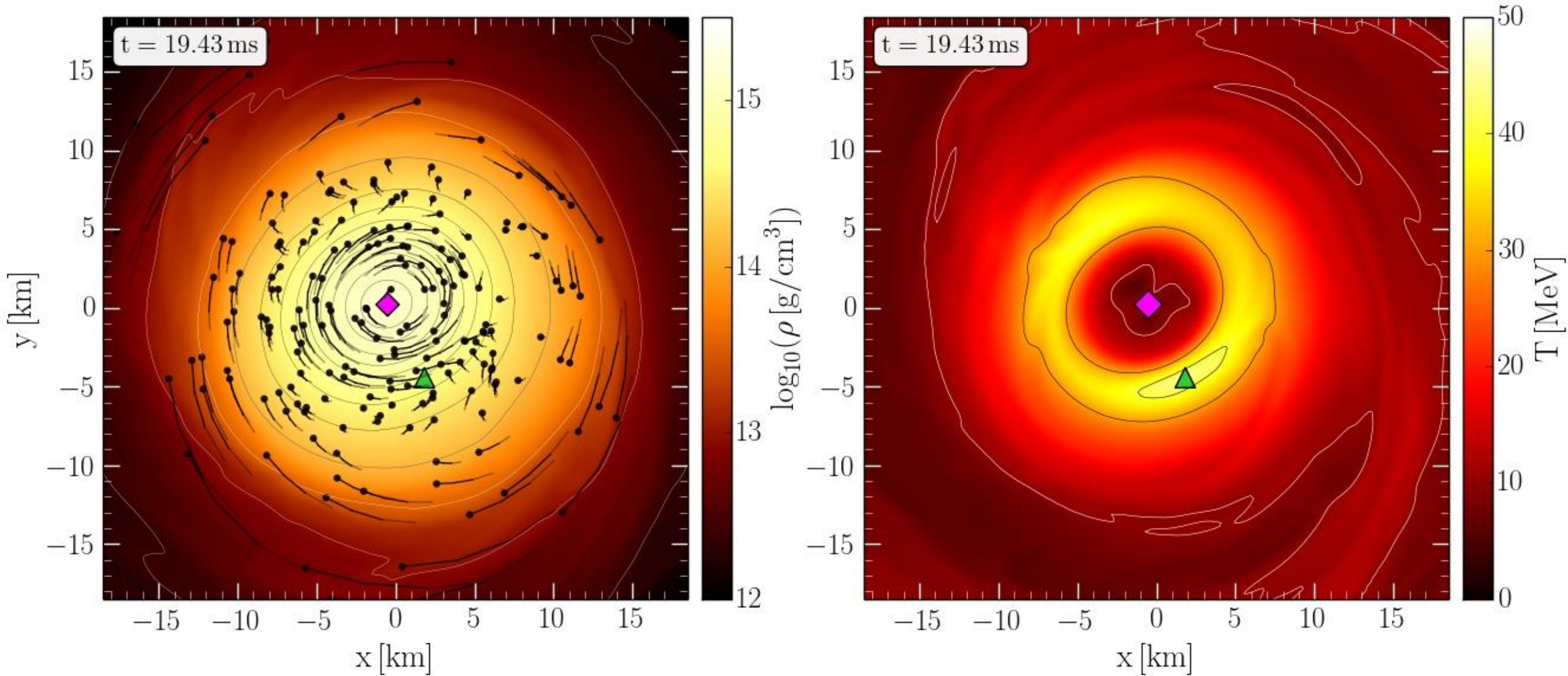
# Density and Temperature Evolution inside the HMNS



Rest mass density on the equatorial plane

Temperature on the equatorial plane

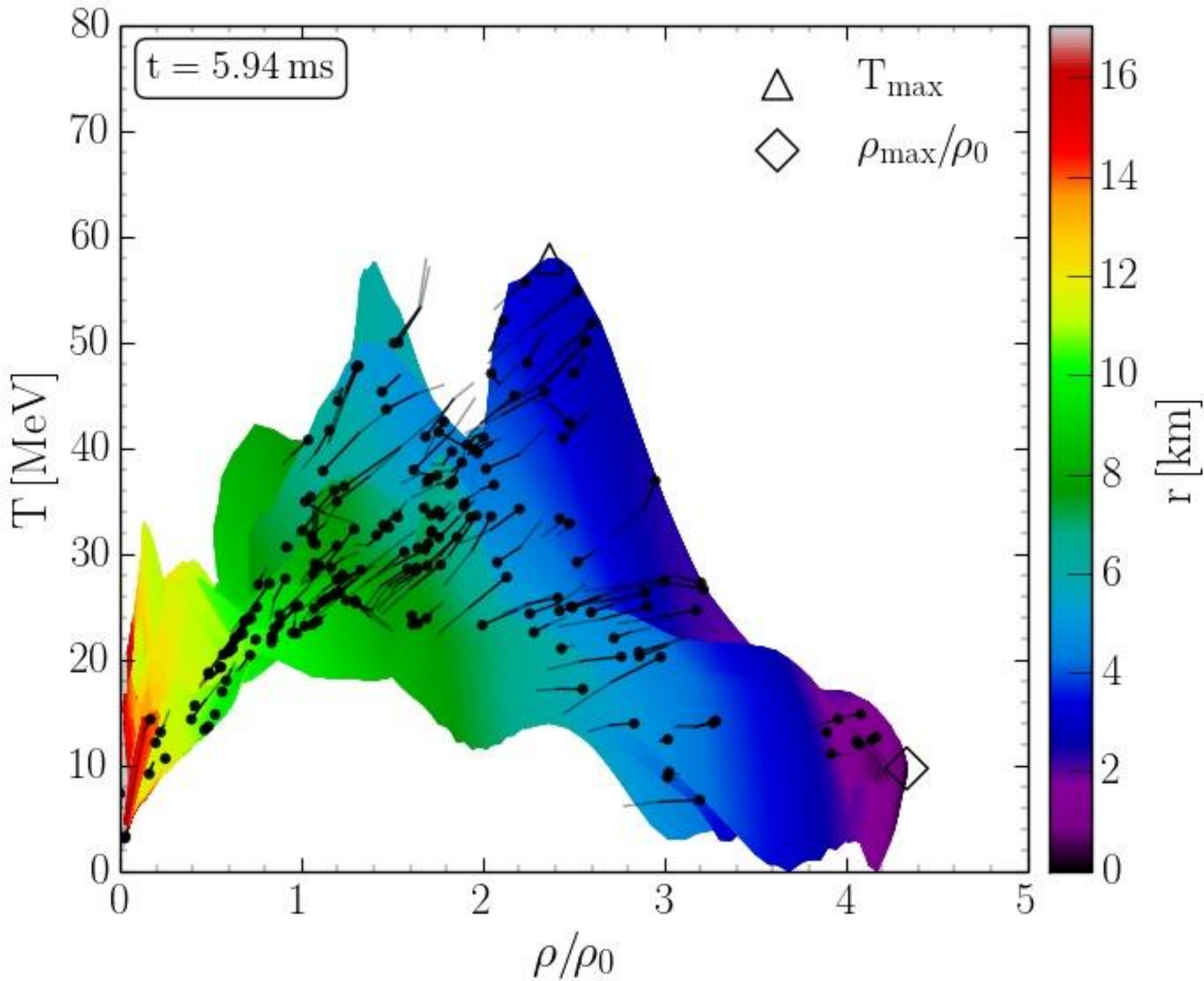
# Density and Temperature Evolution inside the HMNS



Rest mass density on the equatorial plane

Temperature on the equatorial plane

# Binary Neutron Star Mergers in the QCD Phase Diagram



Evolution of hot and dense matter inside the inner area of a hypermassive neutron star simulated within the LS220 EOS with a total mass of  $M_{\text{total}}=2.7 M_{\text{solar}}$  in the style of a  $(T-\rho)$  QCD phase diagram plot

The color-coding indicates the radial position  $r$  of the corresponding  $(T-\rho)$  fluid element measured from the origin of the simulation  $(x, y) = (0, 0)$  on the equatorial plane at  $z = 0$ .

The open triangle marks the maximum value of the temperature while the open diamond indicates the maximum of the density.

# The Angular Velocity in the (3+1)-Split

The angular velocity  $\Omega$  in the (3+1)-Split is a combination of the lapse function  $\alpha$ , the  $\phi$ -component of the shift vector  $\beta^\phi$  and the 3-velocity  $v^\phi$  of the fluid (spatial projection of the 4-velocity  $\mathbf{u}$ ):

**(3+1)-decomposition  
of spacetime:**

$$\Omega(x, y, z, t) = \frac{u^\phi}{u^t} = \alpha v^\phi - \beta^\phi$$

$$g_{\mu\nu} = \begin{pmatrix} -\alpha^2 + \beta_i \beta^i & \beta_i \\ \beta_i & \gamma_{ij} \end{pmatrix}$$

Angular velocity  
 $\Omega$

Lapse function  
 $\alpha$

$\Phi$ -component of  
3-velocity  $v^\phi$

Frame-dragging  
 $\beta^\phi$

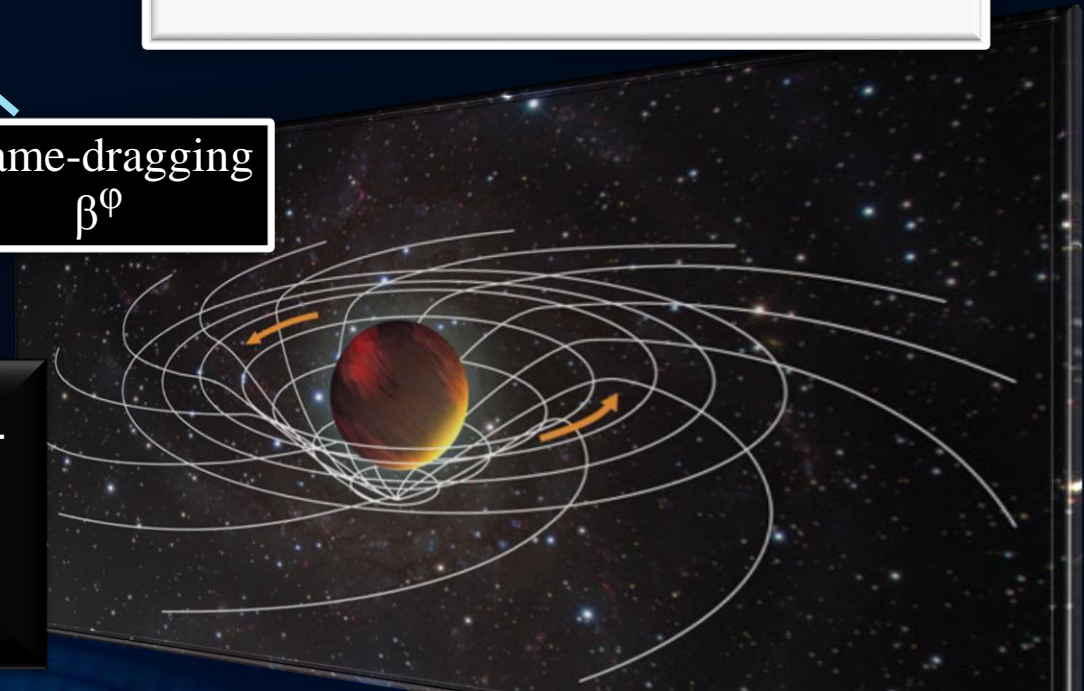
**Focus: Inner core of the differentially rotating HMNS**

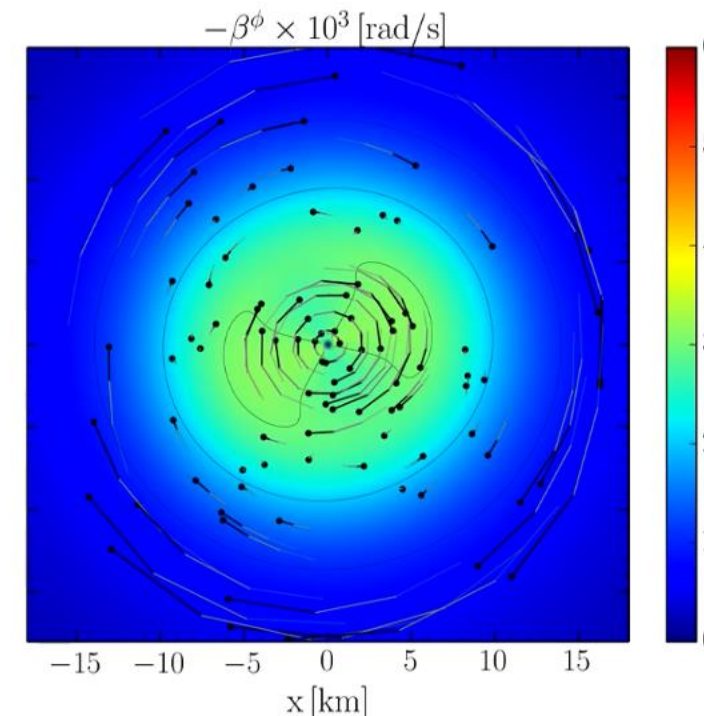
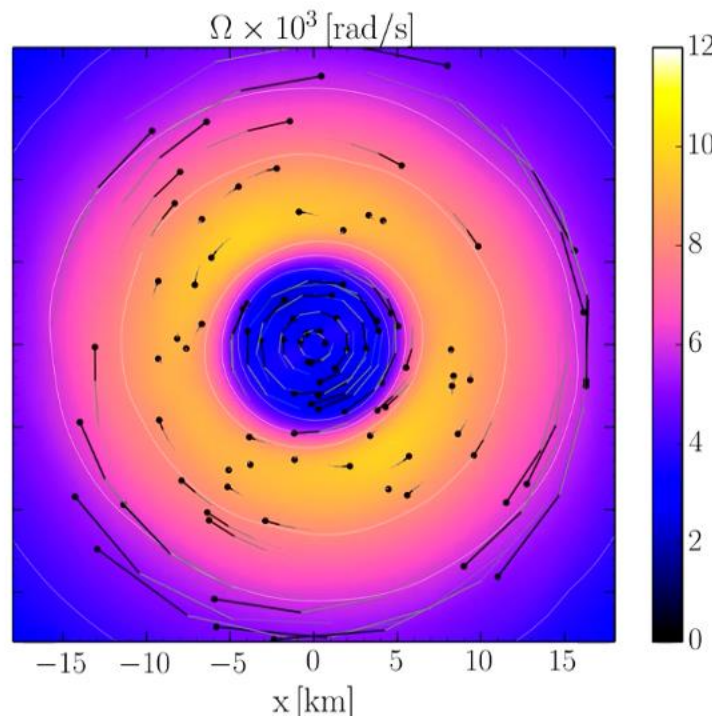
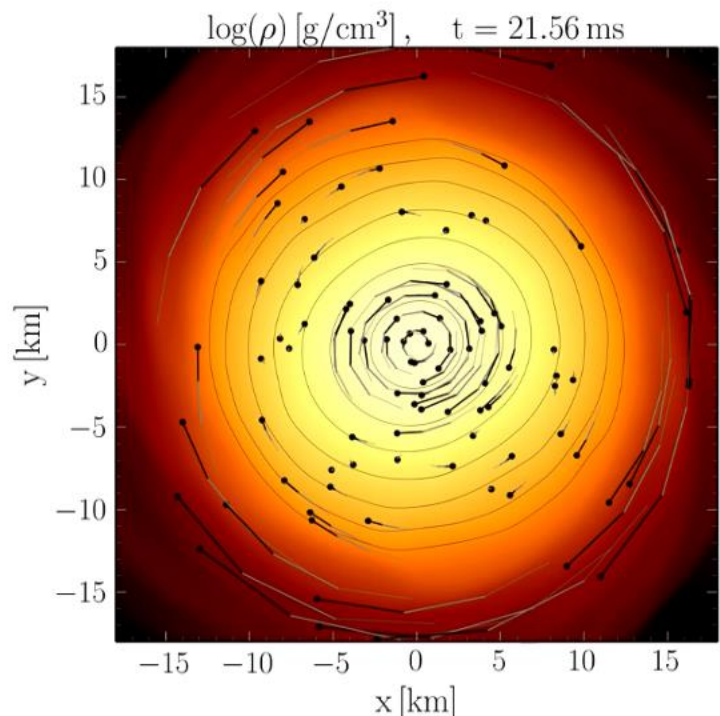
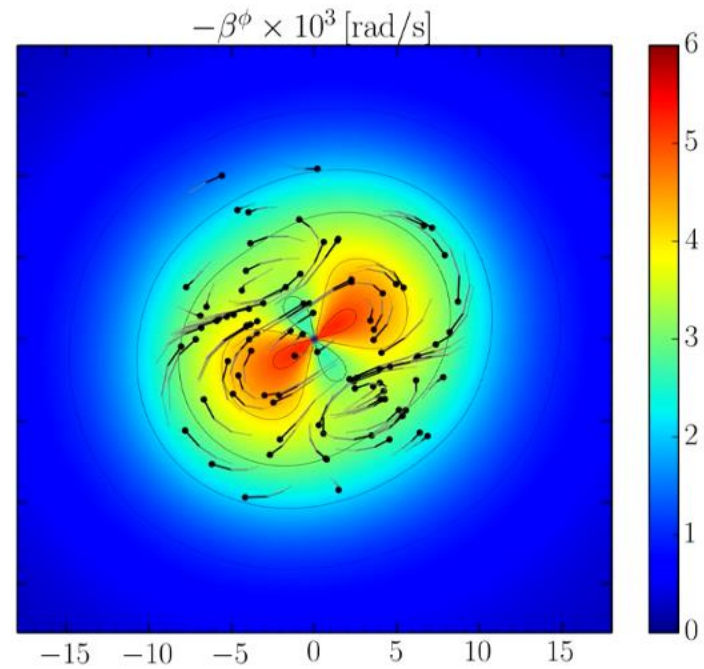
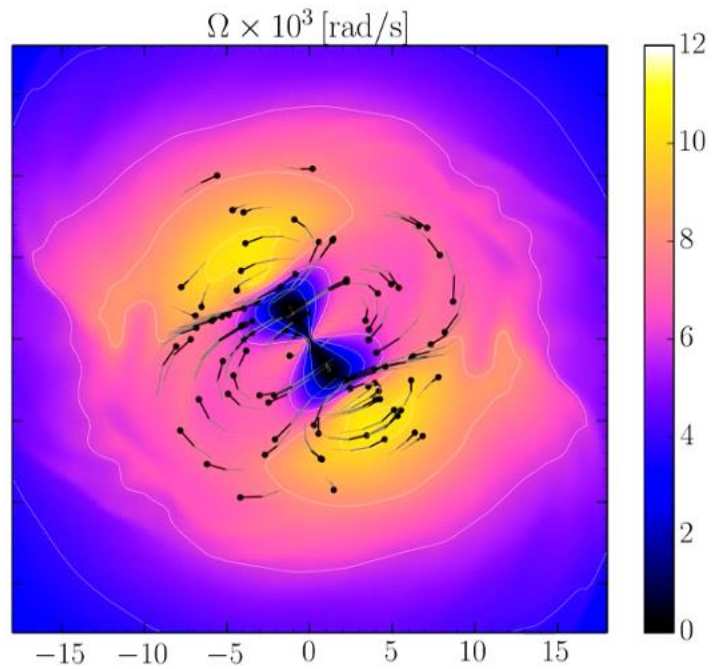
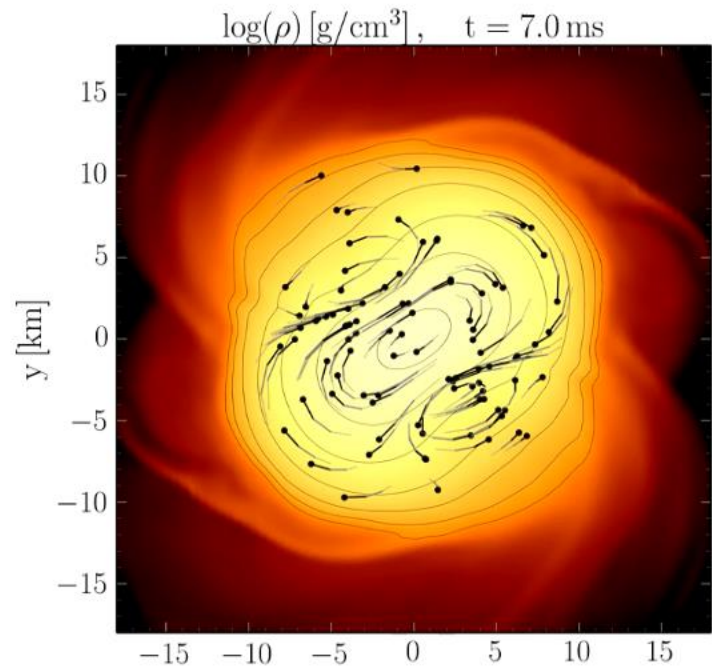
M. Shibata, K. Taniguchi, and K. Uryu, Phys. Rev. D 71, 084021 (2005)

M. Shibata and K. Taniguchi, Phys. Rev. D 73, 064027 (2006)

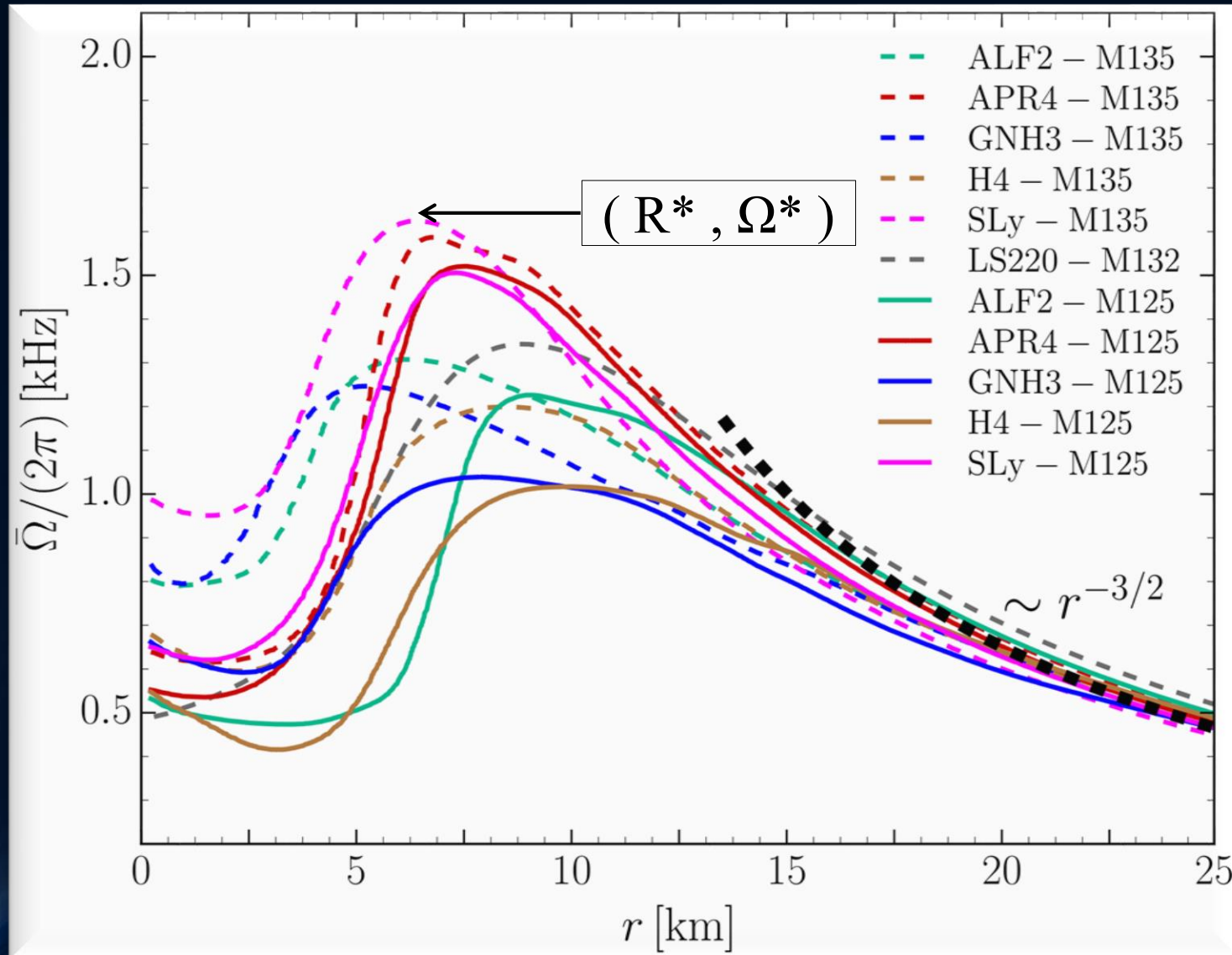
F. Galeazzi, S. Yoshida and Y. Eriguchi, A&A 541, p. A156 (2012)

W. Kastaun and F. Galeazzi, Phys. Rev. D 91, p. 064027 (2015)





# Time-averaged Rotation Profiles of the HMNSs



Soft EoSs:  
Sly  
APR4

Stiff EoSs:  
GNH3  
H4

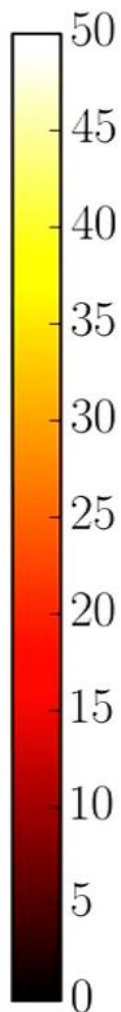
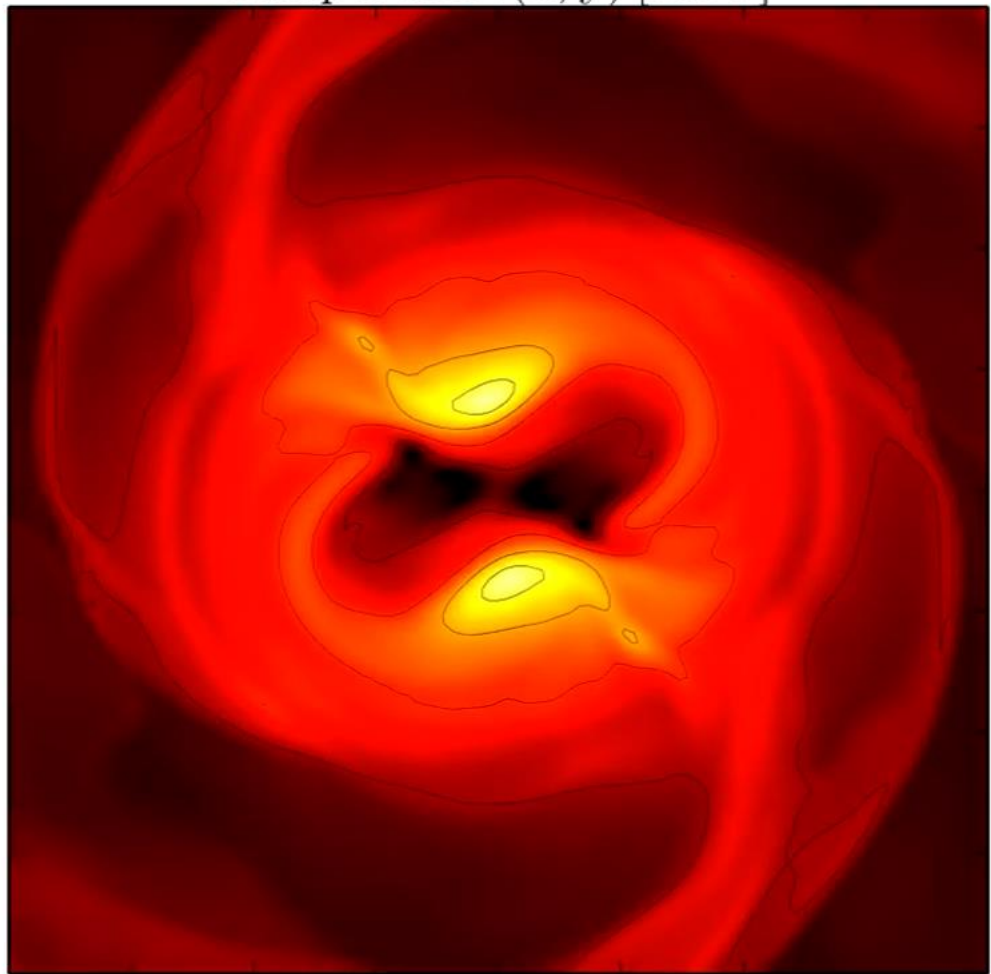
Time-averaged rotation profiles for different EoS  
Low mass runs (solid curves), high mass runs (dashed curves).

Hanuske, et.al. PRD, 96(4), 043004 (2017)

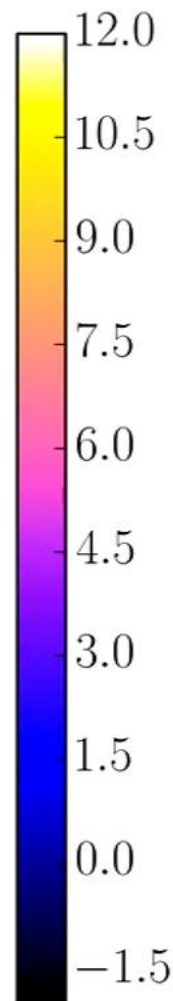
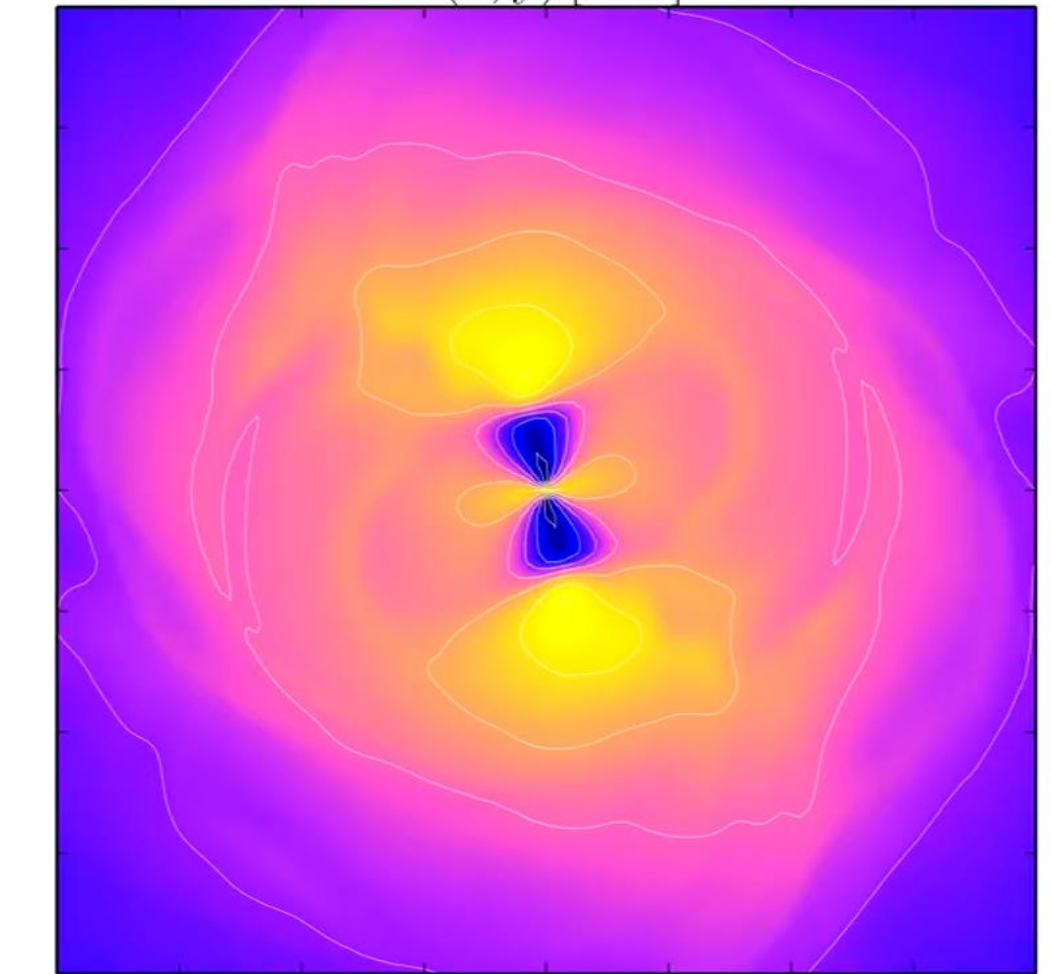
# Temperature

# Angular Velocity

Temperature(x, y) [MeV]



$\Omega(x, y)$  [kHz]



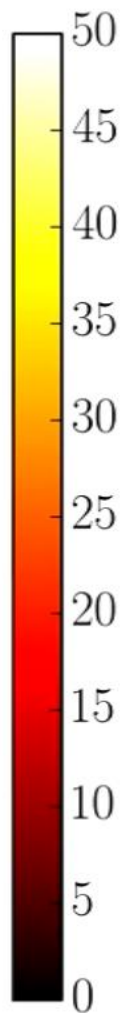
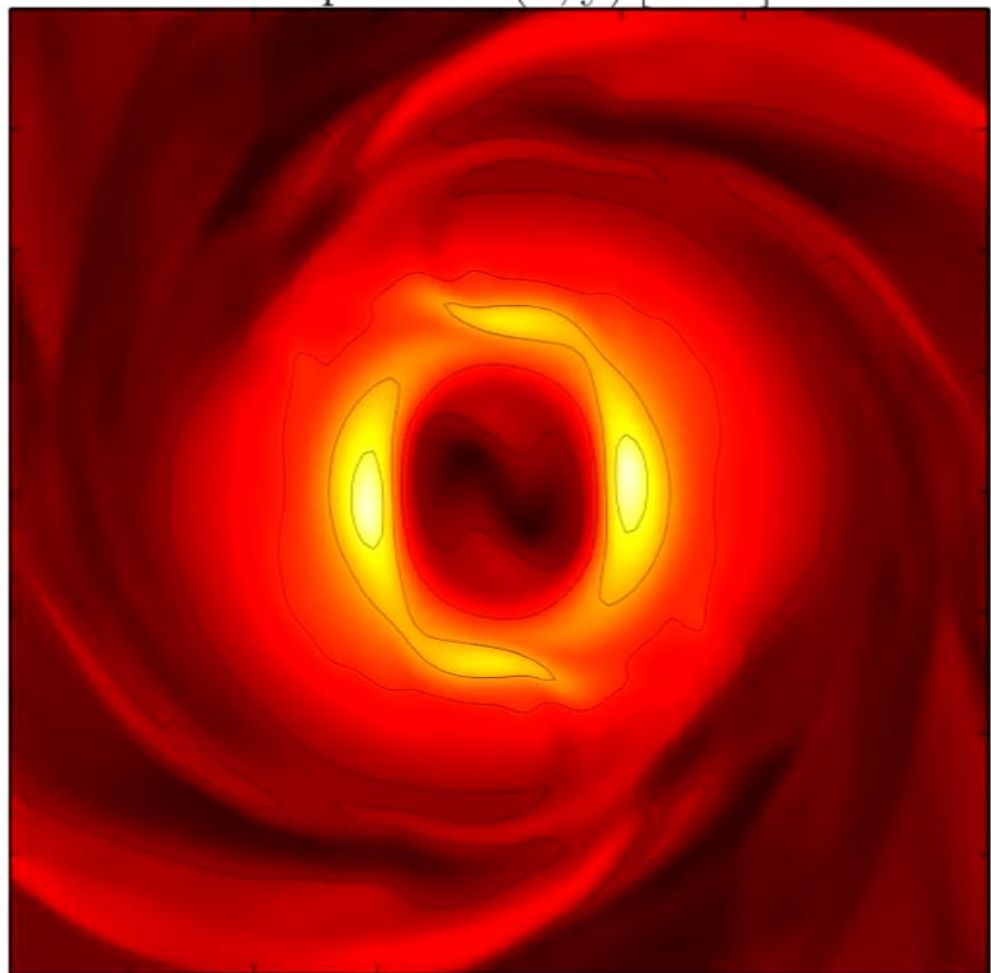
-20 -15 -10 -5 0 5 10 15 20  
x [km]

-20 -15 -10 -5 0 5 10 15 20  
x [km]

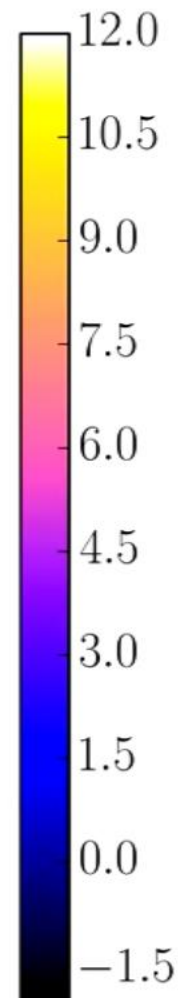
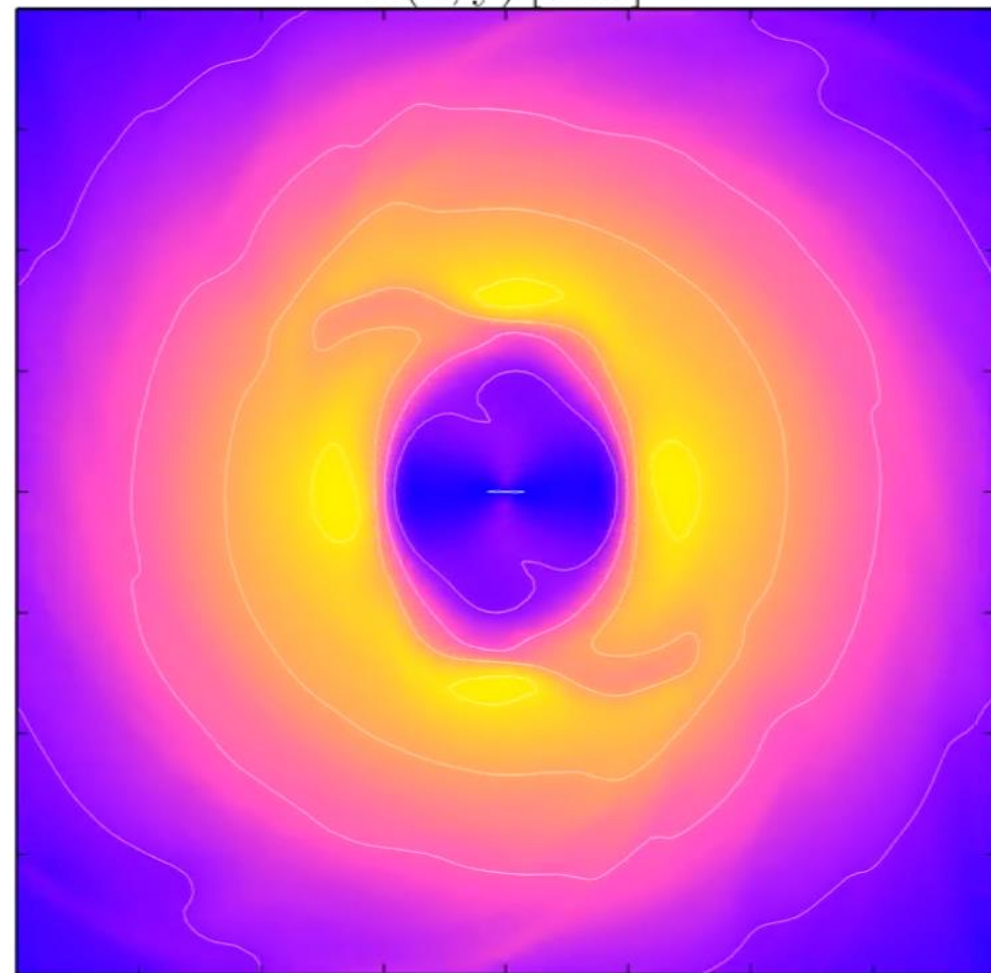
# Temperature

# Angular Velocity

Temperature(x, y) [MeV]



$\Omega(x, y)$  [kHz]



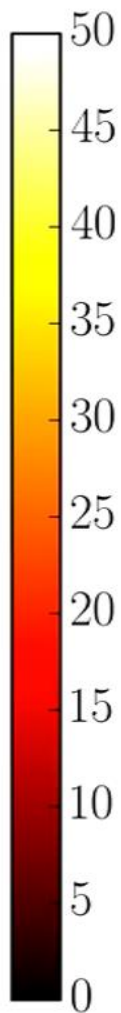
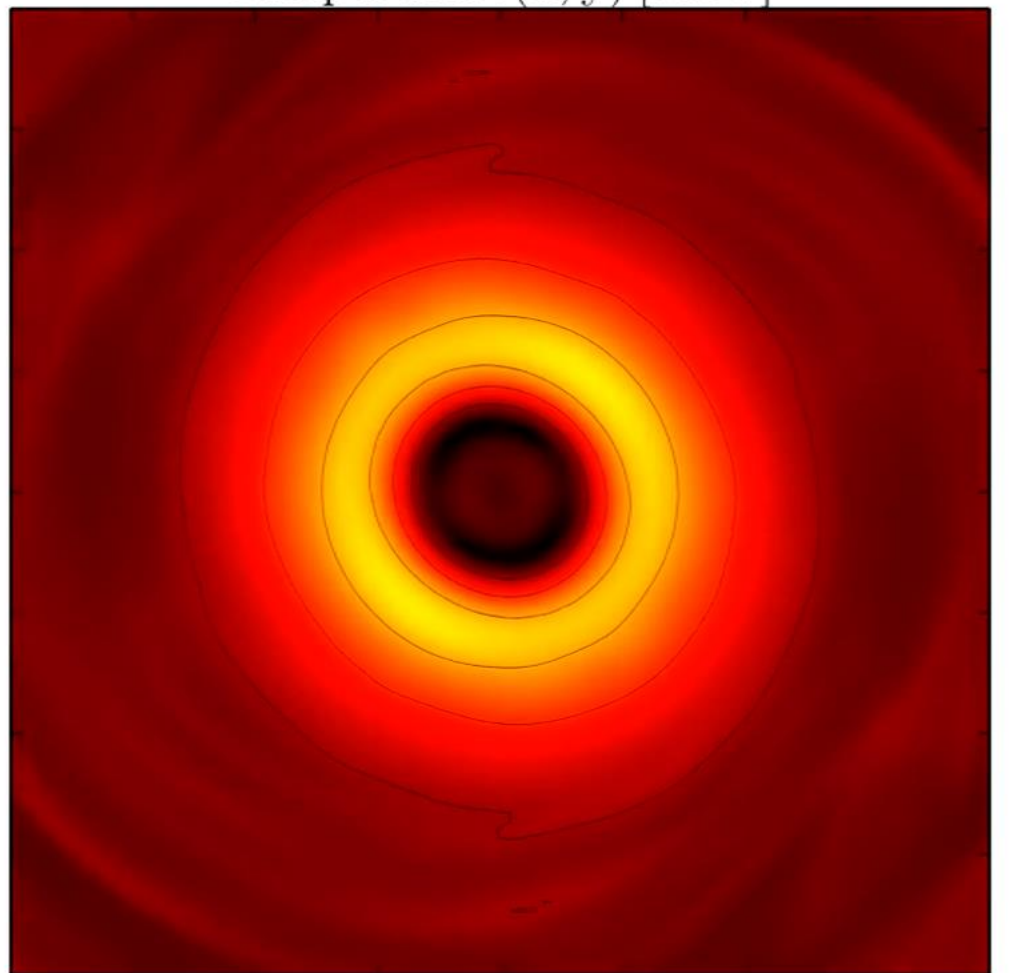
-20 -15 -10 -5 0 5 10 15 20  
x [km]

-20 -15 -10 -5 0 5 10 15 20  
x [km]

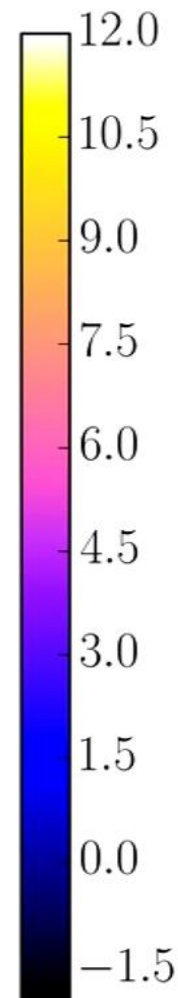
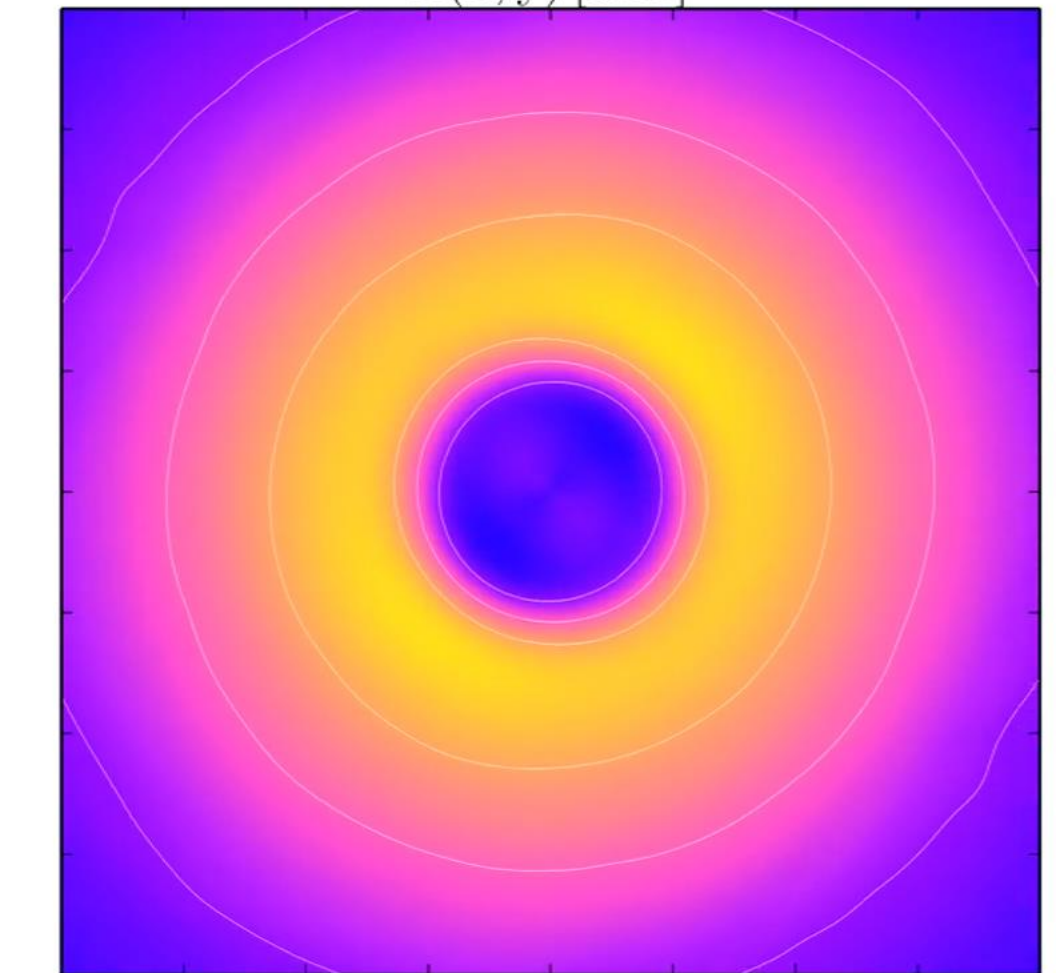
# Temperature

# Angular Velocity

Temperature(x, y) [MeV]

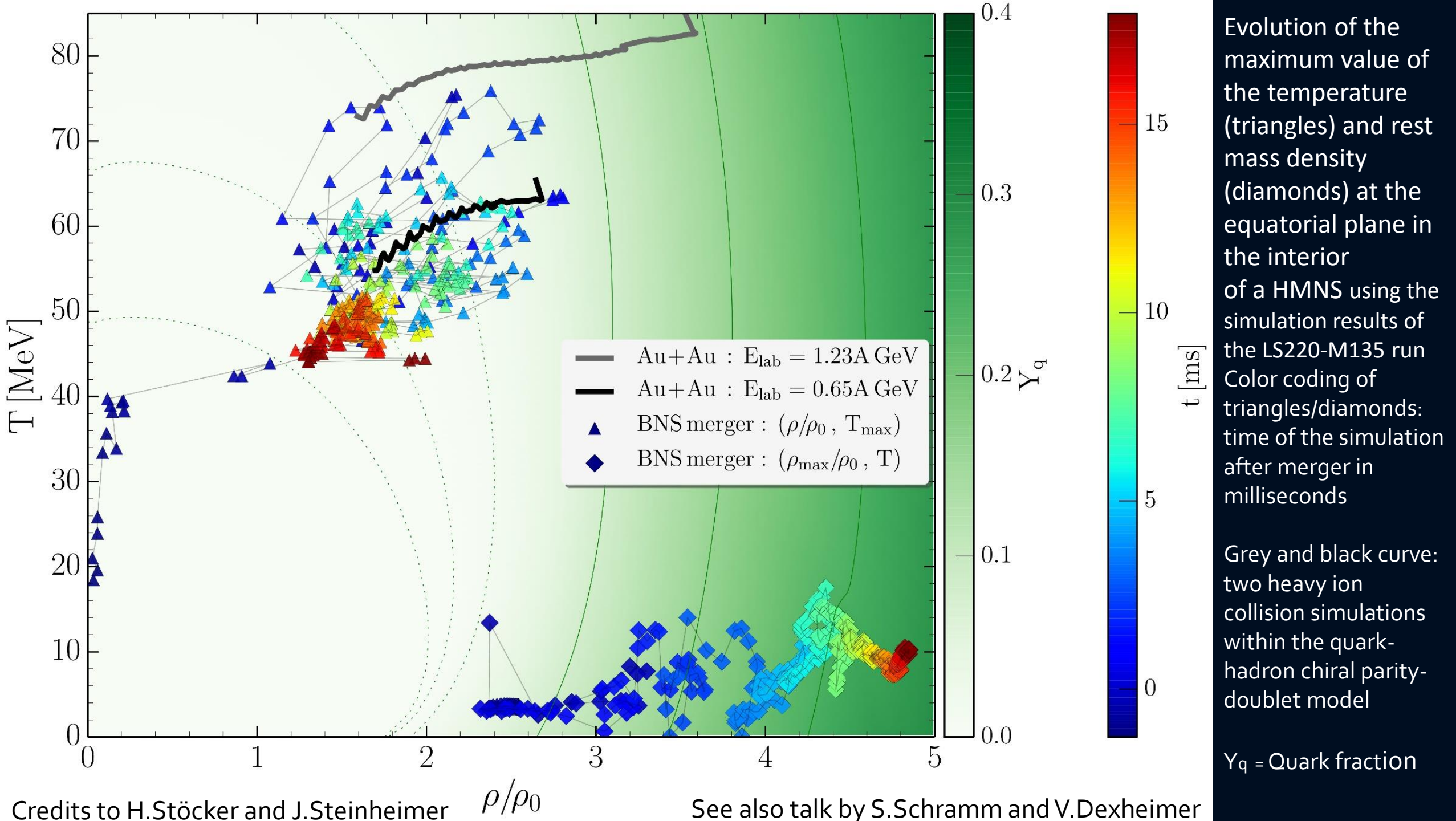


$\Omega(x, y)$  [kHz]

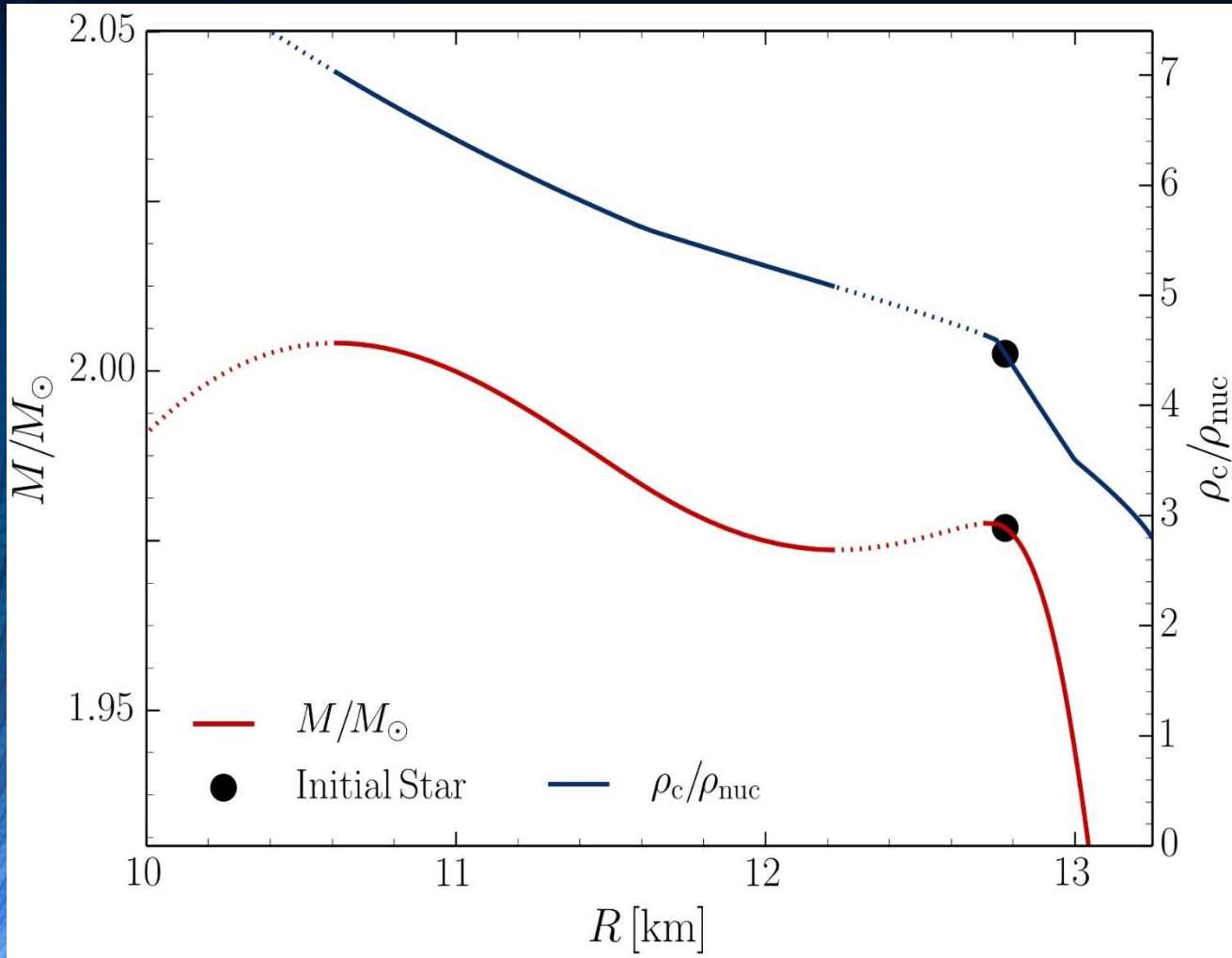


-20 -15 -10 -5 0 5 10 15 20  
x [km]

-20 -15 -10 -5 0 5 10 15 20  
x [km]



# The Hadron-Quark Phase Transition and the Third Family of Compact Stars (Twin Stars)



Gerlach (1968), Glendenning, N. K., & Kettner, C. (1998). Nonidentical neutron star twins. *Astron. Astrophys.*, 353(LBL-42080), L9.

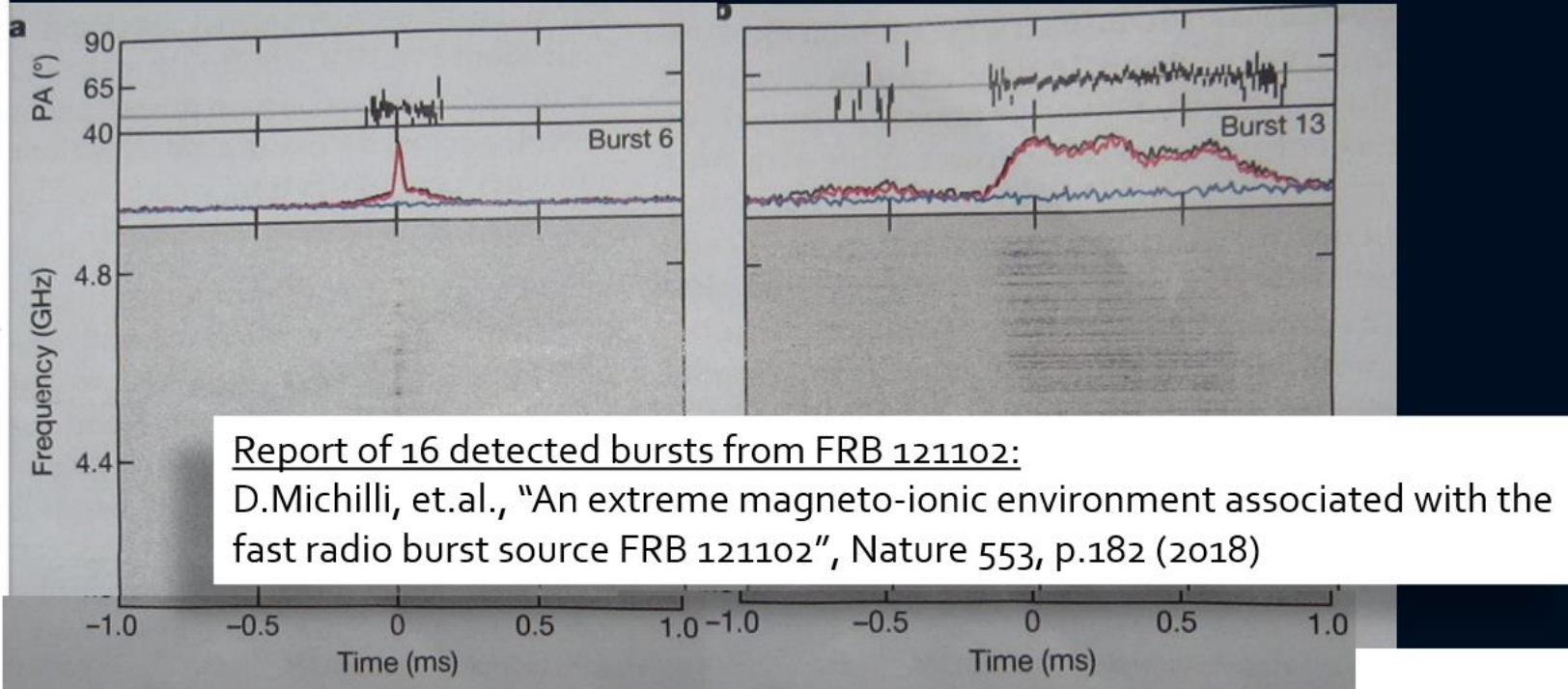
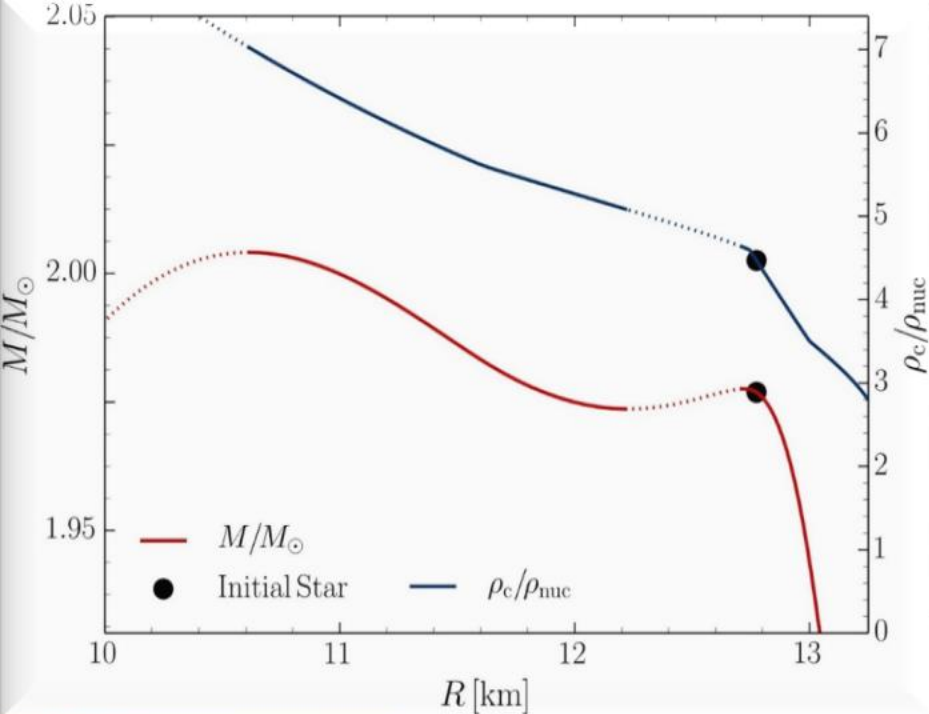
Sarmistha Banik, Matthias Hanauske, Debades Bandyopadhyay and Walter Greiner, Rotating compact stars with exotic matter, *Phys.Rev.D* 70 (2004) p.12304

I.N. Mishustin, M. Hanauske, A. Bhattacharyya, L.M. Satarov, H. Stöcker, and W. Greiner, Catastrophic rearrangement of a compact star due to quark core formation, *Physics Letters B* 552 (2003) p.1-8

M.Alford and A. Sedrakian, Compact stars with sequential QCD phase transitions. *Physical review letters*, 119(16), 161104 (2017).

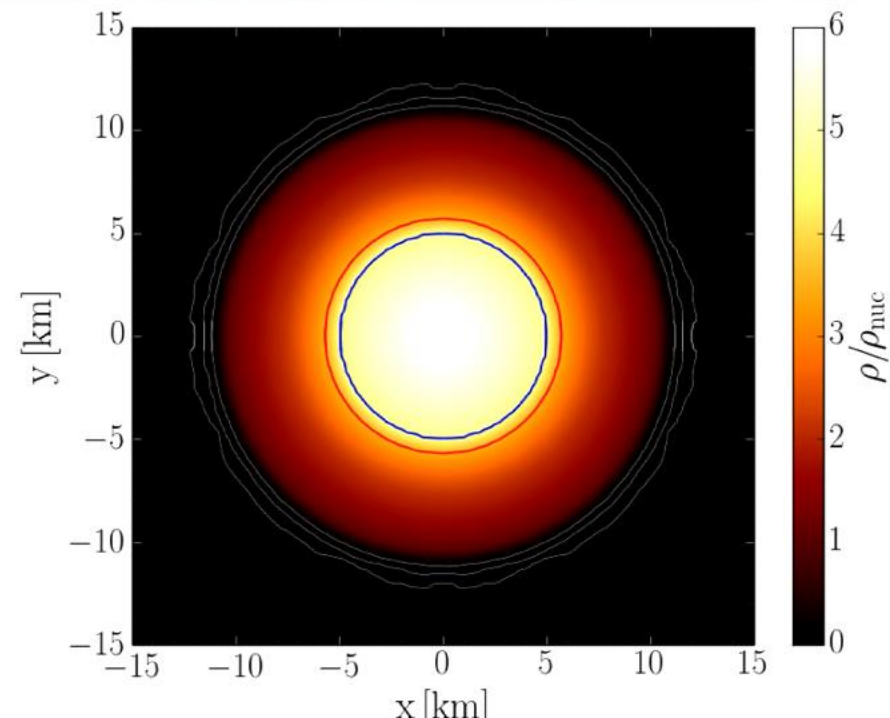
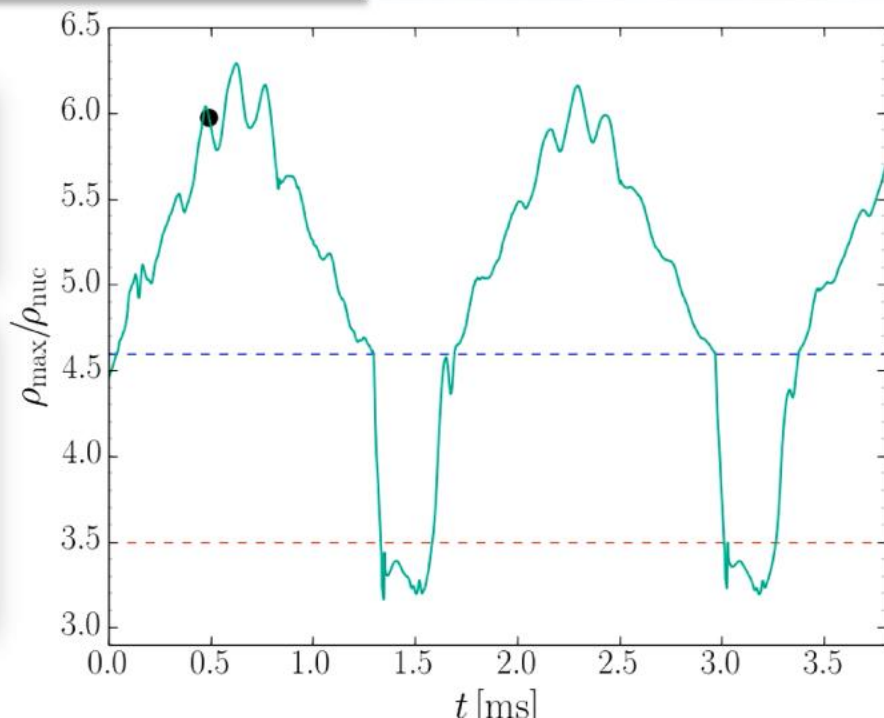
D.Alvarez-Castillo and D.Blaschke, High-mass twin stars with a multipolytrope equation of state. *Physical Review C*, 96(4), 045809 (2017).

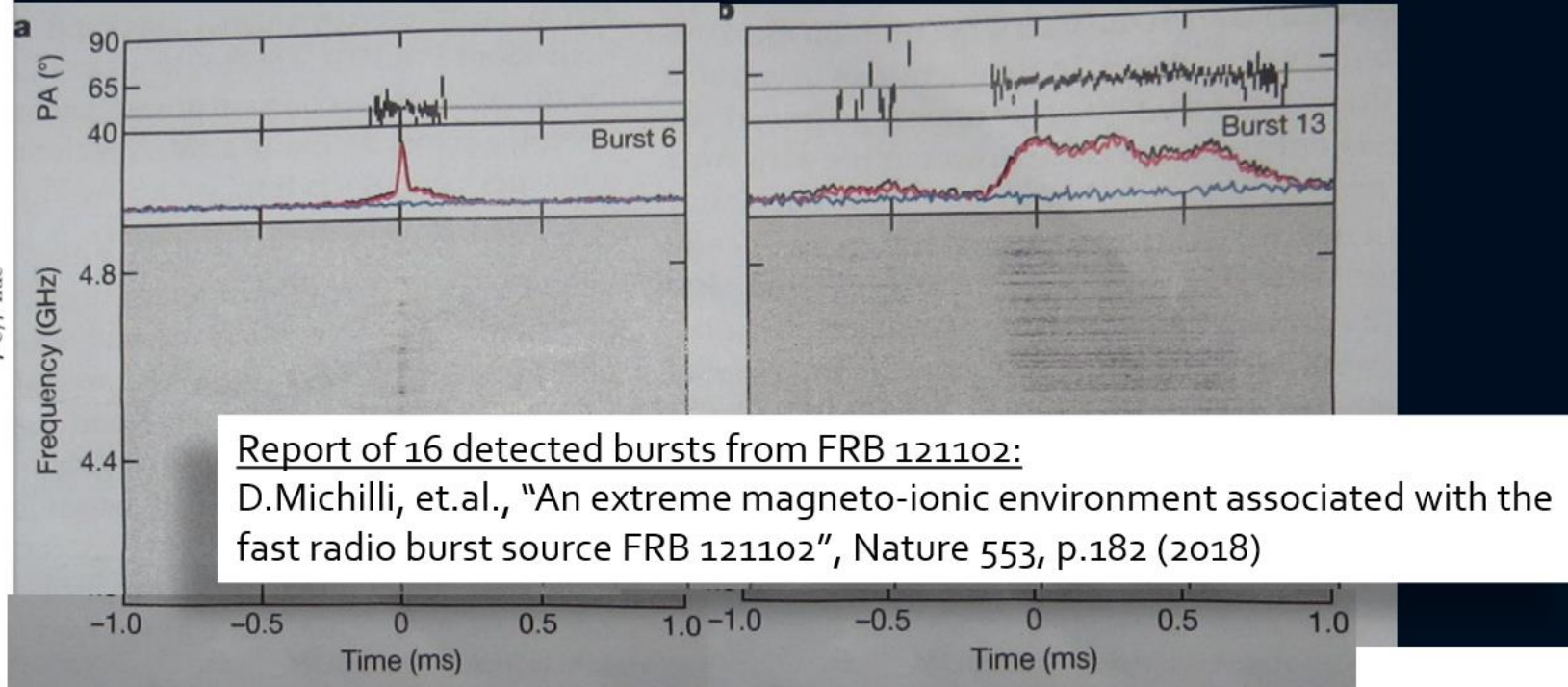
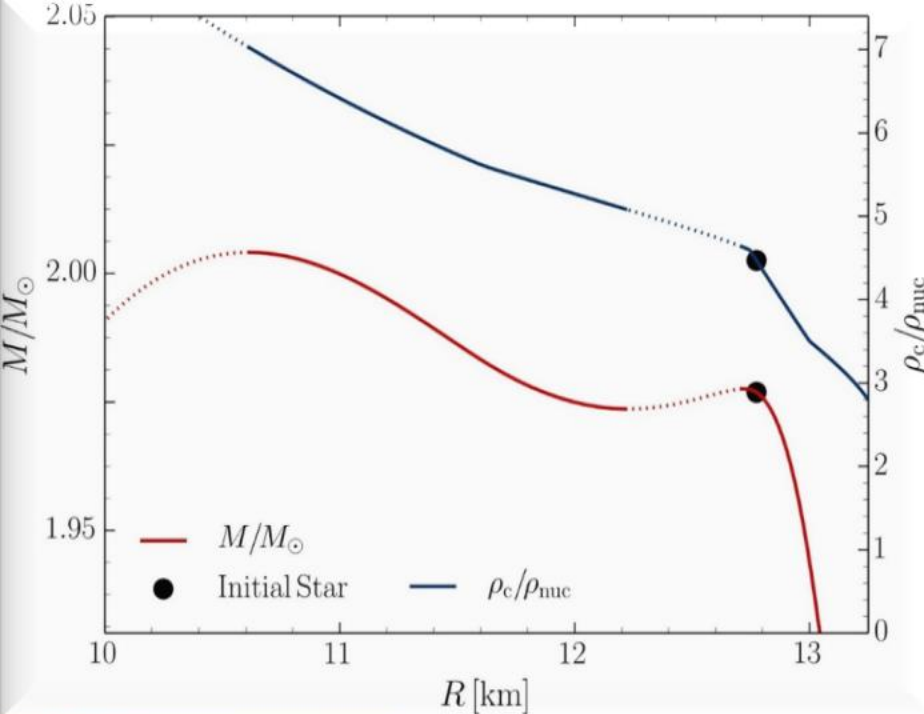
A. Ayriyan, N.-U. Bastian, D. Blaschke, H. Grigorian, K. Maslov, D. N. Voskresensky, How robust is a third family of compact stars against pasta phase effects?, arXiv:1711.03926 [nucl-th]



M.Hanuske, et.al.,  
 "Twin Star Oscillations"  
 (in preparation)

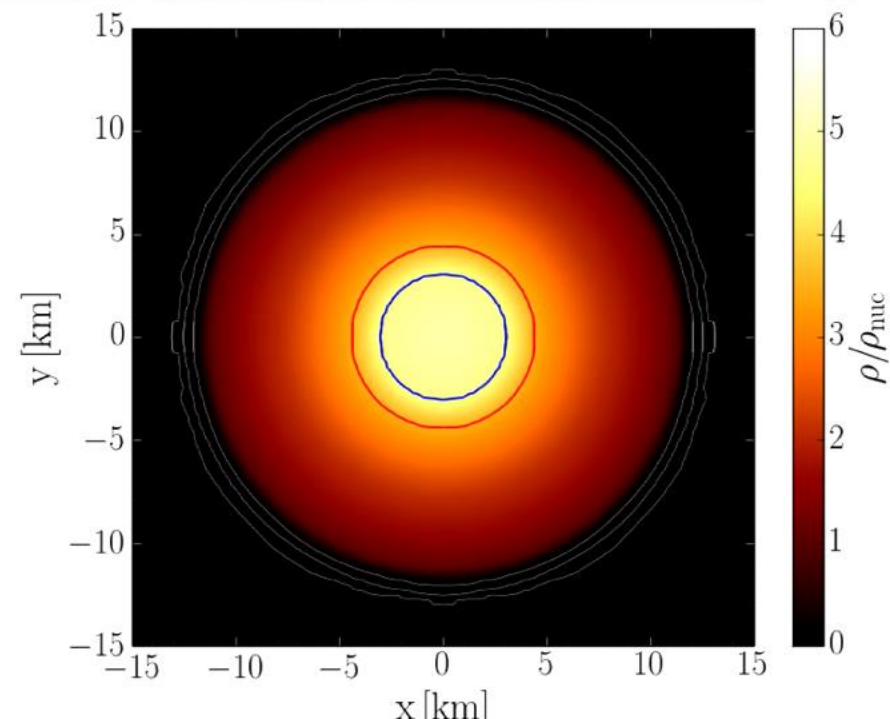
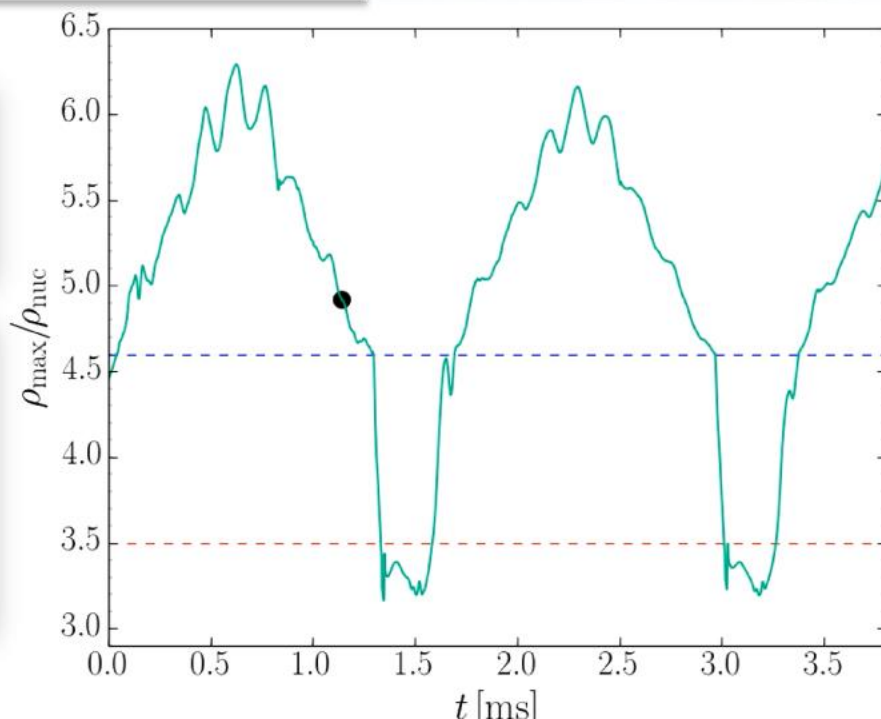
Hanuske, M., Yilmaz,  
 Z.S., Mitropoulos,C.,  
 Rezzolla, L., and  
 Stöcker, H., EPJ Web  
 Conf. 171, 20004 (2018)

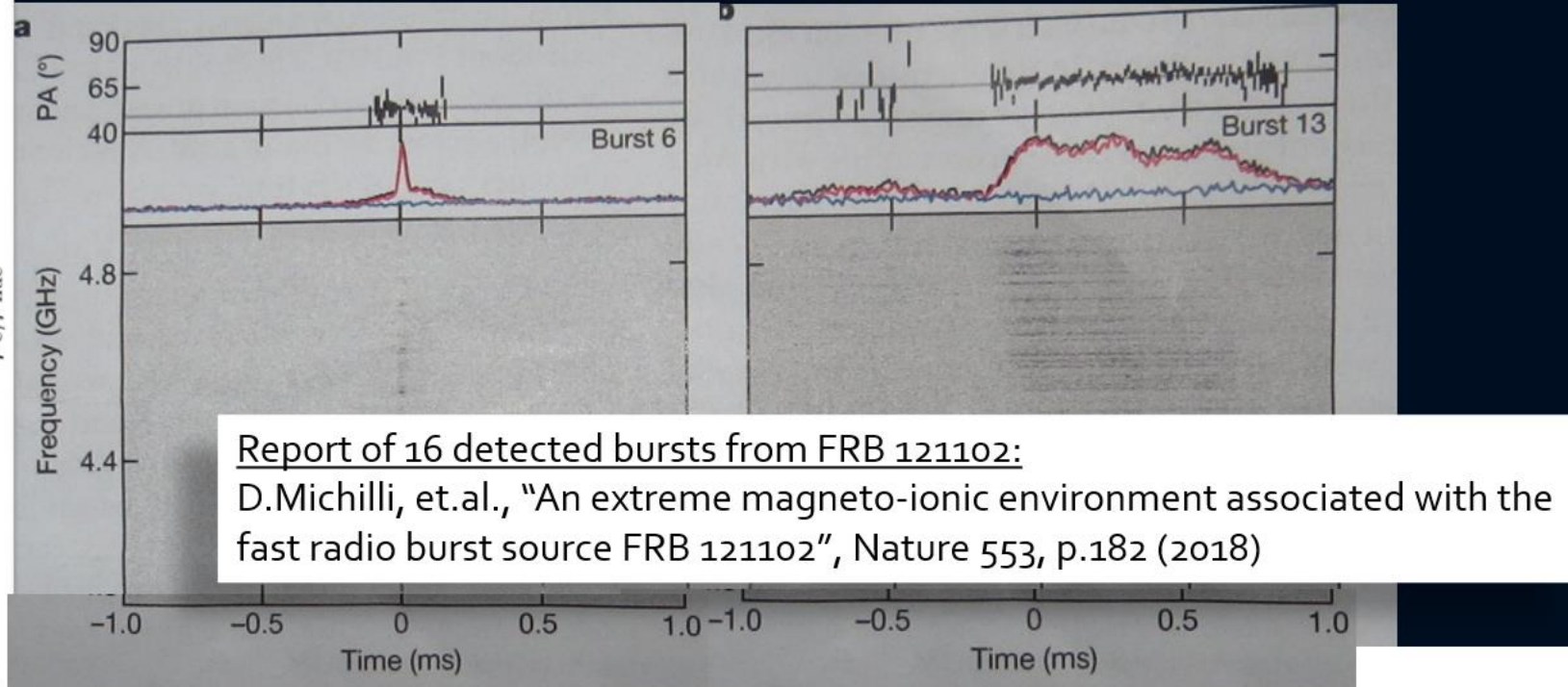
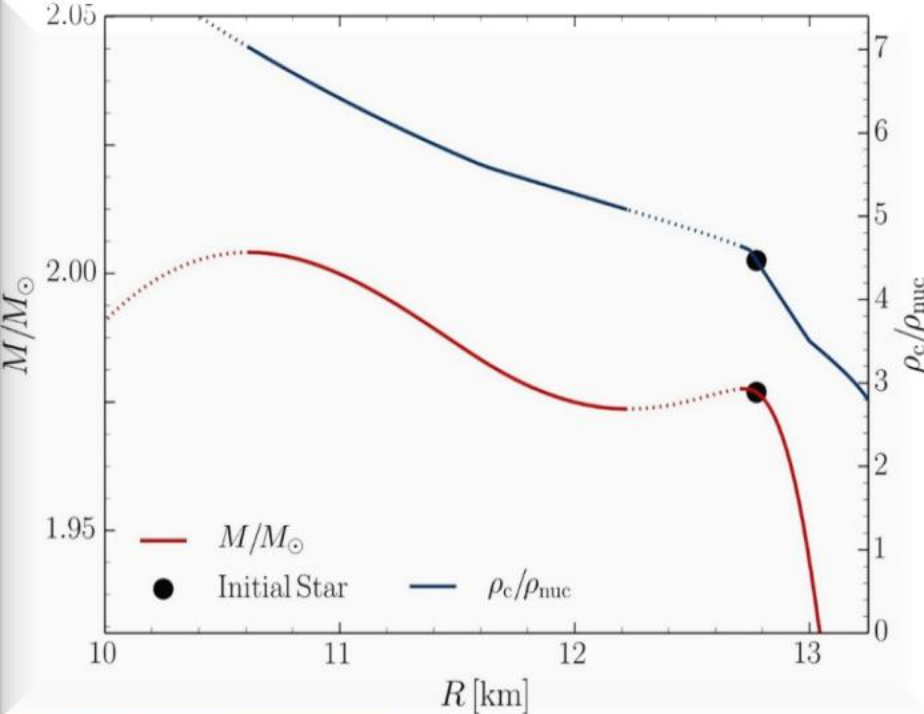




M.Hanauske, et.al.,  
 "Twin Star Oscillations"  
 (in preparation)

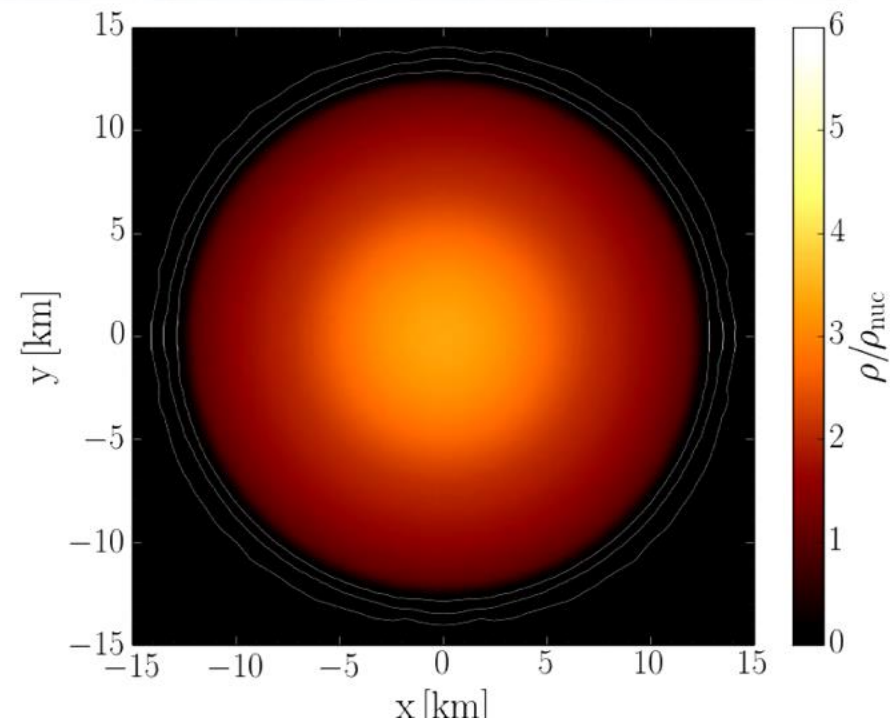
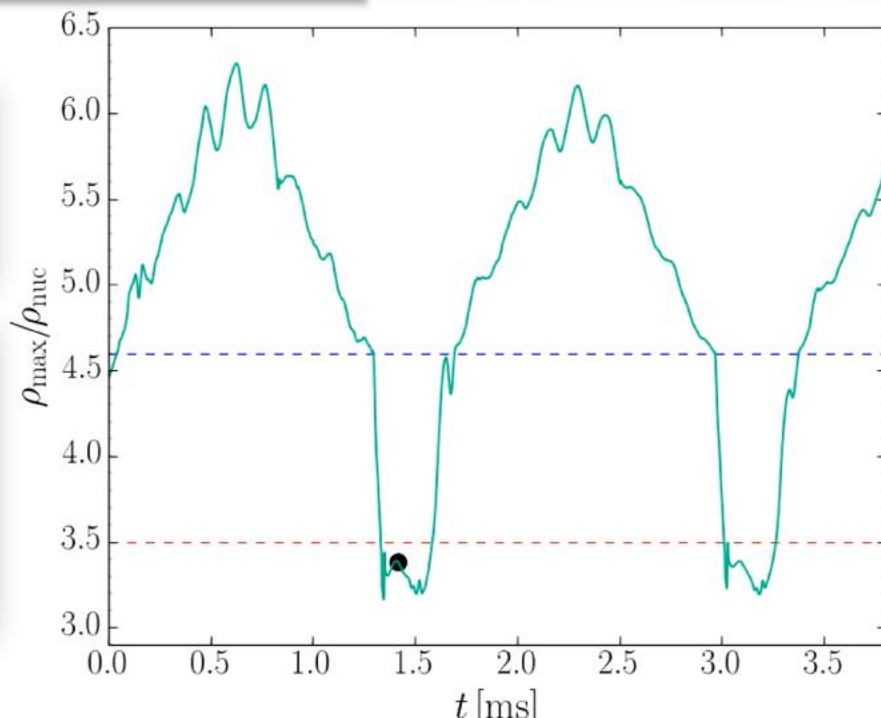
Hanauske, M., Yilmaz,  
 Z.S., Mitropoulos,C.,  
 Rezzolla, L., and  
 Stöcker, H., EPJ Web  
 Conf. 171, 20004 (2018)

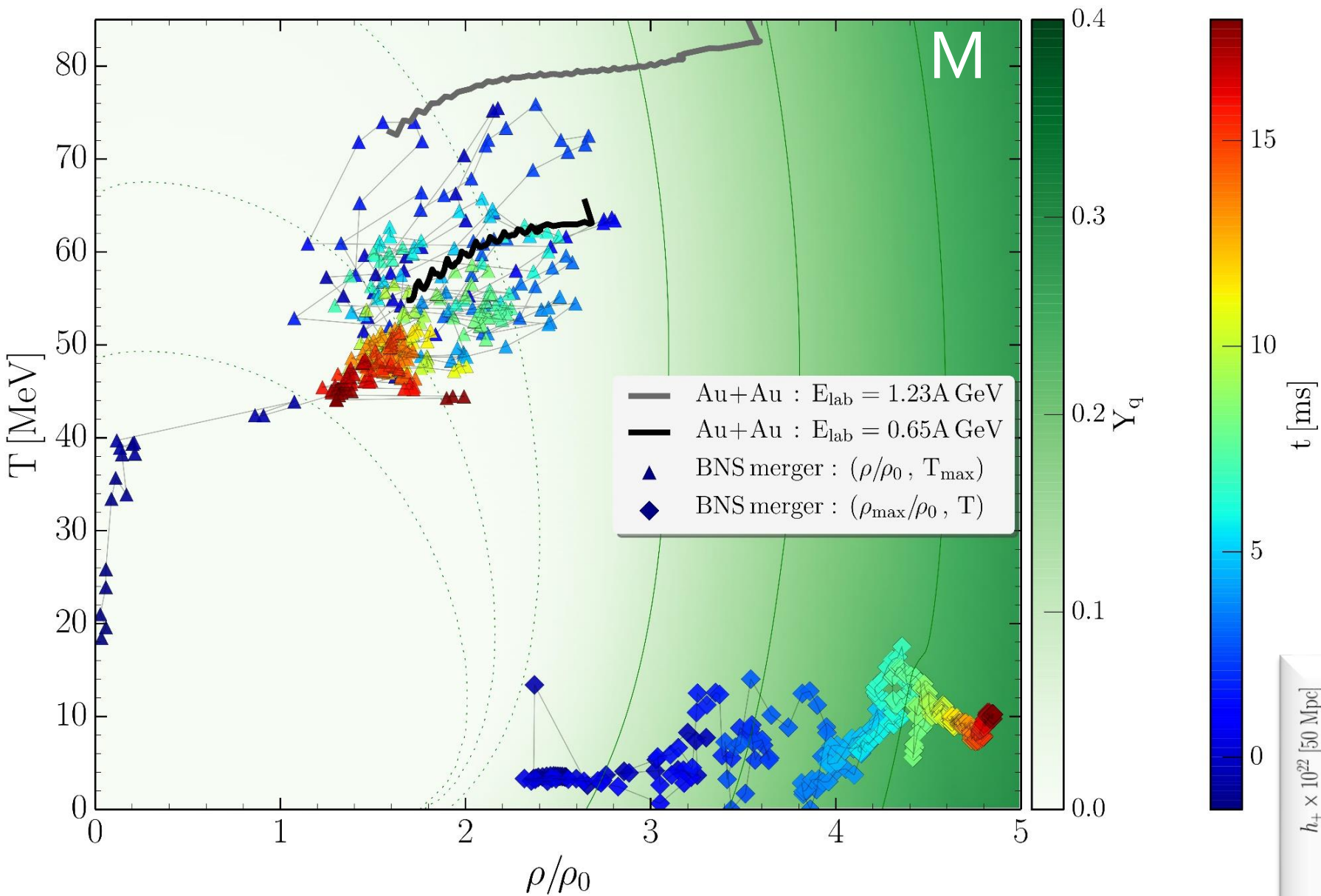




M.Hanauske, et.al.,  
 "Twin Star Oscillations"  
 (in preparation)

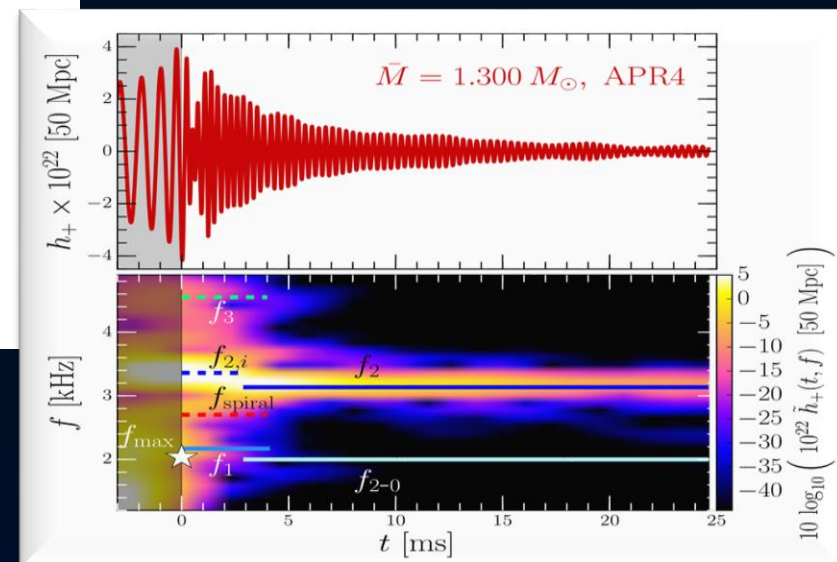
Hanauske, M., Yilmaz,  
 Z.S., Mitropoulos,C.,  
 Rezzolla, L., and  
 Stöcker, H., EPJ Web  
 Conf. 171, 20004 (2018)





# Neutron Star Mergers in the Context of a Twin Star Collapse

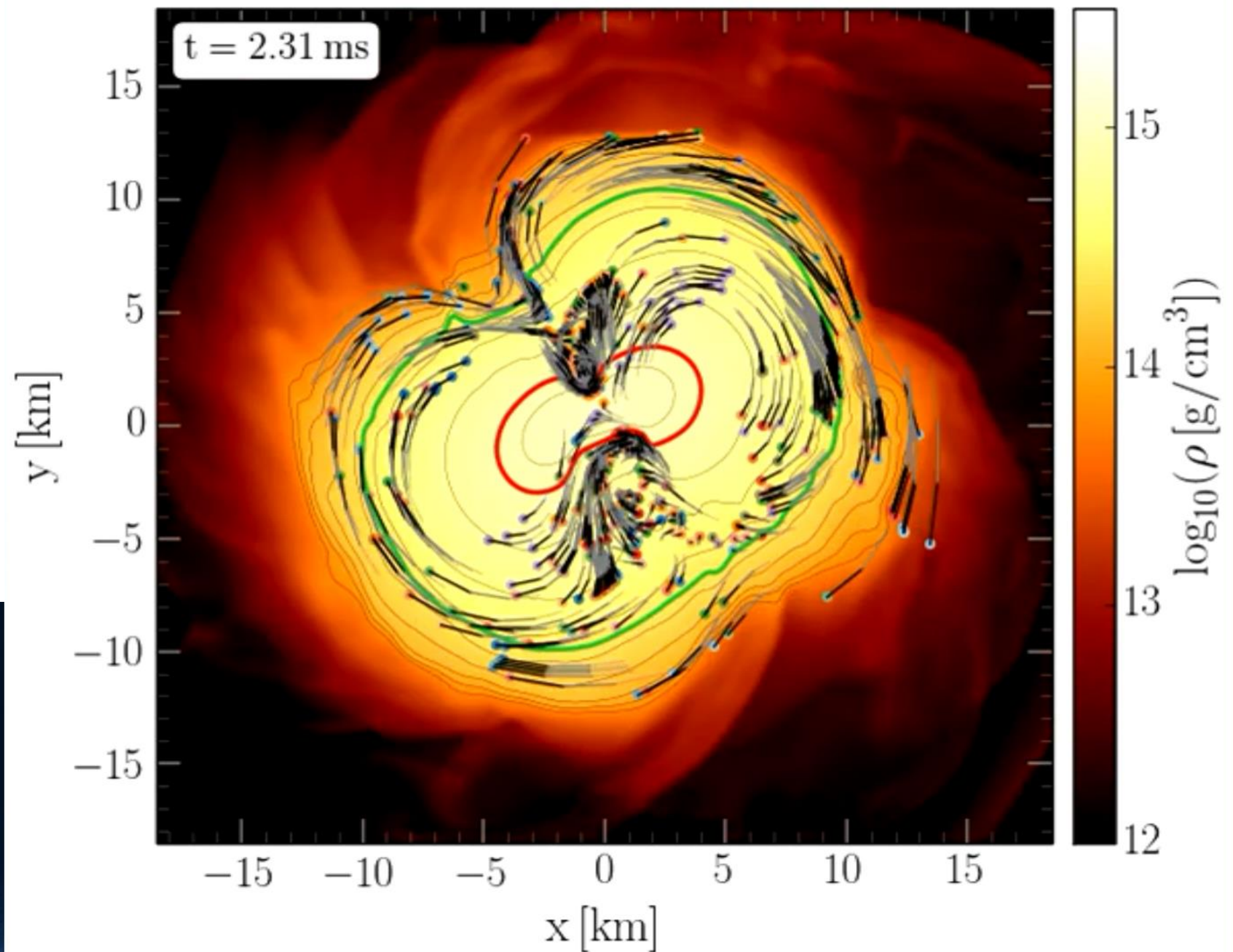
The astrophysical consequences of a rearrangement of a compact star due to the quark core formation, namely a twin star collapse or twin star oscillation, will be imprinted in the emitted GW-signal and would give an additional contribution to the dynamically emitted outflow of mass.

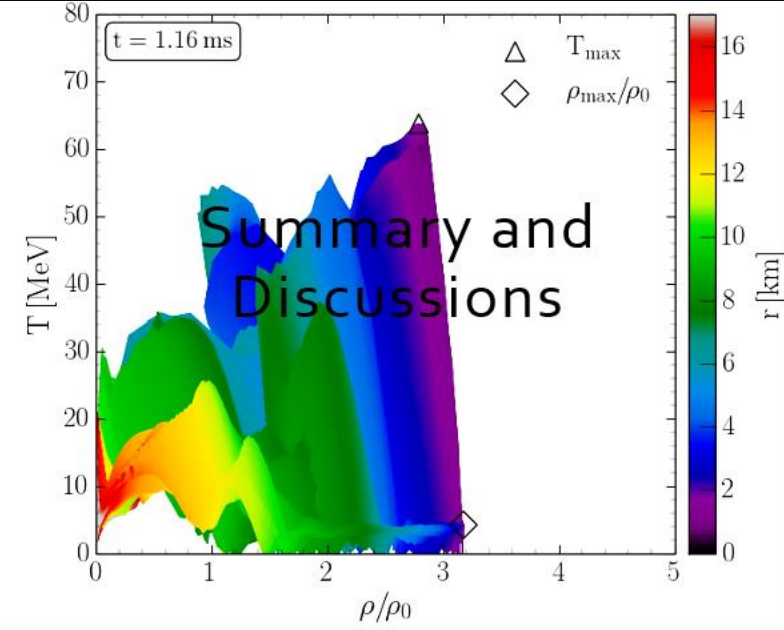
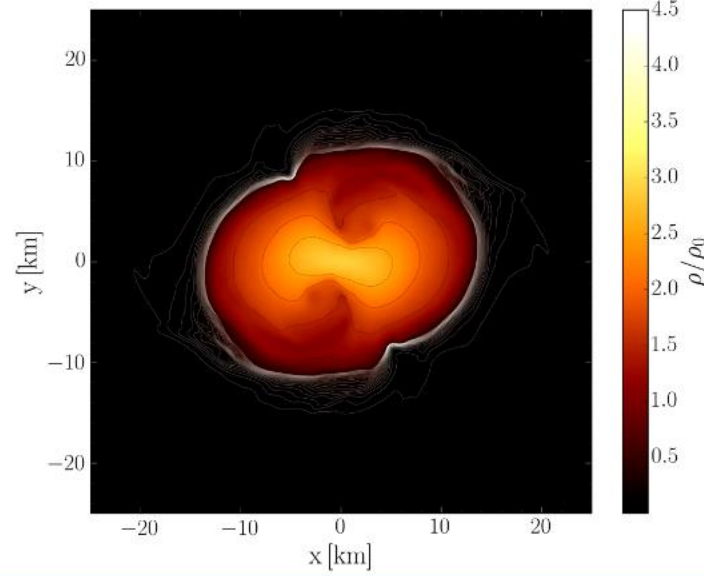
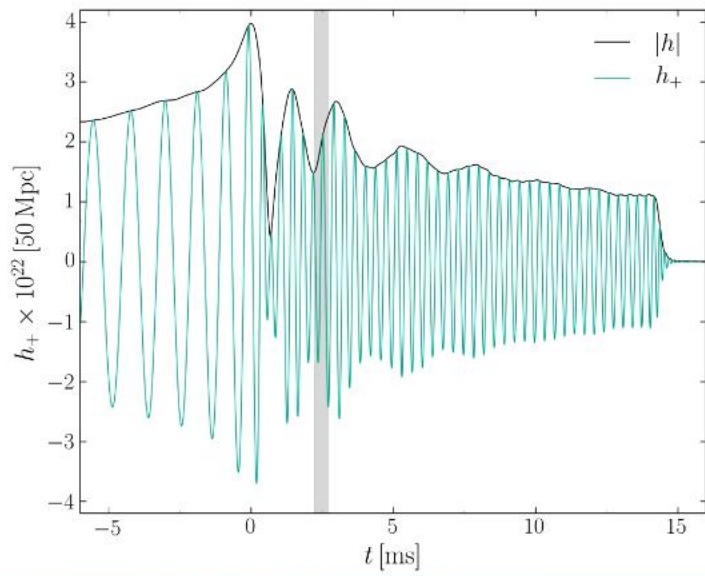


If the unstable twin star region is reached during the "post-transient" phase, the  $f_2$ -frequency peak of the GW signal will change rapidly due to the sudden speed up of the differentially rotating HMNS.

A similar effect as found in non-central ultra-relativistic heavy ion collisions (see lower Ref. ) may be present during the post-merger evolution of a HMNS. The evolution of tracer particles show a swirling behaviour around two pronounced vortices which are centered in the two temperature hot spots of the HMNS. These tracers describe trajectories of fluid elements that could pass the deconfinement transition and confine again within less than 0.3 ms. After the hadronisation process an alignment between the angular momentum of the HMNS and the spin of hadronic particles is expected.

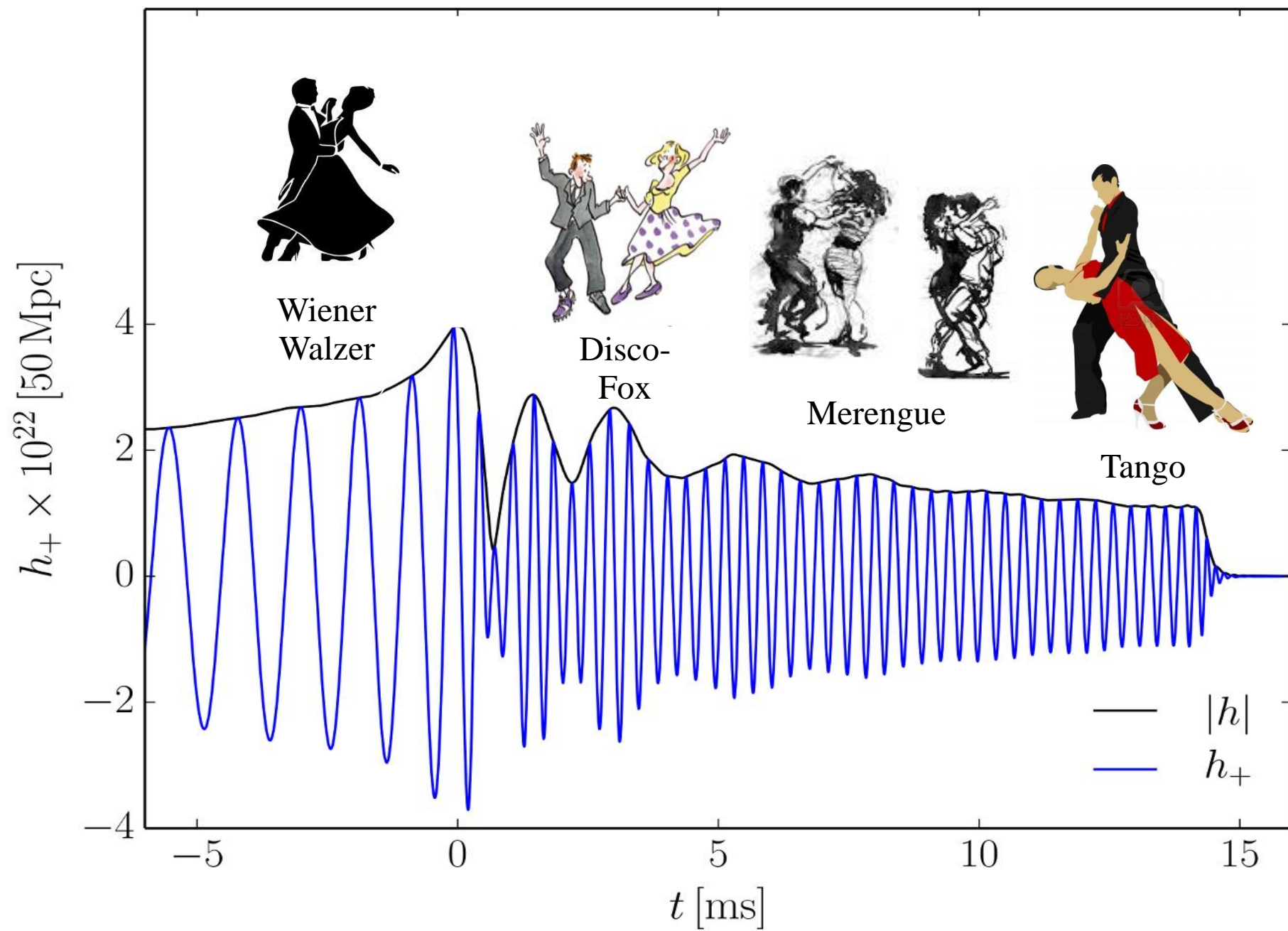
Different rotational behaviour of the quark-gluon-plasma produced in non-central ultra-relativistic heavy ion collisions  
L. Adamczyk et.al., "Global Lambda-hyperon polarization in nuclear collisions: evidence for the most vortical fluid", Nature 548, 2017





- In the post-merger phase of a binary neutron star merger, the density and temperature will reach extreme values and it is expected that a hadron-quark phase transition will be present in the interior region of the supramassive or hypermassive neutron star.
- Astrophysical observables of the hadron-quark phase transition:
  - If a twin star collapse would happen during the post-merger phase it will be imprinted in the GW-signal
  - If the unstable twin star region is reached during the "post-transient" phase, the f2-frequency peak of the GW signal will change rapidly due to the sudden speed up of the differentially rotating HMNS
  - Effects on the kilonova and neutrino emission?
  - Twin Star Collaps/Oszillations and the repeating fast radio burst (FRB 121102).

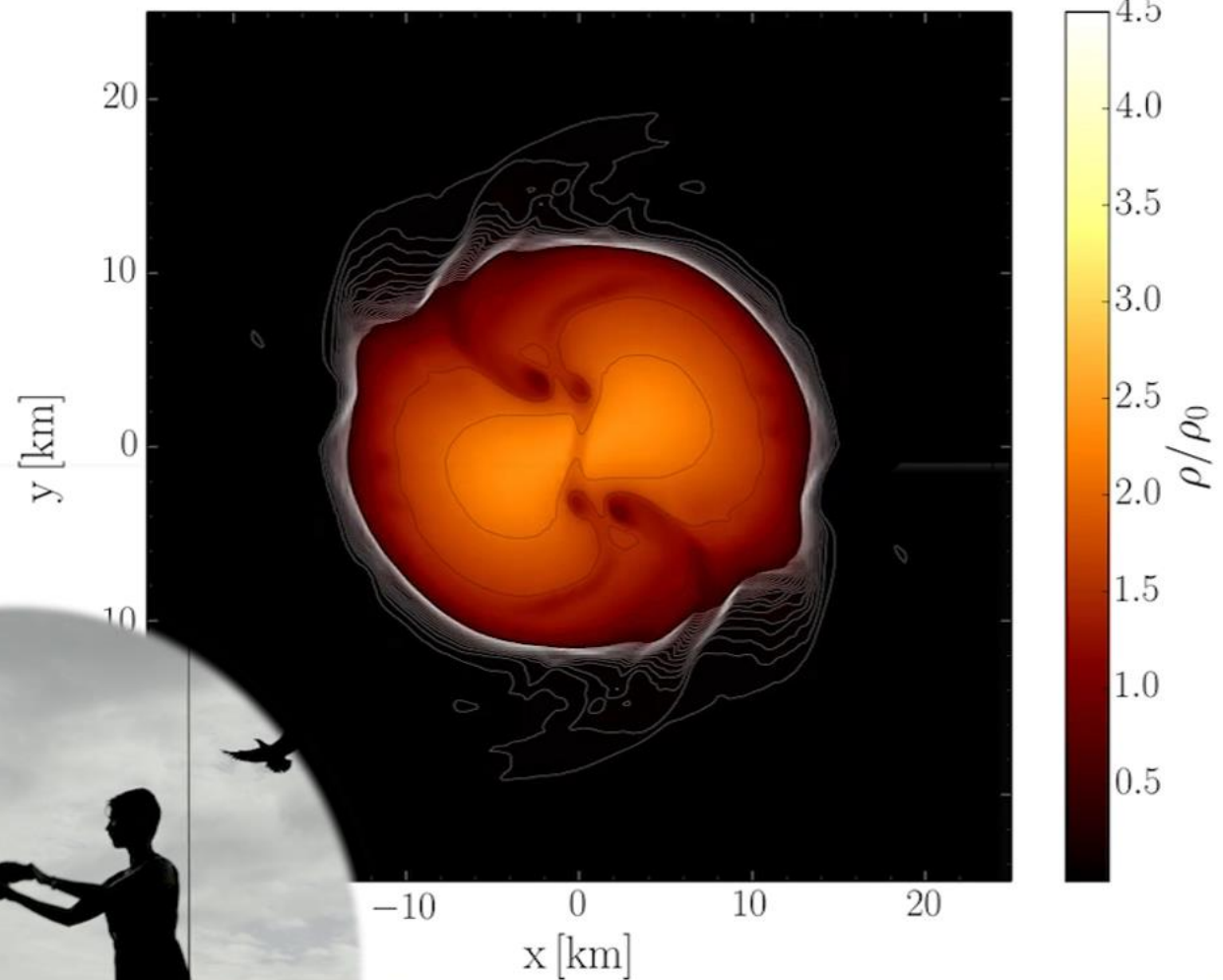
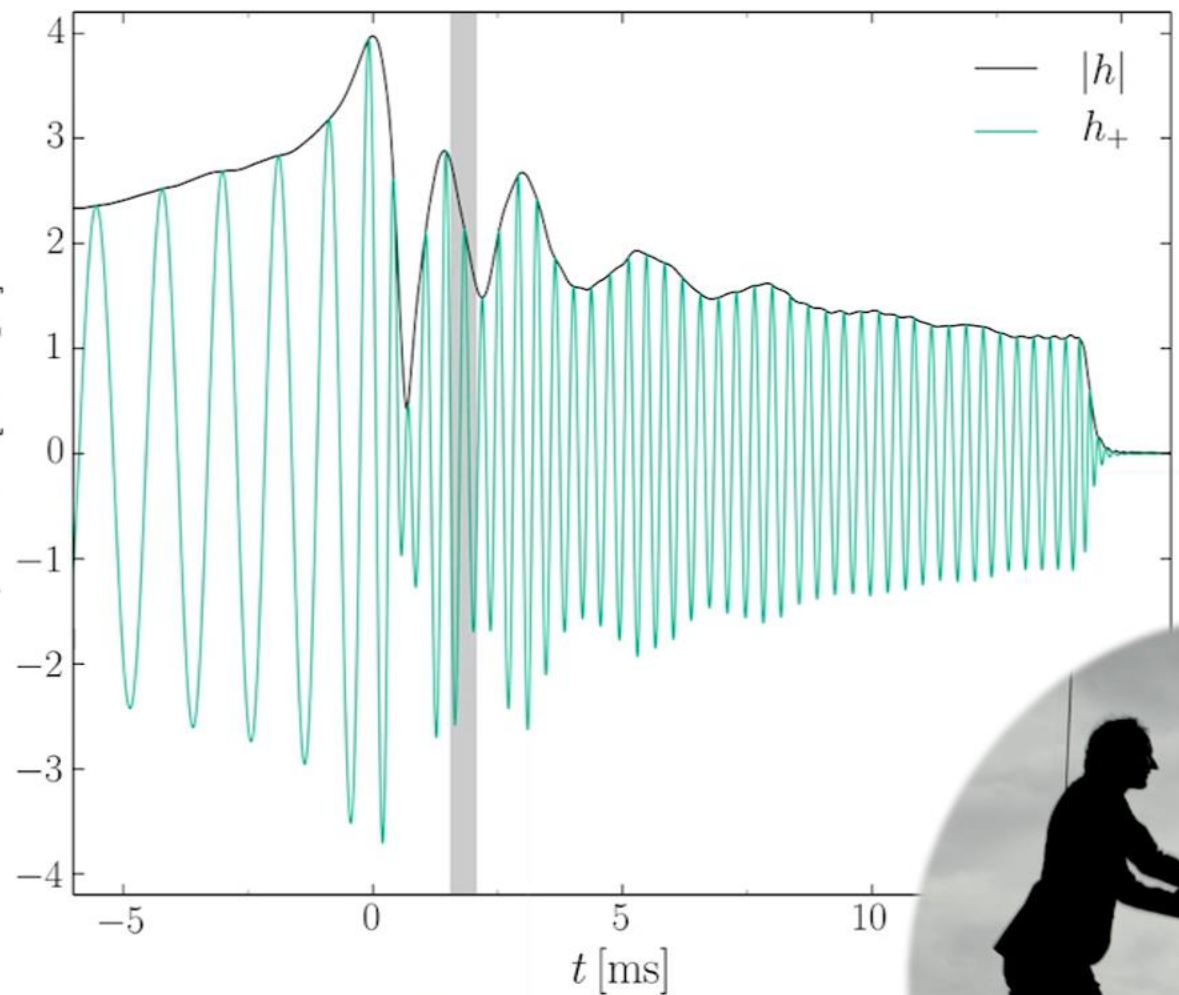
# Different phases of a binary neutron star merger: The Neutronstar Merger Dance





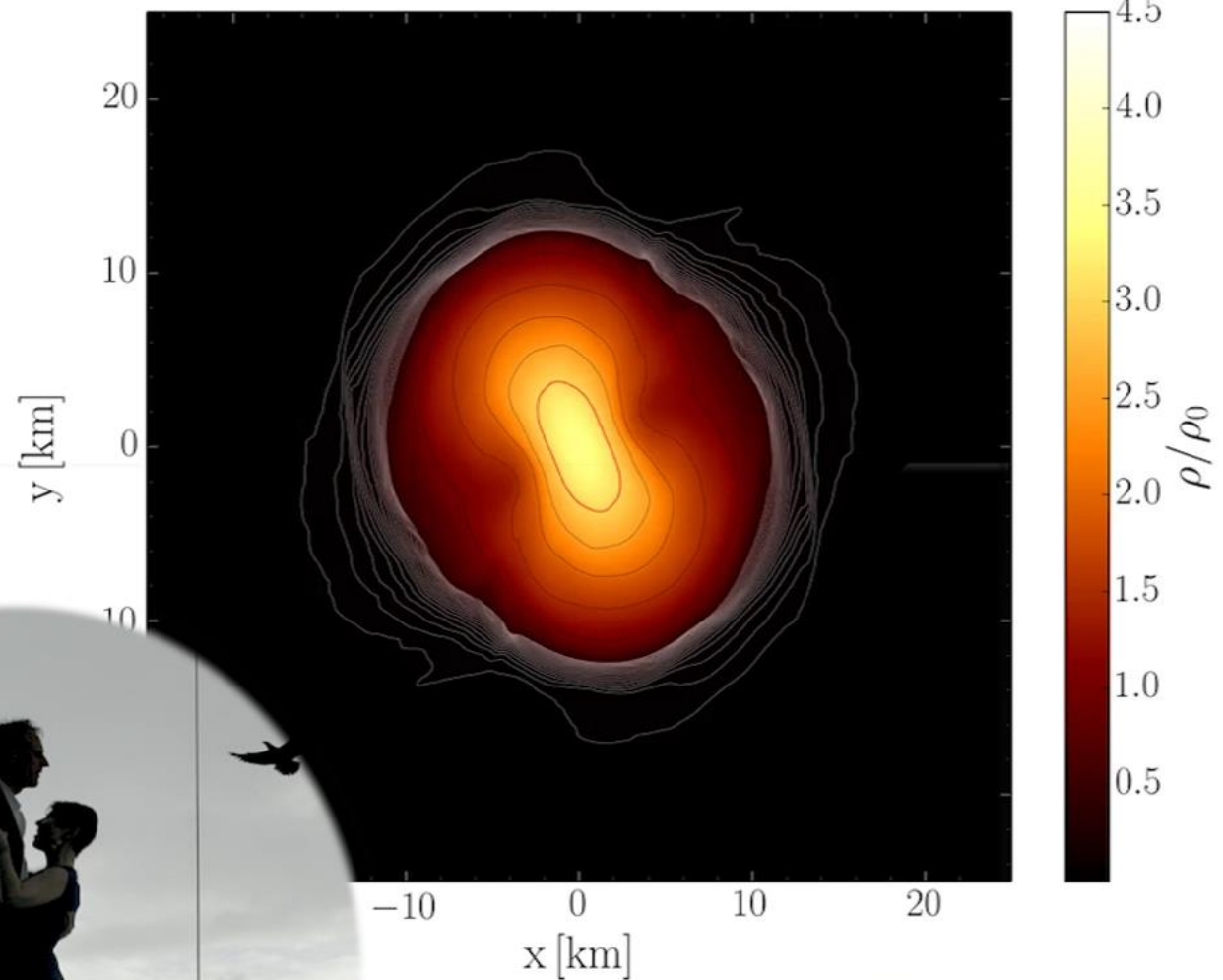
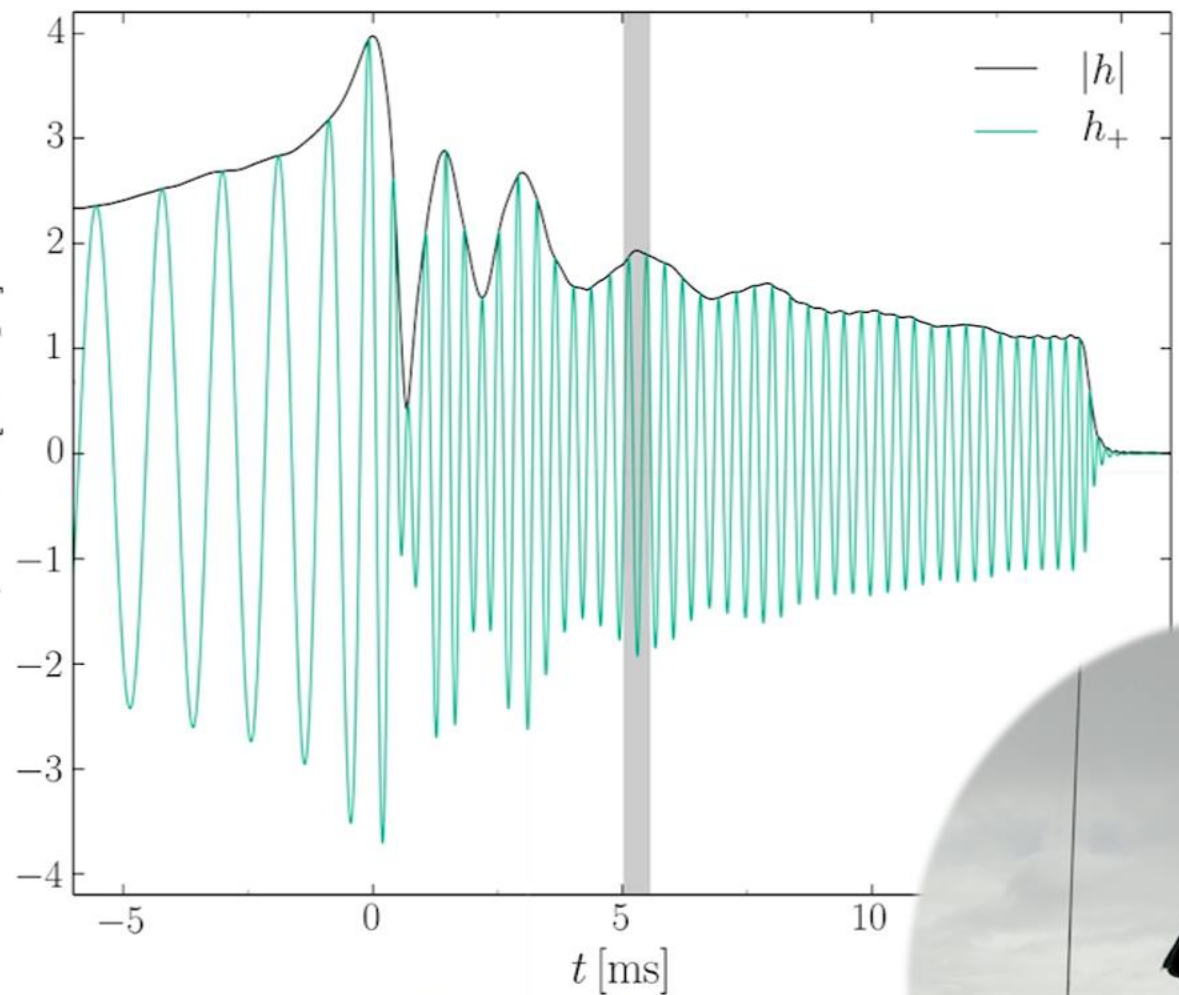
Wiener Walzer

$h_+ \times 10^{22} [50 \text{ Mpc}]$



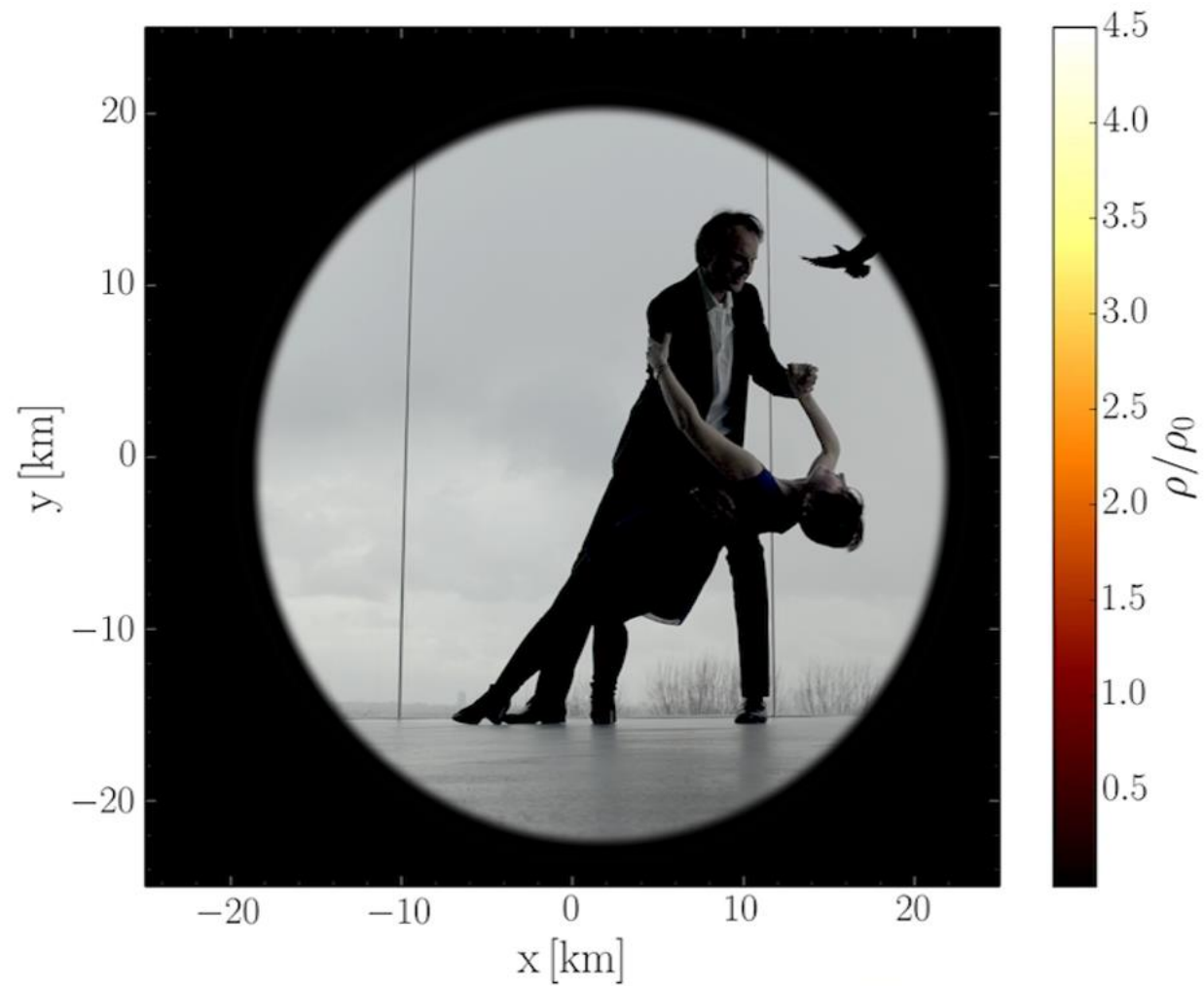
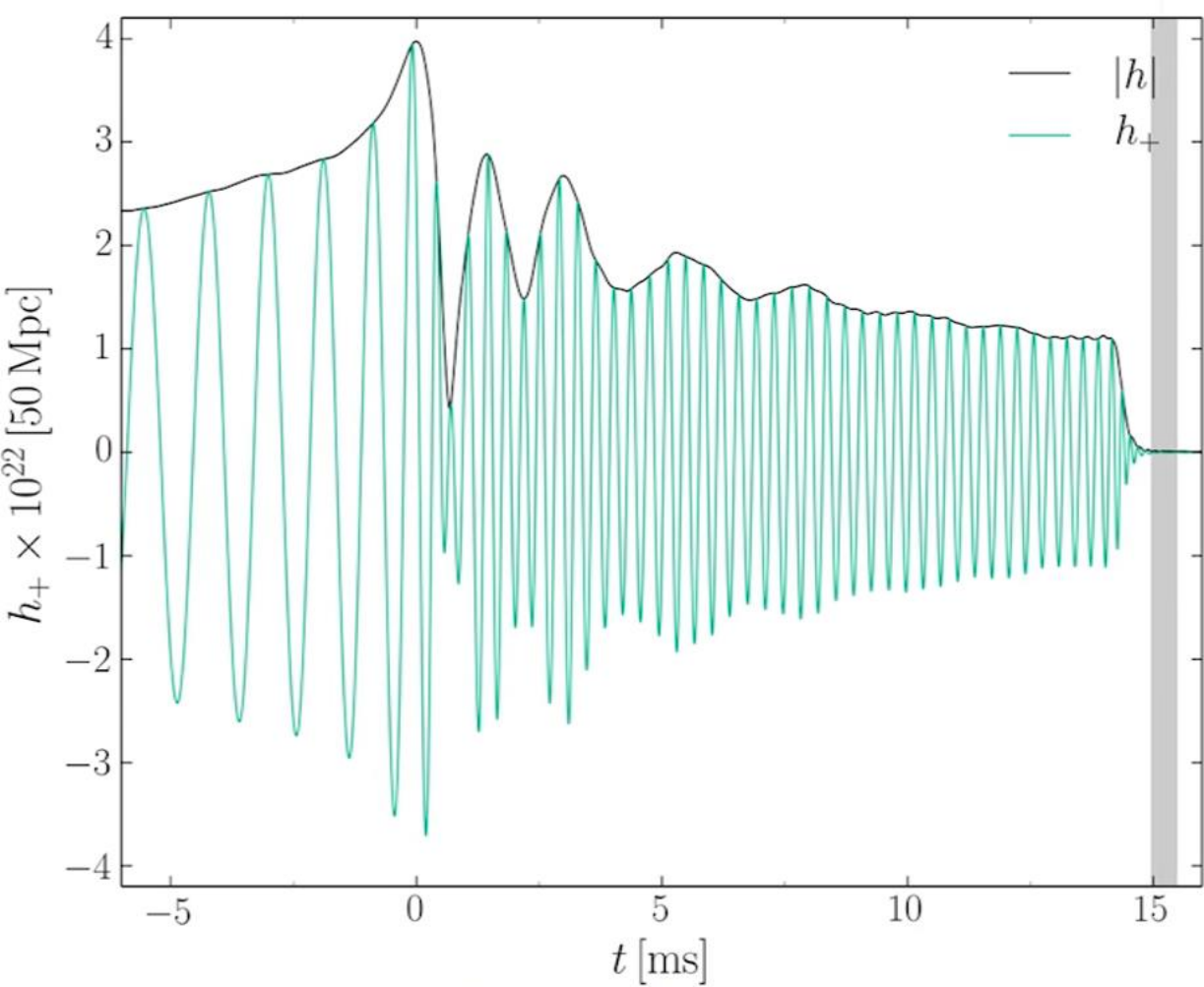
Disco Fox

$h_+ \times 10^{22} [50 \text{ Mpc}]$



Merengue





Tango

*Ludmila* und

**Matthias Hanauske**

**Kamera** Pablo Rengel

Lorena

**Schnitt** Luise Schulte

The Neutron Star Merger Dance  
Credits to Riedberg TV and the  
Hessisches Kompetenzzentrum  
für Hochleistungsrechnen